

## Marbostat 100 defines a new class of potent and selective antiinflammatory and antirheumatic histone deacetylase 6 inhibitors

Andreas Sellmer, Hubert Stangl, Mandy Beyer, Elisabeth Grünstein, Michel Leonhardt, Herwig Pongratz, Emerich Eichhorn, Sigurd Elz, Birgit Striegl, Zsuzsa Jenei-Lanzl, Stefan Dove, Rainer H Straub, Oliver H Krämer, and Siavosh Mahboobi

*J. Med. Chem.*, **Just Accepted Manuscript** • DOI: 10.1021/acs.jmedchem.7b01593 • Publication Date (Web): 28 Mar 2018

Downloaded from <http://pubs.acs.org> on March 28, 2018

### Just Accepted

“Just Accepted” manuscripts have been peer-reviewed and accepted for publication. They are posted online prior to technical editing, formatting for publication and author proofing. The American Chemical Society provides “Just Accepted” as a service to the research community to expedite the dissemination of scientific material as soon as possible after acceptance. “Just Accepted” manuscripts appear in full in PDF format accompanied by an HTML abstract. “Just Accepted” manuscripts have been fully peer reviewed, but should not be considered the official version of record. They are citable by the Digital Object Identifier (DOI®). “Just Accepted” is an optional service offered to authors. Therefore, the “Just Accepted” Web site may not include all articles that will be published in the journal. After a manuscript is technically edited and formatted, it will be removed from the “Just Accepted” Web site and published as an ASAP article. Note that technical editing may introduce minor changes to the manuscript text and/or graphics which could affect content, and all legal disclaimers and ethical guidelines that apply to the journal pertain. ACS cannot be held responsible for errors or consequences arising from the use of information contained in these “Just Accepted” manuscripts.



# Marbostat-100 defines a new class of potent and selective antiinflammatory and antirheumatic histone deacetylase 6 inhibitors

*Andreas Sellmer<sup>1</sup>, Hubert Stangl<sup>2</sup>, Mandy Beyer<sup>3</sup>, Elisabeth Grünstein<sup>1</sup>, Michel Leonhardt<sup>1</sup>, Herwig Pongratz<sup>1</sup>, Emerich Eichhorn<sup>1</sup>, Sigurd Elz<sup>1</sup>, Birgit Striegl<sup>4,5</sup>, Zsuzsa Jenei-Lanzl<sup>2,6</sup>, Stefan Dove<sup>1</sup> ‡, Rainer H. Straub<sup>2</sup> ‡, Oliver H. Krämer<sup>3</sup> ‡, Siavosh Mahboobi<sup>1</sup> ‡\**

<sup>1</sup>Institute of Pharmacy, Faculty of Chemistry and Pharmacy, University of Regensburg, 93040 Regensburg, Germany

<sup>2</sup>Laboratory of Experimental Rheumatology and Neuroendocrine Immunology, Department of Internal Medicine, University Hospital 93042 Regensburg, Germany

<sup>3</sup>Institute of Toxicology, Johannes Gutenberg University Mainz, Universitätsmedizin 55131 Mainz, Germany

<sup>4</sup>Technical University of Applied Sciences (OTH) Regensburg, 93053, Regensburg, Germany

<sup>5</sup>Regensburg Center of Biomedical Engineering (RCBE), OTH and University Regensburg, 93053 Regensburg, Germany

<sup>6</sup>Dr. Rolf M. Schwiete Research Unit for Osteoarthritis, Orthopedic University Hospital, Friedrichsheim GmbH, 60528 Frankfurt/Main, Germany

‡Senior authors who contributed equally

\*Corresponding author, E-mail: [Siavosh.mahboobi@chemie.uni-regensburg.de](mailto:Siavosh.mahboobi@chemie.uni-regensburg.de)

1  
2  
3 KEYWORDS. Acetylated tubulin, HDAC6 inhibitor, Hydroxamic acid, Rheumatoid  
4  
5 arthritis, Tetrahydro- $\beta$ -carboline.  
6  
7  
8  
9  
10

## 11 **Abstract**

12  
13  
14  
15 Epigenetic modifiers of the histone deacetylase (HDAC) family contribute to autoimmunity,  
16  
17 cancer, HIV infection, inflammatory, and neurodegeneration. Hence, histone deacetylase  
18  
19 inhibitors (HDACi), which alter protein acetylation, gene expression patterns, and cell fate  
20  
21 decisions, represent promising new drugs for the therapy of these diseases. Whereas pan-  
22  
23 HDACi inhibit all 11  $Zn^{2+}$ -dependent histone deacetylases (HDACs) and cause a broad  
24  
25 spectrum of side effects, specific inhibitors of histone deacetylase 6 (HDAC6i) are  
26  
27 supposed to have less side effects. We present the synthesis and biological evaluation of  
28  
29 Marbostats, novel HDAC6i, that contain the hydroxamic acid-moiety linked to tetrahydro-  
30  
31  $\beta$ -carboline-derivatives. Our lead compound Marbostat-100 is a more potent and more  
32  
33 selective HDAC6i than previously established, well-characterized compounds *in vitro* as  
34  
35 well as in cells. Moreover, Marbostat-100 is well tolerated by mice and effective against  
36  
37 collagen type II-induced arthritis. Thus, Marbostat-100 represents the most selective known  
38  
39 HDAC6i and the possibility for clinical evaluation of a HDAC isoform-specific drugs.  
40  
41  
42  
43  
44  
45

## 46 **Introduction**

47  
48  
49  
50 Acetylation and deacetylation of histones significantly contribute to the packing of  
51  
52 chromatin and thereby to the control of gene expression. Acetylation/deacetylation cycles  
53  
54 additionally regulate physiologically important functions of non-histone proteins.<sup>1-3</sup>  
55  
56  
57  
58  
59  
60

1  
2  
3 Acetylation of proteins is controlled by two types of enzymes: Histone acetyltransferases  
4 (HAT) attach acetyl groups to lysine residues of histone and non-histone proteins, and  
5 histone deacetylases (HDACs) catalyze the removal of those acetyl groups.<sup>1, 2, 4</sup>  
6  
7

8  
9  
10 HDACs can be divided into four classes (I-IV): While class I, II, and IV are zinc  
11 dependent, class III deacetylases need  $\text{NAD}^+$  as a cofactor. Class II is further subdivided  
12 into two subgroups, IIa (HDAC4, 5, 7, 9) and IIb (HDAC6 and 10).<sup>1, 2, 4, 5</sup> HDAC6 belongs  
13 to class IIb and is mainly distributed in the cytoplasm due to its nuclear export signal.<sup>5</sup>  
14 HDAC6 is the only enzyme of the HDAC family which has two catalytically active  
15 domains. It further became clear that HDAC6 has no *in vivo* activity against histones.<sup>4, 6</sup>  
16 Targets of HDAC6 are HSP90, tubulin, and other proteins that contribute to cancer  
17 development and progression.<sup>4, 6</sup> Hence, agents that selectively target HDAC6 could be  
18 valuable anti-cancer drugs.<sup>4</sup> Moreover, HDAC6 inhibitors are assumed as a promising  
19 therapeutic strategy in the treatment of neurodegenerative diseases.<sup>7, 8</sup>  
20  
21  
22  
23  
24  
25  
26  
27  
28  
29  
30  
31  
32

33 Histone deacetylase inhibitors (HDACi) modulate protein acetylation and thereby gene  
34 expression patterns, protein stability, intracellular targeting of proteins, and other protein  
35 functions.  
36  
37  
38  
39

40 Due to the target structure, the classical pharmacophore model for HDACi, exemplified  
41 by SAHA (**1**) (Figure 1) consists of (i) a zinc-binding group (ZBG) which chelates the  
42 central zinc-ion and thus inhibits the enzymatic activity of HDACs, (ii) a linker passing  
43 through the hydrophobic ion channel and (iii) a surface recognition region (head group)  
44 interacting with amino acid residues at the substrate binding site.<sup>4, 9, 10</sup> Clinical problems  
45 that arose with pan-HDACi, which inhibit all  $\text{Zn}^{2+}$ -dependent HDACs, were due to an  
46 associated broad spectrum of side effects.<sup>11</sup> In contrast, HDAC6-specific inhibitors  
47  
48  
49  
50  
51  
52  
53  
54  
55  
56  
57  
58  
59  
60

(HDAC6i) are supposed to have less side effects,<sup>6</sup> because HDAC6 knock-out mice are fully viable and healthy throughout their lives.<sup>12</sup> The first selective HDAC6i reported was tubacin **2**,<sup>13</sup> but it has a non-drug like structure with a high lipophilicity (CLOGP = 6.36<sup>14</sup>) and a high molecular mass. However, as a research tool it contributed to information about structure-activity-relationships (SAR) for the generation of better HDAC6-selective compounds.<sup>15, 16</sup> Due to the fact that HDAC6 has the largest active binding site within the HDAC family, selectivity for HDAC6 can arise from interactions between a bulky head group and specific amino acid residues within the substrate binding site.<sup>10, 14</sup> Butler, Kalin *et al.*<sup>14</sup> first synthesized tubastatin A (**3**), and they characterized further HDAC6-selective compounds with a tetrahydro- $\gamma$ - or tetrahydro- $\beta$ -carboline structure, showing a very good activity and a high selectivity for HDAC6 (over 1000-fold *versus* HDAC1).<sup>14, 17</sup> Most of the currently available HDAC6i co-inhibit other HDACs and cause lethal effects instead of a genuine inhibition of HDAC6. The co-inhibition of other HDAC-family members has led to misinterpretations regarding the biological roles of HDAC6 (see e.g., ref.<sup>18</sup>) and cytotoxic events prevent the interpretation of HDAC6 functions in vital cells. While several agents target HDAC6 in the nanomolar range *in vitro*, biological effects are often only described for micromolar and even higher doses, which may additionally block other HDACs (e.g.,<sup>19-22</sup>). A promising exception are effects against pancreatic cancer cells. These have been achieved with drugs targeting HDAC6 and HDAC3 in the nanomolar range.<sup>23</sup> One also has to consider the caveat that recently developed drugs that may specifically impair HDAC6 have often not been tested against all other Zn<sup>2+</sup>-dependent HDACs.

1  
2  
3 Here we present novel, highly selective and very active inhibitors of HDAC6. These are  
4 based on a modified tetrahydro- $\beta$ -carboline function, incorporating a hydantoin increment  
5 as the elementary part of the head group. We attached this group to a hydroxamic acid by  
6 different benzyl linkers. Our new inhibitors are genuine HDAC6i that reflect the benign  
7 phenotype of HDAC6 knock-out mice. Furthermore, they act very fast, in the nM-range,  
8 and more potently and, to the best of our knowledge, more selective than most previously  
9 established agents targeting HDAC6.<sup>1,2,4</sup>

19 HDACi are also able to ameliorate inflammatory processes and conditions *in vitro* and *in*  
20 *vivo*. Various studies show the possibility to treat inflammatory conditions, like arthritis,  
21 with HDACi. Often, beneficial effects are based on reduced cytokine responses that derive  
22 from human peripheral blood mononuclear cells under inhibition of multiple HDACs,<sup>24</sup>  
23 class I HDACs,<sup>25</sup> HDAC3,<sup>26</sup> and HDAC8.<sup>27</sup> Other cell types that are relevant for the  
24 pathogenesis of RA, like fibroblast-like synoviocytes (FLS)<sup>28</sup> and chondrocytes,<sup>29</sup> display  
25 decreased inflammatory responses under unspecific HDAC inhibition by trichostatin A or  
26 givinostat as well. However, pan-HDACi may also cause undesired effects due to a  
27 feedback loop, in which the pro-inflammatory cytokines TNF and IL-1 $\beta$  downregulate  
28 HDAC5 expression in RA-FLS.<sup>30</sup>

42 Of note, emerging evidence suggests beneficial effects of HDAC6i for the treatment of  
43 chronic immune and inflammatory disorders. As demonstrated with the selective HDAC6  
44 inhibitor tubastatin A (**3**) in a mouse-model, anti-inflammatory and antirheumatic effects  
45 can be obtained by modulation of HDAC6 activity, at least in part, by modulating IL-6  
46 expression.<sup>21</sup> However, tubastatin A (**3**) was recently described to inhibit HDAC10,<sup>18</sup>  
47 making an interpretation of HDAC6 as a drug target in arthritis animal models difficult. A  
48  
49  
50  
51  
52  
53  
54  
55  
56  
57  
58  
59  
60

1  
2  
3 caveat of this study<sup>21</sup> is that tubastatin A (**3**) also inactivates other HDACs at the high doses  
4  
5 that were used to collect the data.  
6  
7

8 Here we present novel HDAC6i with superior pharmacological and toxicological properties  
9  
10 in vitro, in cells, and in an animal model of rheumatoid arthritis.  
11  
12  
13  
14  
15  
16  
17  
18  
19  
20  
21  
22  
23  
24  
25  
26  
27  
28  
29  
30  
31  
32  
33  
34  
35  
36  
37  
38  
39  
40  
41  
42  
43  
44  
45  
46  
47  
48  
49  
50  
51  
52  
53  
54  
55  
56  
57  
58  
59  
60

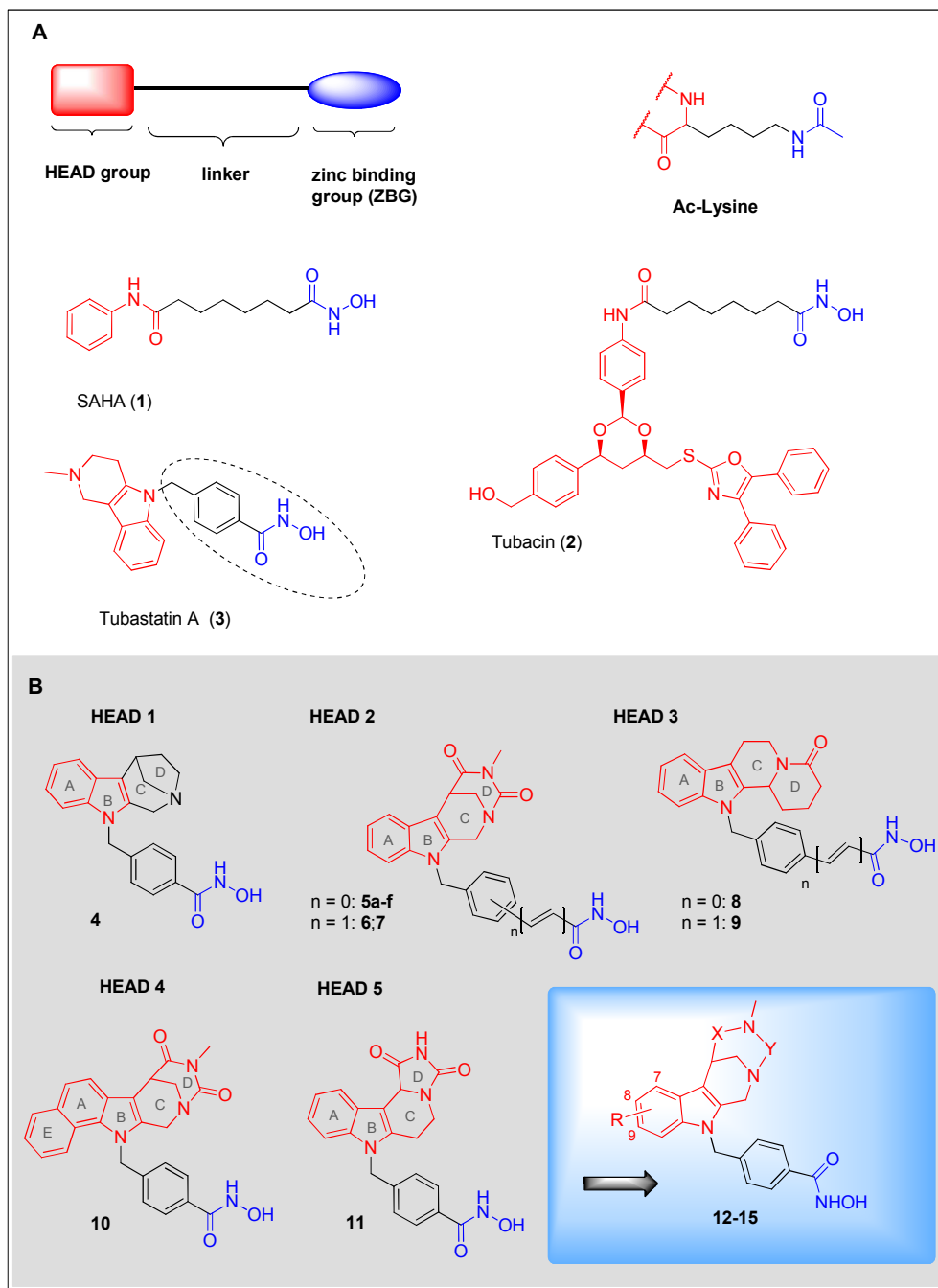


**Figure 1. Schematic segmentation of the common pharmacophore of HDACi.** A) Typical pharmacophore of HDACi (left) which is designed according to acetylated lysine, i.e. the biological substrate. The cap group (red) binds at the entrance of the HDAC catalytic cleft, a linker interacts with the cleft, and the polar ZBG group (blue) chelates the catalytically active zinc ion in the HDAC pocket.<sup>4</sup> These structures are exemplified by the FDA approved HDACi SAHA (1), tubacin(2), or tubastatin (3). B) Structures and general structures of compounds investigated (4-15). To obtain isoenzyme-selectivity, different tetracyclic bulky head groups were investigated. Modifications of head 2 were performed in the following.

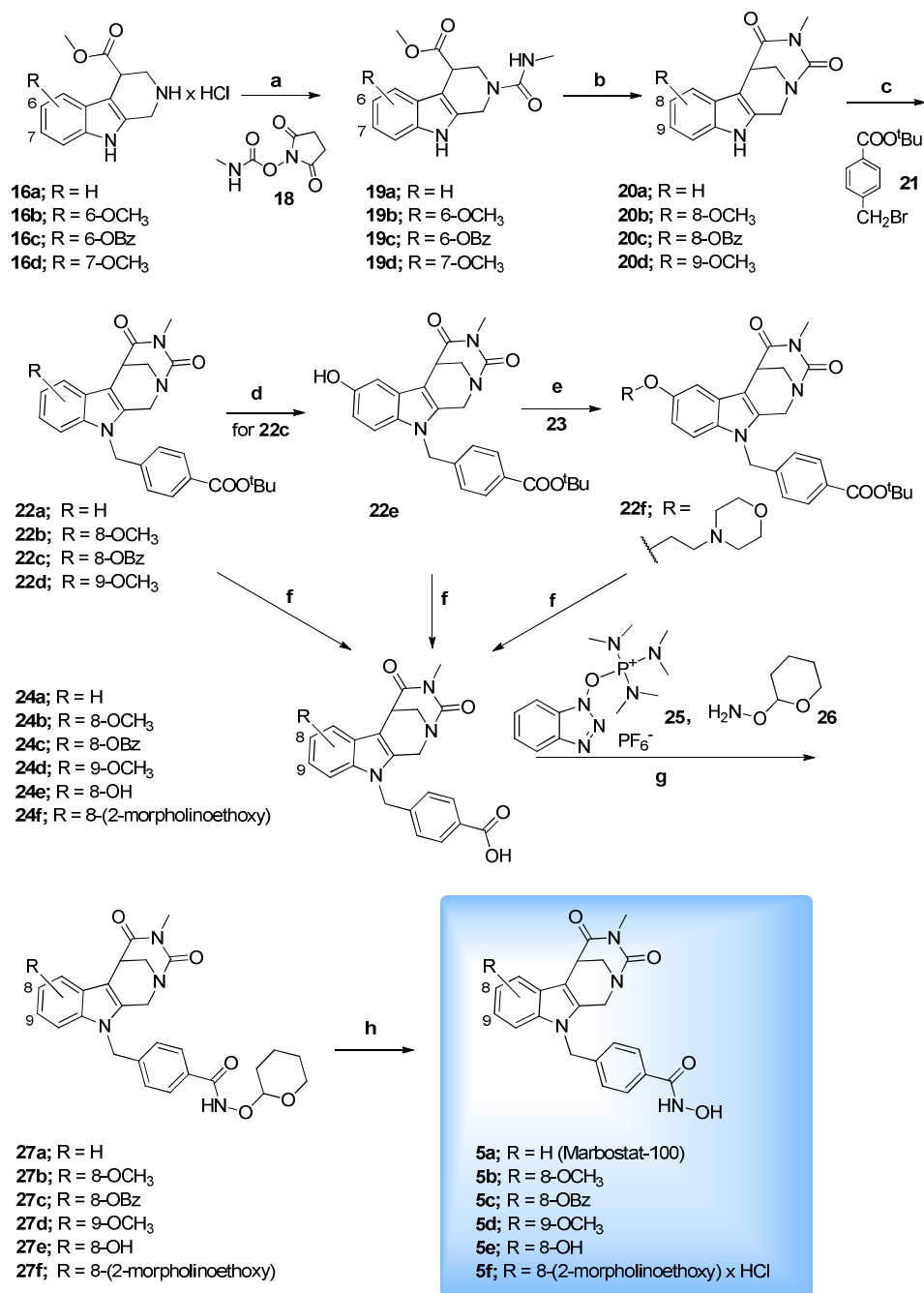
## Results

### Chemistry

The general synthetic strategy to obtain derivatives bearing head group 2 and derivatives thereof, and head group 4, which contains an additional benzene ring, respectively, is shown in scheme 1. The methyl-2,3,4,9-tetrahydro-1*H*-pyrido[3,4-*b*]indole-4-carboxylate hydrochlorides **16a-d**<sup>31</sup>, respectively **17**, were accessible according to literature procedures (see also supporting information schemes S4 and S7).<sup>31-35</sup>

The six-membered D-ring can be obtained by reaction of **16a-d** with 2,5-dioxopyrrolidin-1-yl methylcarbamate (**18**) and subsequent cyclization of the methyl-2-(methylcarbamoyl)-2,3,4,9-tetrahydro-1*H*-pyrido[3,4-*b*]indole-4-carboxylates **19a-d** to yield **20a-d**.

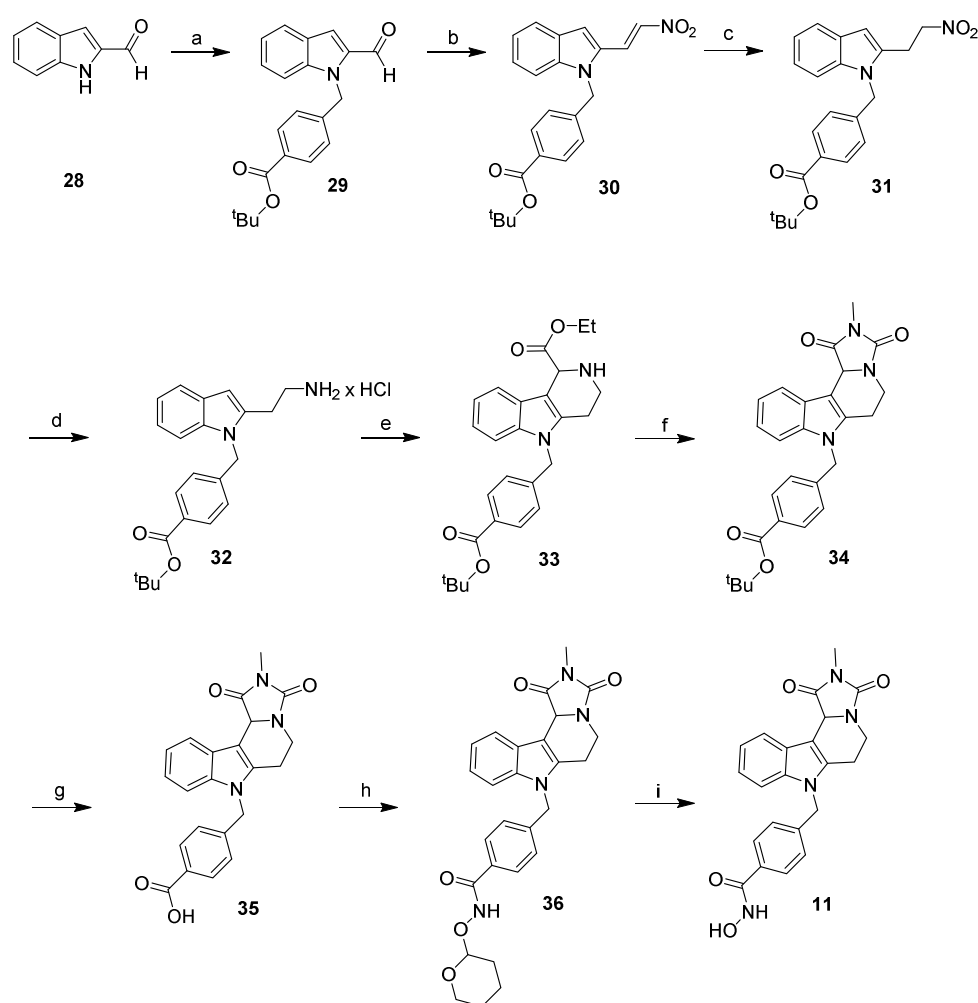
As shown in scheme 1, introduction of the benzyl spacer bearing a hydroxamic acid as a Zn<sup>2+</sup>-chelating function was performed in 4 steps: Alkylation of the indole nitrogen using *tert*-butyl 4-(bromomethyl)benzoate (**21**)<sup>36</sup> led to **22a-d**. The benzyloxy-derivative **22c** was further modified to give **22e** and **22f**. Acidic removal of the *t*-butyl protecting group to form **24a-f**, BOP **25** catalyzed amidation with NH<sub>2</sub>OTHP **26** and acidic cleavage of the resulting acetals **27a-f** finally led to the target compounds **5a-f**.



**Scheme 1:** Synthesis of **5a-f**, by modification of head group 2. Reagents and conditions: (a) MeCN, EtN(isopropyl)<sub>2</sub>, 2,5-Dioxopyrrolidin-1-yl methylcarbamate (18), rt, 16 h. (b) Dioxane, Cs<sub>2</sub>CO<sub>3</sub>, 110 °C, 2 h. (c) i; DMF, NaH, 0 °C, 15 min. ii; rt, 1 h. (d) Pd/C, H<sub>2</sub>. (e) 2-Butanone, 4-(2-Chloroethyl)morpholine hydrochloride (23), Δ, 4 d. (f) TFA, rt, 30 min. (g) DMF, rt, 2-3 h. (h) MeOH, HCl<sub>aq</sub>, rt. Following in principle the same synthetic pathway, compound 10, bearing head group 4, was prepared.

The structure of **5a**, hereafter named Marbostat-100, was confirmed by x-ray structure analysis, in addition to characterization by <sup>1</sup>H- and <sup>13</sup>C-NMR spectroscopic data.

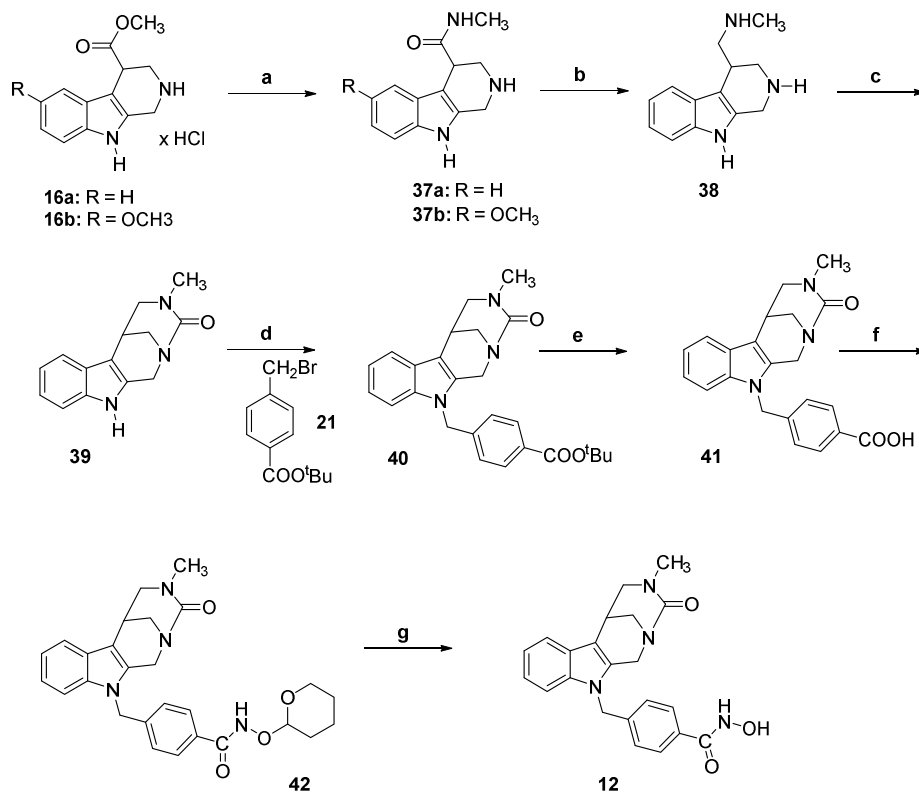
In principle by the same way the fusion of the 4-methylen-*N*-hydroxybenzamide element taken from tubastatin A (**3**) and head groups 1-4 was performed (Figure 1,  $n = 0$ ). For head groups 2 and 3 an elongation of the spacer was investigated in addition ( $n = 1$ ). Moreover, we introduced the hydantoin increment at the tetrahydro- $\gamma$ -carboline structure (head 5,  $\gamma$ -Marbostat, **11**) to compare this system with tubastatin A (**3**) and Marbostat-100 (**5a**). Because of tautomerism of the hydantoin ring system followed by alkylation of the oxygen of the amide group, we modified the synthetic route as shown in scheme 2.



**Scheme 2:** Synthesis of  $\gamma$ -Marbostat-100 **11** bearing an angular fused hydantoin increment Reagents and conditions: (a) DMF, NaH, *tert*-butyl 4-(bromomethyl)benzoate (**21**). (b)  $\text{NH}_4\text{OAc}$ ,  $\text{CH}_3\text{NO}_2$  (c)  $\text{CHCl}_3$ , *i*Prop,  $\text{NaBH}_4$ ,  $\text{SiO}_2$ . (d) i)  $\text{HOAc}$ , Zn, ii)  $\text{NH}_4\text{OH}$ , iii) THF, HCl. (e) MeOH,  $\text{SiO}_2$ , ethyl glyoxalate. (f) i) MeCN,  $\text{EtN}(\text{t}^{\text{Prop}})_2$ , 2,5-dioxopyrrolidin-1-yl methylcarbamate (**18**), rt, 16 h. ii)  $\text{Cs}_2\text{CO}_3$ , dioxane,  $\Delta$ , (g)  $\text{CF}_3\text{COOH}$ . (h) DMF, BOP (**25**),  $\text{NH}_2\text{OTHP}$  (**26**), rt, 2 - 3 h. (i) MeOH,  $\text{HCl}_{\text{aq}}$ , rt.

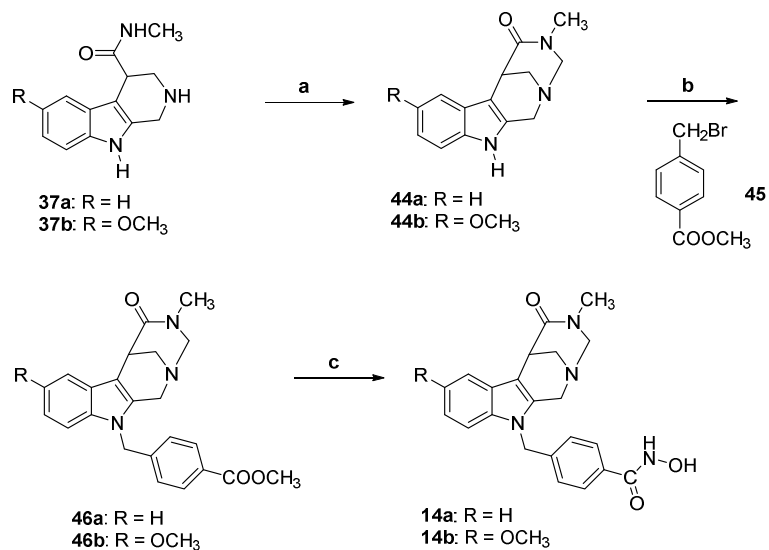
1  
2  
3  
4  
5  
6 In the enzymatic as well as in the cellular assays Marbostat-100 (**5a**) exhibited the most  
7 potent and selective HDAC6 inhibitory activity. Therefore, to investigate the  
8 pharmacophore requirements for compounds based on this lead structure in more detail,  
9 derivatives by modification of the D-ring system were prepared. Hereby we focused on the  
10 influence of the carbonyl functions, structural elements that lack in the original parental  
11 structure of tubastatin A (**3**). To obtain derivative **12**, lacking the amide carbonyl group as  
12 well as derivatives **14a** and **14b** without the urea carbonyl-group (Figure 3) the synthetic  
13 routes were slightly modified as shown in schemes 3 and 4.  
14  
15  
16  
17  
18  
19

20 To obtain **12**, in the first step methyl 2,3,4,9-tetrahydro-1*H*-pyrido[3,4-*b*]indole-4-  
21 carboxylate (**16a**) was transformed to the amide **37a** by treatment with methylamine in  
22 methanolic solution (Scheme 3). In the same way **37b** as an intermediate was obtained. **37a**  
23 was reduced using LiAlH<sub>4</sub> and the urea structure in **39** was formed by CDI. The benzylic  
24 linking element was introduced by alkylation with *tert*-butyl 4-(bromomethyl)benzoate  
25 (**21**)<sup>36</sup>. After acidic cleavage of the *t*butylbenzoate **40** the hydroxamic acid was introduced in  
26 2 steps as shown.  
27  
28  
29  
30  
31  
32  
33  
34  
35  
36  
37  
38  
39  
40  
41  
42  
43  
44  
45  
46  
47  
48  
49  
50  
51  
52  
53  
54  
55  
56  
57  
58  
59  
60



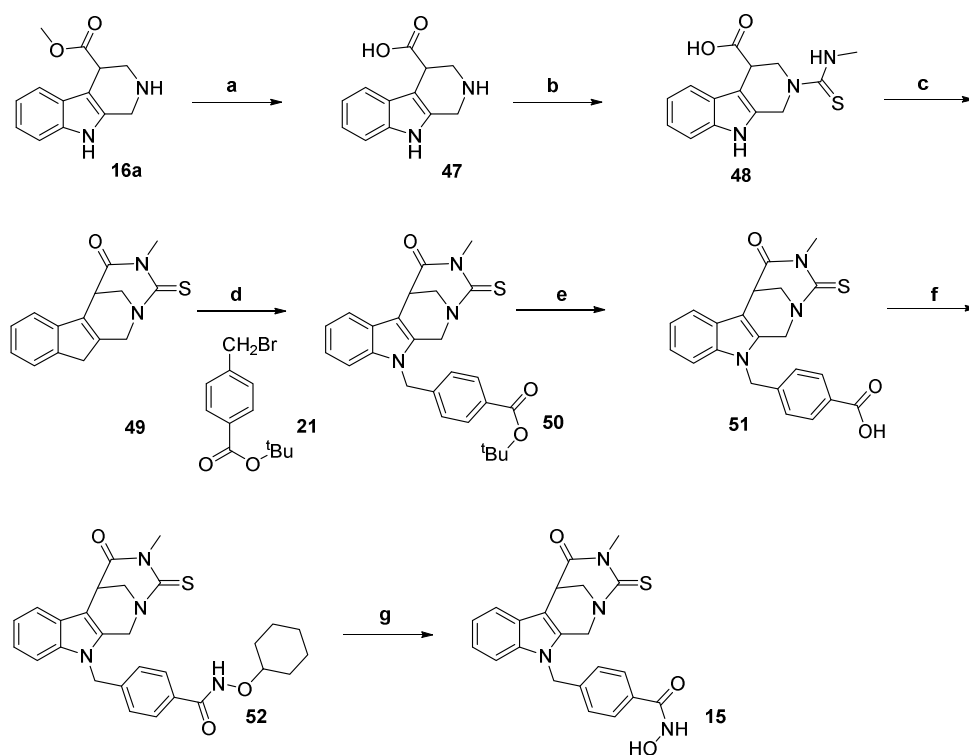
**Scheme 3:** Synthesis of **12**, an inhibitor based on the basic structure the 4-methyl-4,5,6,11-tetrahydro-2,6-methano[1,3]diazocino[5,6-*b*]indole-3(*1H*)-on. Reagents and conditions: (a) CH<sub>3</sub>NH<sub>2</sub> (40 % in MeOH), rt, 3 d. (b) LiAlH<sub>4</sub>, THF, 16 h, Δ. (c) CDI, THF, 16 h, Δ. (d) NaH, THF, rt. (e) CF<sub>3</sub>COOH, CH<sub>2</sub>Cl<sub>2</sub>, 3.5 h, rt. (f) THF, BOP, NH<sub>2</sub>OThp, rt, 2 - 3 h. (g) MeOH, HCl<sub>i</sub>Prop, rt.

To obtain derivatives without the urea carbonyl-group (Scheme 4) the amides **37a** and **37b** were treated with formaldehyde **43** to form the methylene bridged D-ring system (**44a**, **44b**). After alkylation with methyl 4-(bromomethyl)benzoate **45** the hydroxamic acids (**14a**, **14b**) were formed from the methylesters **46a** and **46b** using hydroxylamine in alkaline solution.



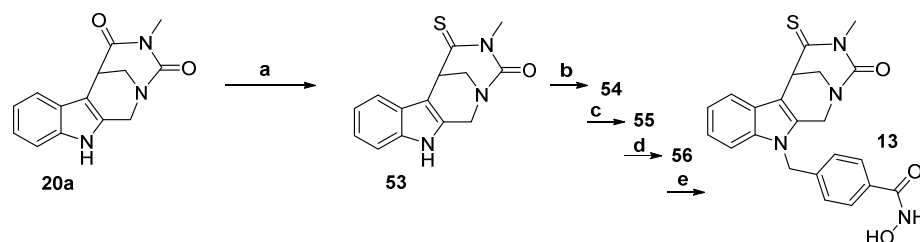
**Scheme 4:** Synthesis of inhibitors based on the 4-methyl-3,4,6,11-tetrahydro-2,6-methano[1,3]diazocino[5,6-*b*]indole-5(1*H*)-on – basic structure exemplified by compounds **14a** and **14b**. Reagents and conditions: (a) (CH<sub>2</sub>O), CH<sub>3</sub>OH, 70 °C, 2 h. (b) NaH, THF, rt, 30 min. (c) NH<sub>2</sub>OH, CH<sub>3</sub>OH, KOH, 0 °C.

The thiourea analogs of Marbostat-100 (**5a**), compound **15** (Figure 3), can be obtained by alkaline cleavage of the ester **16a**, reaction of the resulting 2,3,4,9-tetrahydro-1*H*-pyrido[3,4-*b*]indole-4-carboxylic acid (**47**) with methyl isothiocyanate<sup>37</sup> and ring closure by use of CDI<sup>38</sup>, followed by the steps used for the synthesis of Marbostat-100 (**5a**) (scheme 5).



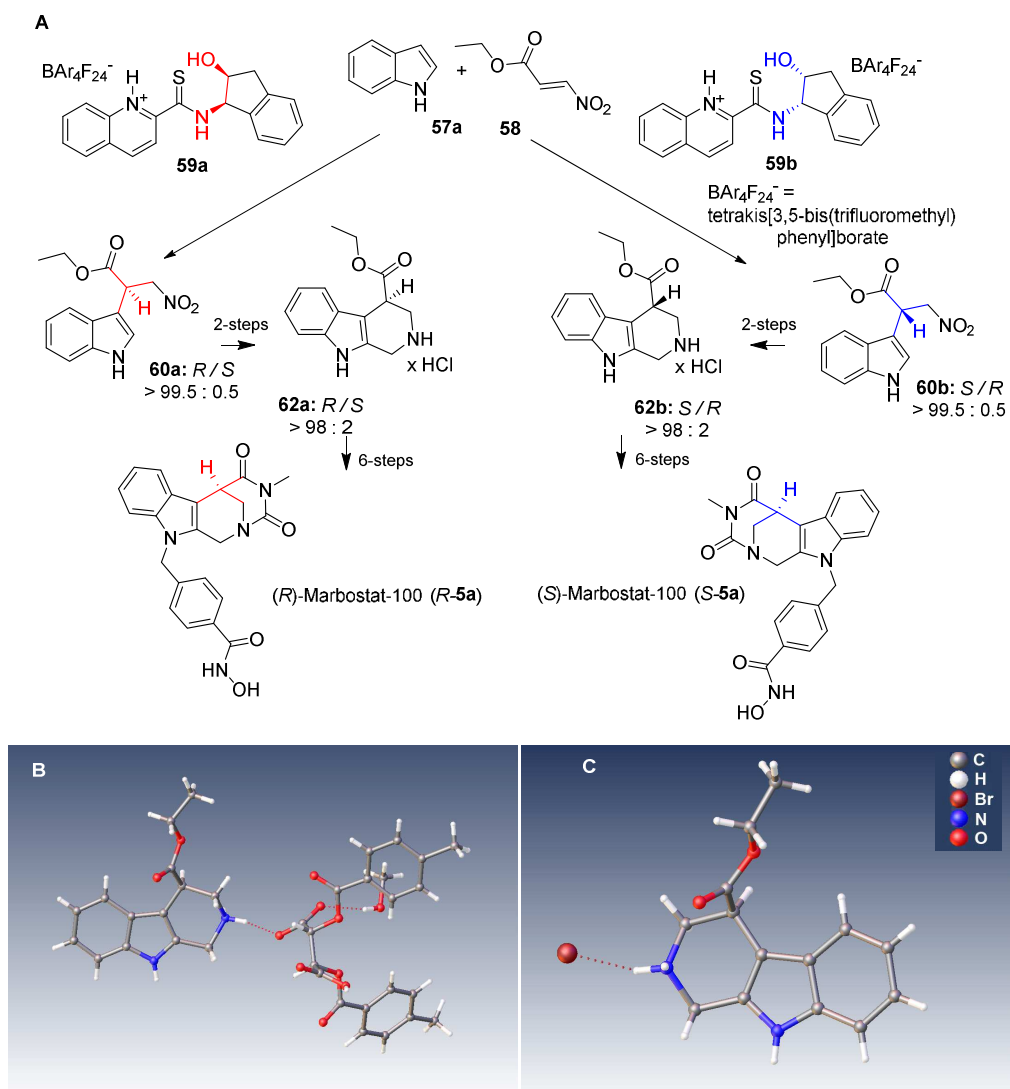
**Scheme 5:** Synthesis of **16**, the thiourea derivative of Marbostat-100 (**5a**) Reagents and conditions: (a) LiOH, H<sub>2</sub>O, MeOH, THF, rt, 16h, Δ, 2h, HOAc. (b) methylisothiocyanate, acetone, DMSO, Δ, 2 h. (c) CDI, CH<sub>3</sub>CN, rt, 30 min. (d) NaH, DMF, rt. (e) CF<sub>3</sub>COOH, rt, 30 min. (f) NH<sub>2</sub>OTHP, BOP, DMF, NEt<sub>3</sub>, (g) HCl<sub>aqu.</sub>, MeOH, H<sub>2</sub>O.

Moreover, thioamide derivative **13** (scheme 6) was prepared by reaction of **20a** with Lawesson's reagent and the resulting 4-methyl-3-thioxo-3,4,6,11-tetrahydro-2,6-methanoindeno[2,1-*e*][1,3]diazocin-5(1*H*)-one (**53**) was transformed to the final test compound **13** in four steps.



**Scheme 6:** Synthesis of **13**, a thioamide derivative of Marbostat-100 (**5a**) Reagents and conditions: (a) Lawesson's reagent, THF, Δ, 48 h. (b) **21**, NaH, DMF, rt. (c) CF<sub>3</sub>COOH, rt, 30 min. (d) NH<sub>2</sub>OTHP, BOP, DMF, NEt<sub>3</sub>, (e) HCl<sub>aqu.</sub>, MeOH, H<sub>2</sub>O.

1  
2  
3  
4  
5 To investigate the influence of the stereochemistry of head group 2 on the biological  
6 activity, a stereoselective synthesis of Marbostat-100 (**5a**) by chiral catalysis<sup>39</sup> was  
7 developed. Using 1.5 equiv. of indole (**57a**) and an enhanced catalyst loading of 25 mol%  
8 of the respective catalyst **59b** prepared *in situ*, the reported enantiomeric excess of 95 % for  
9 the formation of (*S*)-ethyl-2-(1*H*-indol-3-yl)-3-nitropropanoate (**60b**)<sup>39</sup> by coupling of **57a**  
10 with **58** was optimized to an enantioselectivity  $\geq 99$  %. Following the same protocol, also  
11 the enantiomeric *R*-derivative **60a** was obtained in a yield of 50 % and an ee of  $\geq 99$  %.  
12  
13 Based on the synthetic route shown in Scheme 1, the synthesis of (*R*)- and (*S*)-  
14 Marbostat-100 (**R-5a** and **S-5a**) was performed from **60a** and **60b** in the following as shown  
15 in the supporting information scheme 8. To avoid racemization at least in part at the CH  
16 acidic stereocenter, the reaction conditions were modified.  
17  
18  
19  
20  
21  
22  
23  
24  
25  
26  
27  
28  
29  
30  
31  
32  
33  
34  
35  
36  
37  
38  
39  
40  
41  
42  
43  
44  
45  
46  
47  
48  
49  
50  
51  
52  
53  
54  
55  
56  
57  
58  
59  
60



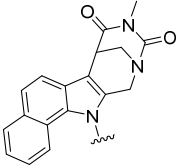
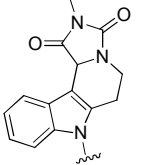
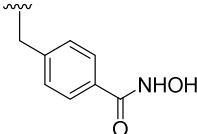
**Scheme 7:** **A:** Enantioselective synthesis of (*R*)- and (*S*)-Marbostat-100. The enantiomeric excess was determined by HPLC analysis. To confirm the stereochemistry, structures of (*R*)-ethyl 2,3,4,9-tetrahydro-1*H*-pyrido[3,4-*b*]indole-4-carboxylate (**62a**) crystallized with (-)-di-*p*-toluoyl-*L*-tartaric acid from MeOH (**B**), and of (*S*)-ethyl 2,3,4,9-tetrahydro-1*H*-pyrido[3,4-*b*]indole-4-carboxylate (**62b**) as a hydrobromide (**C**), respectively were determined by x-ray diffraction analysis.

### HDAC6 inhibition and selectivity of Marbostat-100 and derivatives

We synthesized a series of hydroxamic acids bearing tetrahydrocarbolines as parts of different tetracyclic head groups and investigated whether different linker groups enhance HDAC6 selectivity which was derived from  $K_i$  values of HDAC6, HDAC2 and HDAC8 inhibition measured in assays using recombinant purified human HDAC proteins

**Table 1.**  $K_i$ -values [nM] for HDAC-subtypes HDAC2, HDAC6 and HDAC8 compared to the pan-HDACi Trichostatin A (TSA) (Enzymatic Inhibitory Activities)<sup>a</sup>

Head group 1	Spacer	Cpd. No.	HDAC2	HDAC6	HDAC8
		<b>4</b>	6 097	6.51	1 540
<b>Head group 2</b>					
		<b>Marbostat-100 (5a)</b>	774	0.70	173
		<b>R-5a</b>	3 195	2.01	294
		<b>S-5a</b>	5 205	0.70	999
		<b>6</b>	66.51	4.15	205
		<b>7</b>	768	72.24	13.09
		<b>24a</b>	>10 000	>20 000	>40 000
<b>Head group 3</b>					
		<b>8</b>	7 244	30.20	1678
		<b>9</b>	234	14.13	720
<b>Head group 4</b>					

		<b>10</b>	ND	1.78	ND
<b>Head group 5</b>					
		<b>11</b>	995	1.86	761
<b>TSA</b>			3.55	0.58	145
<b>Tubastatin A</b>			> 1 130	7.56	1 697

<sup>a</sup>Compounds were tested in a 10-dose IC<sub>50</sub> mode with 3-fold serial dilution starting from 100 μM solutions for HDAC2 and HDAC8, respectively, starting from 1 μM solutions for HDAC6. IC<sub>50</sub> values were extracted by curve-fitting of the dose/response slopes and K<sub>i</sub> values were calculated from the respective IC<sub>50</sub> values, determined in duplicate, according to the *Cheng-Prusoff* equation<sup>40</sup> as given in the SI. TSA was used as an internal standard. ND: Not Determined. Assays were performed by Reaction Biology Corporation, USA.

All compounds inhibit HDAC6 preferentially (Table 1). Compound **4** (Figure 1), featuring a methylene-bridged tetrahydro-β-carboline in conjunction with a benzyl linker, has an HDAC6 K<sub>i</sub> value of 6.51 nM with approximately 940-fold selectivity for HDAC6 over HDAC2. Modification of the D-ring system and introduction of a hydantoin increment (Figure 3), combined with the addition of a benzyl linker led to Marbostat-100 (**5a**) with an K<sub>i</sub> of 0.7 nM for HDAC6 and conserved selectivity for HDAC6 (Table 1). **S-5a** represents the eutomer (K<sub>i</sub>, 0.7 nM), but the eudismic ratio amounts to only 0.35 (K<sub>i</sub> of **R-5a**, 2.01 nM) (Table 1).

**Table 2:** Influence the stereochemistry and of modifications of head group 2 in the enzymatic fluorescence assay on inhibition of HDAC-subtypes HDAC2, HDAC6 and HDAC8 ( $K_i$ -values [nM])<sup>a</sup>

Modifications of head group 2			Cpd. No.	HDAC2	HDAC6	HDAC8
R	X	Y				
8-OCH <sub>3</sub>	C=O	C=O	<b>5b</b>	310	0.15	124
8-O-Bz	C=O	C=O	<b>5c</b>	ND	0.08	ND
8-OH	C=O	C=O	<b>5e</b>	ND	0.42	ND
8-(2-morpholinoethoxy) x HCl	C=O	C=O	<b>5f</b>	313	0.48	721
9-OCH <sub>3</sub>	C=O	C=O	<b>5d</b>	70.8	0.32	93.3
H	CH <sub>2</sub>	C=O	<b>12</b>	484	0.51	528
H	C=O	CH <sub>2</sub>	<b>14a</b>	1 356	0.23	427
8-OCH <sub>3</sub>	C=O	CH <sub>2</sub>	<b>14b</b>	370	0.16	299
H	C=S	C=O	<b>13</b>	943	0.88	701
H	C=O	C=S	<b>15</b>	469	0.45	40.4

<sup>a</sup>Compounds were tested in a 10-dose IC<sub>50</sub> mode with 3-fold serial dilution starting from 100 μM solutions for HDAC2 and HDAC8, respectively, starting from 1 μM solutions for HDAC6. IC<sub>50</sub> values were extracted by curve-fitting of the dose/response slopes and  $K_i$  values were calculated from the respective IC<sub>50</sub> values, determined in duplicate, according to the *Cheng-Prusoff* equation<sup>40</sup> as given in the SI. TSA was used as an internal standard. ND: Not Determined. Assays were performed by Reaction Biology Corporation, USA.

Connecting the tetracyclic head group 2 with a *para*- or *ortho*-substituted cinnamic acid-*N*-hydroxamide (compounds **6** and **7** Table 1) significantly reduces HDAC6 inhibition and

1  
2  
3 selectivity. The angular fused D-ring system in compounds **8** and **9** lowers activity  
4 compared to the bridged tetracylic system of Marbostat-100 (**5a**), probably because of steric  
5 hindrance. Reduced activity can also be observed for compound **10**, where an additionally  
6 fused E-ring might hinder penetration of the drug to the channel-rim. The *para*-substituted  
7 cinnamic acid-*N*-hydroxamide in case of **9** enhances activity at HDAC2, HDAC6 and  
8 HDAC8 compared to **8**, but there is still a preference for HDAC6. Elongation of the linker  
9 possibly compensates steric hindrance due to the head group and allows better penetration  
10 into the catalytic channel rim. As expected, the carboxylic acid **24a** (Scheme 1), the  
11 analogue of Marbostat-100 (**5a**) lacking the hydroxamic acid asZn<sup>2+</sup>-chelating group,  
12 showed no activity on HDAC2 and HDAC6 and a significantly reduced potency on  
13 HDAC8.  
14  
15  
16  
17  
18  
19  
20  
21  
22  
23  
24  
25  
26  
27  
28  
29

30 Marbostat-100 (**5a**), the most potent compound in this series, served as lead for further  
31 modifications of head group 2. The introduction of a methoxy group at C-8 enhances  
32 activity towards HDAC6 in the enzymatic assay (**5b**, **14b**) (Table 2). Substitution at C-8 by  
33 OH (**5e**) and by bulkier benzyloxy (**5c**) or 2-morpholinoethoxy (**5f**) groups is also tolerated  
34 as well as a methoxysubstituent at C-9 (**5d**). Replacing one of the carbonyl moieties by a  
35 sulfocarbonyl or a CH<sub>2</sub> group does not significantly affect HDAC6 inhibition (**13**, **14a**, **14b**,  
36 **15**).  
37  
38  
39  
40  
41  
42  
43  
44  
45  
46

47 To further validate the selectivity of this series of compounds, Marbostat-100 (**5a**) was  
48 profiled against a broader panel of isoenzymes. As shown by the data in Table3,  
49 Marbostat-100 (**5a**) exhibited significant selectivity for HDAC6 over all nine  
50 Zn<sup>2+</sup> dependent HDAC isoenzymes investigated, ranging from about 250-fold vs. HDAC8 to  
51  
52  
53  
54  
55  
56  
57  
58  
59  
60

2600-fold vs. HDAC4. The HDAC6 selectivity of tubastatin A (**3**), the most selective inhibitor to date, in contrast is about 150-fold (vs. HDAC8), with respect to the  $K_i$ -values determined in our test system.

**Table 3:** Enzyme inhibition data ( $K_i$ -values [nM]) for Marbostat-100 HDAC-subtypes HDAC1, HDAC2, HDAC3, HDAC4, HDAC5, HDAC6, HDAC7, HDAC8, HDAC10 and HDAC11 compared to the pan-HDACi TSA and the highly potent, selective and cell-permeable class IIa HDAC inhibitor **TMP 269**,<sup>41</sup> as reference compounds <sup>a</sup>.

Compound	HDAC Subtype									
	1	2	3	4	5	6	7	8	10	11
<b>Marbostat-100 (5a)</b>	358	774	306	1821	701	0.7	442	173	452	495
<b>TSA</b>	0.64	3.55	0.84	ND	ND	0.58	ND	145	4.76	401
<b>TMP 269</b>	ND	ND	ND	90.5	86.9	ND	46.3	2706	ND	ND

<sup>a</sup>Compounds were tested in a 10-dose  $IC_{50}$  mode with 3-fold serial dilution starting from 100  $\mu$ M solutions for all HDAC subtypes and starting from 1  $\mu$ M solutions for HDAC6, respectively.  $IC_{50}$  values were extracted by curve-fitting the dose/response slopes and  $K_i$  values were calculated from the respective  $IC_{50}$  values, determined in duplicate, according to the *Cheng-Prusoff* equation<sup>40</sup> as given in the SI. TSA and **TMP 269** were used as an internal standard. ND: Not Determined. Assays were performed by Reaction Biology Corporation USA.

### Binding Mode of Marbostat-100 (5a)

Recently, Christianson et al.<sup>42,43</sup> released 18 crystal structures of HDAC6 (one human catalytic domain (CD) II, one zebrafish CD I, 16 zebrafish CD II), mostly in complex with an inhibitor or a substrate analog, in the Brookhaven Protein Databank (PDB). The ultrahigh resolution structure of zebrafish HDAC6 CD II (PDB 5WGK) in complex with N-hydroxy-4-[[[2-hydroxyethyl)(phenylacetyl)amino]methyl]benzamide is most suited for docking approaches, since CD II is the major functional catalytic domain of HDAC6<sup>44</sup> and since the binding mode of the phenylhydroxamic acid moiety is provided.<sup>43</sup> Although the sequence identity of human and zebrafish HDAC6 amounts to only 40%, the latter species isoform may be used for docking of Marbostat-100 because of 100% identical binding sites

1  
2  
3 and a root mean square deviation of the backbone of 13 amino acids 3.5Å around  
4  
5 Marbostat-100 of only 0.27Å.  
6  
7

8  
9 Considering that the  $K_i$  values of (*R*)- and (*S*)-Marbostat-100 differ by a factor not greater  
10  
11 than 2.9 (Table 1), both enantiomers were manually docked in energy minimum  
12  
13 conformations close to the x-ray structure (supporting information) retaining the binding  
14  
15 mode of the phenylhydroxamic acid moiety present in the PDB structure 5WGK.<sup>43</sup> The  
16  
17 detailed binding modes are shown in Figure 2 (amino acid numbers correspond to human  
18  
19 HDAC6). Both isomers do not differ with respect to the docking mode of the hydroxamic  
20  
21 acid moiety and the benzyl linker. The former binds in a rather unusual monodentate  
22  
23 hydroxamate-Zn<sup>2+</sup> coordination mode<sup>36,43</sup>. The Zn<sup>2+</sup>-ion is coordinated with D649, H651  
24  
25 and D742 (Zn<sup>2+</sup>-O/N distances ca. 2.0 Å), with a catalytic water molecule and with the  
26  
27 hydroxylamine oxygen of Marbostat-100 (**5a**) (distance 2.0 Å). The hydroxylamine oxygen  
28  
29 forms a hydrogen bond with the hydroxy group of Y782. Furthermore, the catalytic water  
30  
31 molecule links H610, H611 and the amide oxygen of the hydroxamate group via hydrogen  
32  
33 bonds. The benzyl linker penetrates a partially hydrophobic channel (Figure 2) and contacts  
34  
35 the side chains of F620, F680 and Y782 as well as G619.  
36  
37  
38  
39  
40

41  
42 The “surface recognizing cap group” of both isomers, represented by the 4-methyl-6,11-  
43  
44 dihydro-2,6-methano[1,3]diazocino[5,6-*b*]indole-3,5(1*H*,4*H*)-dione moiety, is optimally  
45  
46 fitted onto the entrance of the binding pocket. Figure 2C shows an extended hydrophobic  
47  
48 surface region, mainly formed by P501 and L749, and a small hydrophobic cavity with  
49  
50 F679 at the bottom. In case of the (*R*)-isomer, the 4-methyl group fits between P501 and  
51  
52 L749, and the diazocino moiety contacts P501 and F620. The phenyl plane covers the  
53  
54 cavity forming van der Waals contacts with H651 and F680. The (*S*)-isomer binds in a  
55  
56  
57  
58  
59  
60

1  
2  
3 laterally reversed position. The phenyl plane faces P501, L749 and F620. The edge of the  
4  
5 diazocino moiety contacts the phenyl planes of F679 and F680, and the 4-methyl group fits  
6  
7 between the side chains of F679 and L749. Both carbonyl groups may be involved in water-  
8  
9 mediated hydrogen bonds with the imidazolyl NH of H651 and the backbone O of L749 on  
10  
11 one hand and with the backbone O of P748 on the other hand. Possibly, these additional  
12  
13 interactions account for the slightly higher affinity of the (*S*)-isomer (eutomer). Both  
14  
15 binding modes correspond to the structure-activity relationships of Marbostat-100  
16  
17 derivatives substituted at the phenyl moiety (Table 1), since the substituents may project  
18  
19 into the solvent, leading to only small variations of the affinity. Moreover, at least one  
20  
21 diazocino carbonyl group may be exchanged by a thiocarbonyl moiety or by CH<sub>2</sub> without  
22  
23 significant effects on interactions.  
24  
25  
26  
27  
28  
29  
30  
31  
32

### 33 **Characterization of the Novel HDACi in Cellular Systems**

34  
35  
36  
37 Having assessed the activities of Marbostat-100 (**5a**) and further derivatives *in vitro* (Tables  
38  
39 1-2), we tested these compounds for biological activities. HDAC6 has a number of different  
40  
41 cytosolic substrates, such as  $\alpha$ -tubulin, HSP90,<sup>45</sup> beta-catenin<sup>46</sup> and Akt..<sup>47</sup> A reliable  
42  
43 marker for the inhibition of HDAC6 is hyperacetylation of tubulin, as tubulin is a *bona fide*  
44  
45 target of the cytoplasmic HDAC6 in cells.<sup>4</sup> We assessed this parameter by Western blot.  
46  
47 Due to the high relevance of HDAC6 in hematopoietic cells,<sup>4</sup> we used such cells for our  
48  
49 assays.  
50  
51  
52  
53  
54  
55  
56  
57  
58  
59  
60

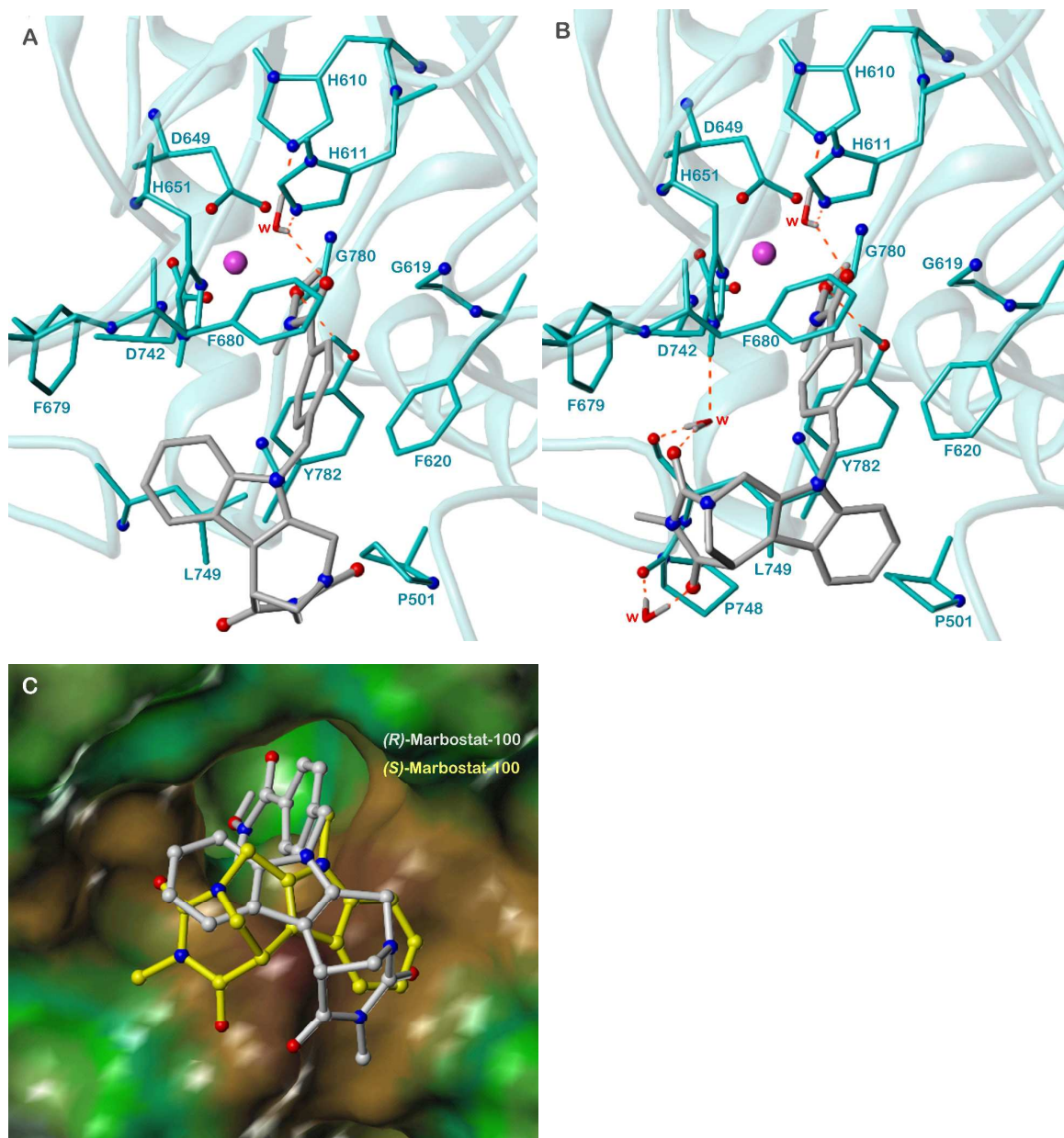
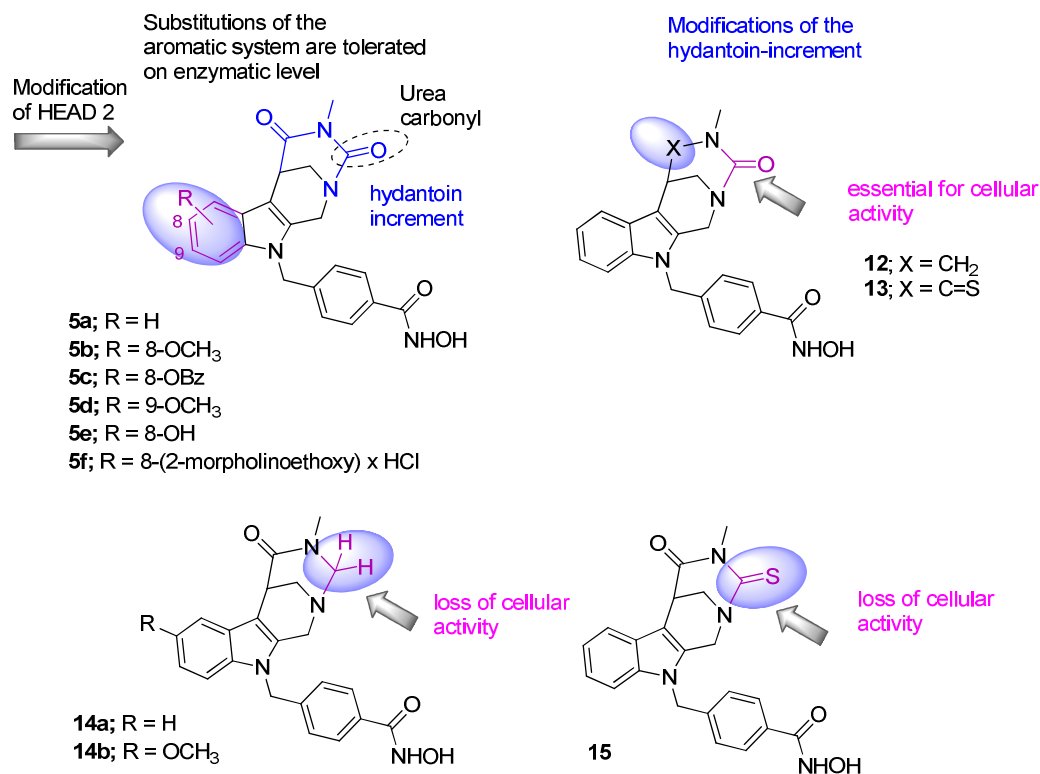


**Figure 2. Probable binding mode of Marbostat-100 at CD II of human HDAC6.** Detailed interactions of **A** (*R*)-Marbostat-100, **B** (*S*)-Marbostat-100 with HDAC6, shown are all amino acids within 3.5 Å around the inhibitor; atom colors N, *blue*, O, *red*, Zn<sup>2+</sup>, *magenta*, C and polar H of Marbostat-100, *grey*, of HDAC6, *cyan*; backbone of the binding site, *light cyan* ( $\alpha$ -helices and  $\beta$ -strands, *ribbons*, loops, *tubes*), w, water molecules, hydrogen bonds, *red dashed lines*. **C** Binding site represented by the lipophilic potential mapped onto a MOLCAD Connolly surface (hydrophobic areas, *brown*, polar areas, *green* and *blue*), (*R*)- and (*S*)-Marbostat-100, ball and stick models (for clarity, the phenylhydroxamic acid moiety of (*S*)-Marbostat-100 is not shown).

1  
2  
3 To define structural requirements for a potent inhibition of HDAC6 *in vivo*, we analyzed  
4 Marbostat-100 (**5a**) and some derivatives thereof (**5b-5f**, **12**, **13**, **14a**, **14b** and **15**). We  
5  
6 applied these agents to exponentially growing human MV4-11 cells, which are derived from  
7  
8 an acute myeloid leukemia case.<sup>48</sup> In contrast to the enzymatic *in vitro* test, a significant  
9  
10 structural dependency on the modifications of head group 2 can be observed in cellular  
11  
12 assays (Table 1). We found that the urea carbonyl-function in the D-ring system (Figure 3)  
13  
14 is essential to block HDAC6, as shown by the induction of tubulin peracetylation mediated  
15  
16 by compounds **5b**, **5d**, **12** and **13**. Compounds **14a**, **14b** and **15** lack this structural element  
17  
18 (figure 3) and fail to inhibit HDAC6 (Figure S1A). Compounds **12** and **13**, which possess  
19  
20 one urea carbonyl function, exhibit slightly reduced activity in comparison to  
21  
22 Marbostat-100 (**5a**) and its derivatives **5b** and **5d** with two carbonyl groups. The 8-  
23  
24 (morpholineethoxy) derivative **5f** with enhanced solubility as well exhibited conserved  
25  
26 selectivity and conserved potency. The 8-  
27  
28  
29  
30  
31  
32  
33  
34  
35  
36  
37  
38  
39  
40  
41  
42  
43  
44  
45  
46  
47  
48  
49  
50  
51  
52  
53  
54  
55  
56  
57  
58  
59  
60



28  
29  
30  
31  
32

**Figure 3.** Structure-activity relationship of **5a** and derivatives. The urea carbonyl function (magenta; compounds **12** and **13**) is essential for cellular activity. Compounds **14a** and **14b** exhibit a methylene-group, respectively **15** a sulfur instead this structural element and lack activity on the cellular level.

33  
34  
35  
36  
37  
38  
39  
40  
41  
42  
43  
44  
45  
46  
47  
48  
49  
50

To ascertain the selectivity of Marbostat-100 (**5a**) for HDAC6, we probed for histone hyperacetylation. HDAC6-specific drugs should not induce this posttranslational modification, because HDAC6 does not recognize histones as substrates *in vivo*.<sup>49</sup> Since class I HDACs catalyze the removal of the acetyl group from histones,<sup>4</sup> we included the benzamide HDACi MS-275 (entinostat) as test compound. MS-275, only inhibits class I HDACs and can be used as a positive control for histone hyperacetylation.<sup>50,51</sup> Potent accumulation of hyperacetylated tubulin and a lack of histone hyperacetylation is observed for both enantiomers of Marbostat-100 (**5a**) (Figure S1b).

51  
52  
53  
54  
55  
56  
57  
58  
59  
60

Since the data above illustrate that Marbostat-100 is the most effective new HDAC6i in enzymatic tests and in cells, we focused our following analyzes on this compound. We

1  
2  
3 treated MV4-11 cells with 5 nM to 1  $\mu$ M Marbostat-100 (**5a**) for 24 h. Western Blot  
4  
5 analyzes revealed that 50 nM Marbostat-100 (**5a**) evoked the accumulation of  
6  
7 hyperacetylated tubulin potently (Figures 4A-B). These *in vivo* findings confirm the *in vitro*  
8  
9 data from the biochemical fluorescence assays (Table 1), which identify Marbostat-100 (**5a**)  
10  
11 as potent HDAC6i. The roughly tenfold difference between the efficacy of Marbostat-100  
12  
13 *in vitro* and in cells positions Marbostat-100 as a highly potent new HDAC6i. Such  
14  
15 differences between drug activity *in vitro* and in cells are typically also seen with highly  
16  
17 potent tyrosine kinase inhibitors.  
18  
19  
20

21  
22 Next, we determined the effects of Marbostat-100 (**5a**) in higher dose ranges. We treated  
23  
24 MV4-11 cells with doses from 50 nM to 10  $\mu$ M Marbostat-100 (**5a**). Lysates of these cells  
25  
26 were tested for hyperacetylated tubulin (Figures 4C and D). While all doses cause an  
27  
28 accumulation of hyperacetylated tubulin, even high doses of Marbostat-100 (**5a**) do not  
29  
30 trigger a hyperacetylation of histones, which verifies Marbostat-100 as a very specific  
31  
32 HDAC6i (Figure 4C). Only a concentration of 10  $\mu$ M leads to a degradation of HDAC6;  
33  
34 this effect is not linked to a further increase in the acetylation of tubulin (Figure 4C). In  
35  
36 contrast, MS-275 induces hyperacetylated H3 in MV4-11 cells (Figure 4A).  
37  
38  
39

40  
41 To exclude cell-type dependent effects, we additionally tested Marbostat-100 (**5a**) in the  
42  
43 human leukemia cell lines Jurkat, HEL, and BV173, and in the human embryonic kidney  
44  
45 cell line HEK293T. Results collected in these systems confirm that Marbostat-100 (**5a**) is  
46  
47 an inhibitor of HDAC6 at nanomolar concentrations (supporting information Figures S2A-  
48  
49 F).  
50  
51  
52  
53  
54  
55  
56  
57  
58  
59  
60

1  
2  
3 Subsequently, we analyzed the kinetics of tubulin hyperacetylation in Marbostat-100 (**5a**)  
4 treated MV4-11 cells. These were incubated with 50 nM Marbostat-100 (**5a**) for 10 min up  
5  
6 to 48 h. Already after 30 minutes, Marbostat-100 (**5a**) causes an accumulation of  
7  
8 hyperacetylated tubulin in MV4-11 cells (Figure 4E, F). To confirm these results, the same  
9  
10 tests were performed in BV173 cells and yielded similar observations (supporting  
11  
12 information, Figure S2G, H).  
13  
14  
15

16  
17 To further ascertain the specificity of Marbostat-100 (**5a**), we used a HEK293T cell  
18  
19 overexpression model using HDAC6-FLAG and pcDNA3.1 as empty vector control. When  
20  
21 we treated these cells with increasing doses of Marbostat-100 (**5a**), we noted that no further  
22  
23 increase in tubulin acetylation could be detected with concentrations above 500 nM  
24  
25 Marbostat-100 (**5a**) (supporting information, Figure S2I). We therefore treated the  
26  
27 transfected HEK293T cells with 500 nM Marbostat-100 (**5a**). As expected,<sup>4</sup> the  
28  
29 overexpression of HDAC6 reduces the levels of endogenous tubulin acetylation  
30  
31 (Figure 4G). Treatment of HEK293T cells expressing pcDNA3.1 or HDAC6-FLAG with  
32  
33 Marbostat-100 (**5a**) augments the acetylation of tubulin (Figure 4G). These data confirm  
34  
35 that Marbostat-100 (**5a**) can antagonize HDAC6-dependent effects *in vivo*.  
36  
37  
38  
39  
40

41 Tubastatin A (**3**) (Figure 1) is currently one of the most frequently used drugs to inhibit  
42  
43 HDAC6.<sup>4</sup> Therefore, we compared Marbostat-100 (**5a**) with tubastatin A (**3**) and with  
44  
45 LBH589 (panobinostat). The hydroxamic acid and pan-HDACi LBH589 is currently tested  
46  
47 in several clinical trials and one of the most potent pan-HDACi.<sup>14</sup> Remarkably, at equimolar  
48  
49 doses, Marbostat-100 (**5a**) is superior to tubastatin A (**3**) regarding both the strength as well  
50  
51 as the duration of tubulin hyperacetylation in MV4-11 cells (Figure 4H). Tubastatin A (**3**)  
52  
53 only leads to a similar hyperacetylation of tubulin as Marbostat-100 (**5a**) when used in 100-  
54  
55  
56  
57  
58  
59  
60

1  
2  
3 fold higher concentrations than Marbostat-100 (**5a**) (50 nM Marbostat-100 (**5a**) vs. 5  $\mu$ M  
4 tubastatinA (**3**)) (supporting information, Figure S2J). Thus, Marbostat-100 (**5a**) is superior  
5  
6 over tubastatin A (**3**). In comparison to LBH589, one of the most potent pan HDACi that is  
7  
8 also highly active against HDAC6,<sup>50, 51</sup> Marbostat-100 (**5a**) evokes the hyperacetylation of  
9  
10 tubulin more rapidly and efficiently. In addition, the treatment with LBH589 induces  
11  
12 acetylated histone H3 and a degradation of HDAC6 after 24 h (Figure 4H). An equimolar  
13  
14 dose of Marbostat-100 does not produce this proteolytic effect (Figure 4H).  
15  
16  
17

18  
19 Based on these findings, we tested if Marbostat-100 (**5a**), tubastatin A (**3**), LBH589,  
20  
21 andMS-275 lead to cell cycle alterations and cell death. As presented in Figure 4I,  
22  
23 Marbostat-100 (**5a**), in contrast to LBH589 and MS-275, did not cause such effects.  
24  
25  
26  
27  
28  
29  
30  
31  
32  
33  
34  
35  
36  
37  
38  
39  
40  
41  
42  
43  
44  
45  
46  
47  
48  
49  
50  
51  
52  
53  
54  
55  
56  
57  
58  
59  
60  
LBH589 and MS-275 led to changes in cell cycle distribution and higher amounts of cells  
with fragmented DNA (subG1 fraction; Figure 4I).

To corroborate these data, we treated further cell lines and normal peripheral blood  
mononuclear cells (PBMCs) with Marbostat-100 (**5a**) and investigated them for cell cycle  
alterations and cell death. Again, we used Marbostat-100 (**5a**) in a dose-escalating manner  
and compared its effects with those induced by MS-275. While MS-275 dysregulates the  
cell cycle and triggered apoptosis in these cells, Marbostat-100 (**5a**) turns out as a non-  
cytotoxic, genuine inhibitor of HDAC6 (Figure 4I and supporting information Figure S2A,  
B).

For further drug assessment, we treated male DBA/1J mice with 0.6 mg Marbostat-100 (**5a**)  
for 15 days. Livers and kidneys from treated and control mice were examined for  
hyperacetylated tubulin by Western Blot. Figure 4J shows that tubulin is hyperacetylated in  
mice that received the inhibitor. Hence, Marbostat-100 (**5a**) also impairs HDAC6 activity in

whole animals. These results encouraged us to test Marbostat-100 (**5a**) in a murine inflammation model.

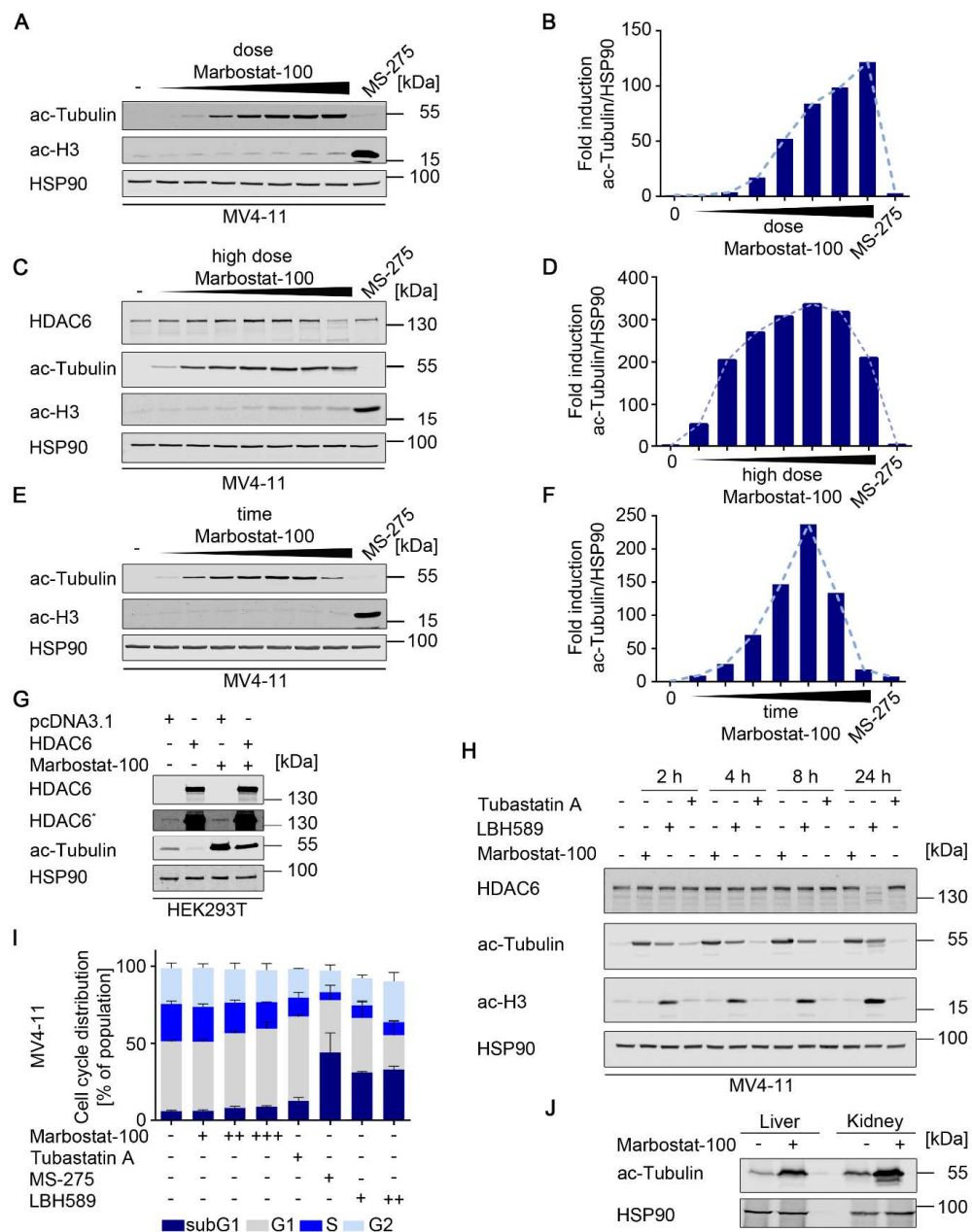


**Figure 4. Potency of Marbostat-100 (5a).** MV4-11 cells were treated with 5, 20, 50, 100, 250, 500 and 1000 nM Marbostat-100 or 5  $\mu$ M MS-275 (24 h). **(B)** Densitometric analysis ac-Tubulin/HSP90; ac-Tubulin, acetylated tubulin. **(C)** MV4-11 cells were treated with 0.05, 0.5, 1, 2, 4, 5 and 10  $\mu$ M Marbostat-100 or 5  $\mu$ M MS-275 (24 h). **(D)** Densitometry ac-Tubulin/HSP90. **(E)** MV4-11 cells were treated 10-30 min, 1, 2, 16, 24 and 48 h with 50 nM Marbostat-100 or 24 h with 5  $\mu$ M MS-275. **(F)** Densitometry of ac-tubulin/HSP90. **(G)** HEK293T cells were transfected with pcDNA3-HDAC6-FLAG or pcDNA3.1. Cells were incubated with

1  
2  
3 500 nM Marbostat-100 (48 h); immunoblot was done as indicated; HDAC6\* is a higher exposure for the  
4 detection of HDAC6. (H) MV4-11 cells were treated with 50 nM Marbostat-100, LBH589 or Tubastatin A as  
5 indicated. (I) MV4-11 cells were treated with 50 nM, 500 nM, and 1  $\mu$ M Marbostat-100, 5  $\mu$ M Tubastatin A,  
6 5  $\mu$ M MS-275, 30 nM or 50 nM LBH589 for 24 h. Cells were stained with propidium iodide and analyzed by  
7 flow cytometry. (J) Male DBA/1J mice were treated with 0.6 mg Marbostat-100 2.5 h. Organs were stored at  
8  $-80^{\circ}\text{C}$ . Livers and the kidneys were analyzed by immunoblot. All figures shown are representative for at least  
9 two independent experiments.

## 10 11 12 13 14 **Characterization of the novel HDACiMarbostat-100 (5a) in the Collagen-Induced** 15 16 **Arthritis (CIA) model**

17  
18 Treatment of CIA with Marbostat-100 (**5a**) (30mg/kg) was compared against vehicle.  
19  
20  
21 First clinical arthritis symptoms appeared at day 20 post immunization in all groups, which  
22  
23 corresponds to two days prior to first treatment. Treatment with Marbostat-100 (**5a**)  
24  
25 (30mg/kg) significantly ameliorated disease severity, displayed by a reduced clinical score  
26  
27 (Figure 5A), reduced paw thickness (Figure 5B), and reduced loss of body weight  
28  
29 (Figure 5C). These effects first appeared one week after the beginning of treatment  
30  
31 (Figure 5A, B), and at least in case of the clinical score, lasted until the end of the  
32  
33 experiment (Figure 5A).  
34  
35

36  
37 Histological assessment of arthritic paws revealed significantly weaker signs of synovial  
38  
39 inflammation, cellular invasion and degradation of cartilage and bone erosion in joints of  
40  
41 mice treated with Marbostat-100 (**5a**) (30mg/kg,  $p=0.004$ ) (Figure 5D-J). In a second  
42  
43 experiment (Figure 5K-N, 5P, treatment of CIA with equimolar compound **5f** (42.3mg/kg)  
44  
45 was compared against vehicle. Similar to the first experiment and six days after beginning  
46  
47 of treatment, significantly lower clinical arthritis scores were observed in the **5f**-treated  
48  
49 group ( $p<0.05$ , Figure 5K). Evaluating erosions in articular bone of arthritic hind paws by  
50  
51 assessing the ratio of bone surface to bone volume (relative bone surface BS/BV, measured  
52  
53 by  $\mu$ CT, see Figure 5L) revealed significantly lower BS/BV ratios in samples from mice  
54  
55  
56  
57  
58  
59  
60

1  
2  
3 treated with compound **5f** ( $p=0.049$ ) compared to vehicle (Figure 5L). Hind paws obtained  
4 from age-matched healthy control mice displayed no visible erosions (Figure 5M) and a  
5 small variance of the BS/BV ratio (Figure 5L). Visible erosions were present in all arthritic  
6 groups, however, rate and extent were lower in the Marbostat-100 (**5a**) and compound **5f**  
7 treated groups (Figure 5N-P).  
8  
9

10  
11 Concerning toxic effects, analysis of red blood cell count, hemoglobin concentration and  
12 white blood cell count were performed. Neither Marbostat-100 (**5a**) (30 mg/kg) nor  
13 compound **5f** (42.3mg/kg) were toxic in this respect when compared with vehicle control.  
14  
15 All measured values were in normal ranges of typical mouse hematogram data (see  
16 supporting information Figure S3).  
17  
18  
19  
20  
21  
22  
23  
24  
25

26  
27 In summary, Marbostat-100 (**5a**) and compound **5f** show significant preclinical,  
28 histological and radiological effects without major safety concerns when treating CIA.  
29  
30  
31  
32  
33  
34  
35  
36  
37  
38  
39  
40  
41  
42  
43  
44  
45  
46  
47  
48  
49  
50  
51  
52  
53  
54  
55  
56  
57  
58  
59  
60

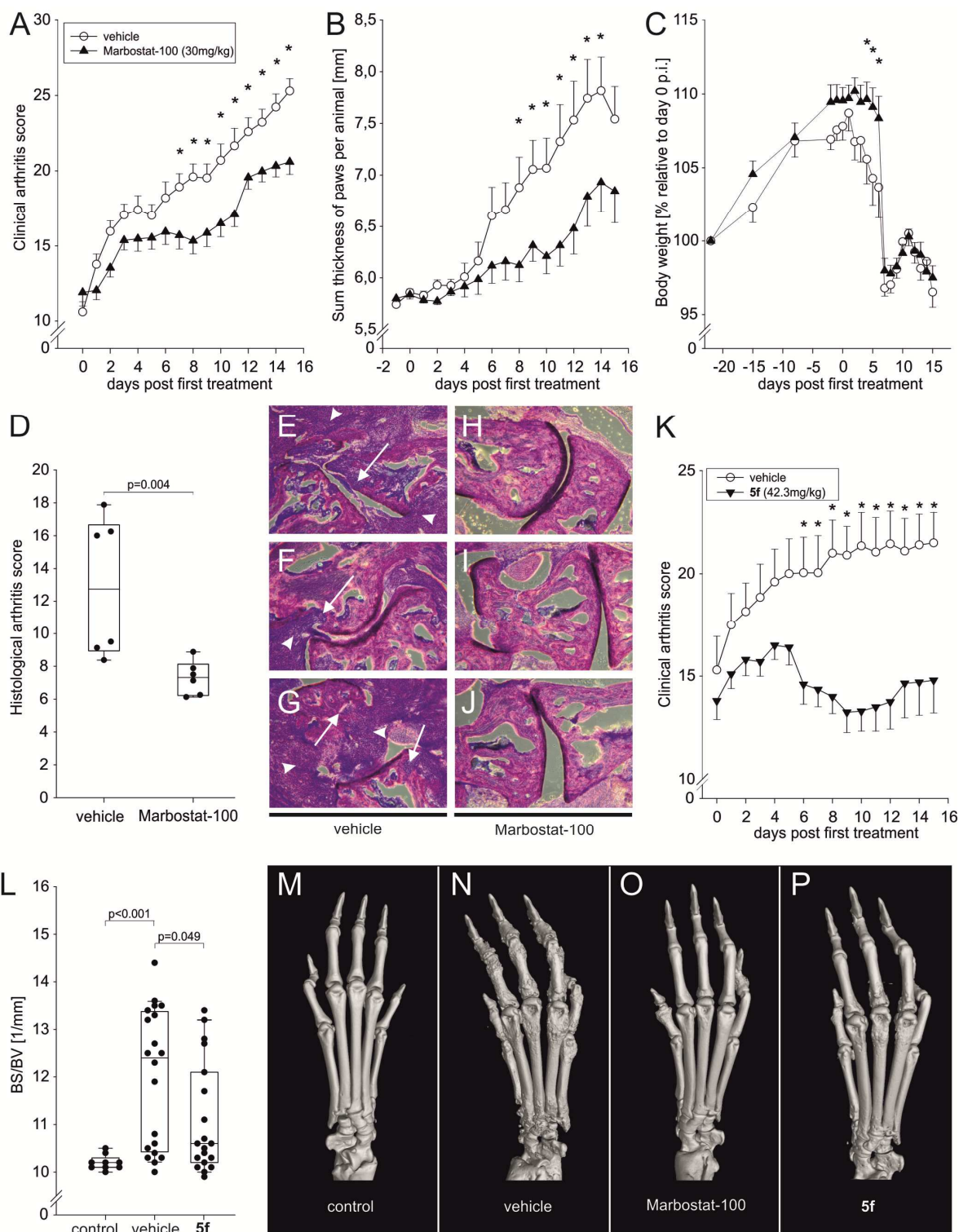


**Figure 5. Clinical, histological, and radiological effects of Marbostat-100 treatment in Collagen-Induced Arthritis (CIA).**

**A-C)** Clinical arthritis score (A), paw thickness (B), and body weight (C) of mice treated with vehicle or Marbostat-100 (**5a**) (n=15 per group, mean±standard error). Stars indicate significance (p<0.05, two-way ANOVA). **D)** Histological arthritis score of mice in A) (n=6 per group analyzed). Box plots demonstrate 10th (whisker), 25th, 50th (median), 75th, and 90th (whisker) percentile. Every dot represents the mean of replicate determinations in one animal. Mann-Whitney test was used to compare groups. **E-J)** Representative DMMB

1  
2  
3 staining of joints in mice from A). Magnification x100. Arrowheads indicate synovial inflammation and  
4 cellular invasion, arrows indicate degradation/erosion of cartilage/bone, exemplarily shown for vehicle. **K**)  
5 Clinical arthritis score of mice treated with vehicle or compound **5f** (n=10 per group). Stars indicate  
6 significance (p<0.05, two-way ANOVA). **L**) Ratio BS/BV as an indicator for bone erosion in hind-paws from  
7 mice in K). Every dot represents the value of one paw. Outliers beyond group mean±2.0\*SD were excluded.  
8 Mann-Whitney test was used to compare groups. **M-P**) Representative microcomputed tomography images  
9 from treated and control mice. Abbreviations: p.i., post immunization; BS, bone surface; BV, bone volume;  
10 DMMB, 1,9-Dimethylmethylene blue; n.s., not significant.

## 11 12 13 **Discussion**

14  
15 Crystal structures of different HDACs and the recent structures of HDAC6,<sup>35</sup> reveal that  
16 the active sites are highly conserved among HDACs. The “cap domain” in contrast differs  
17 greatly in terms of shape and properties between isoforms. Moreover, the HDAC6 channel  
18 appears to be wider and shallower than that of HDAC1, suggesting that large and more rigid  
19 cap groups might lead to HDAC6 selectivity. In our approach for full inhibitory potency  
20 and selectivity on the enzymatic level, a benzylic linker connected with a hydroxamic acid  
21 as Zn<sup>2+</sup>-chelating group, combined with a linearly fused tetracyclic ring system as cap group,  
22 are necessary. On the more complex cellular level, a hydantoin increment additionally is  
23 essential for potent HDAC6 inhibition.  
24  
25  
26  
27  
28  
29  
30  
31  
32  
33  
34

35  
36  
37 Sequence and 3D-structure comparisons enable to speculate about reasons for the high  
38 selectivity of Marbostat-100 (**5a**) for HDAC6. The K<sub>i</sub> values for ten HDAC species (Table  
39 3) indicate that Marbostat-100 has a unique binding mode at HDAC6. The catalytic sites  
40 of HDAC2, HDAC6, HDAC7 and HDAC8 are highly similar, providing no obvious  
41 indication for significantly different docking modes<sup>52</sup>. Structure-based alignments of the  
42 Marbostat-100 binding site (Figure 2) with corresponding amino acids of HDAC2 (PDB  
43 4LXZ<sup>52</sup>), HDAC7 (PDB 3C0Z<sup>44</sup>) and HDAC8 (PDB 1W22<sup>53</sup>) result in root mean square  
44 deviations of backbone atoms of 0.43 Å, 0.69 Å and 0.63 Å, respectively. Only one to two  
45 amino acids differ among the four species. Structure-activity relationships (Table 1) suggest  
46  
47  
48  
49  
50  
51  
52  
53  
54  
55  
56  
57  
58  
59  
60

1  
2  
3 that the outstanding selectivity for HDAC6 versus HDAC2 (observed also e.g. in the case of  
4 tubastatin A) is mainly due to the benzylic linker. Probably, the specific monodentate  
5 hydroxamate-Zn<sup>2+</sup> coordination mode<sup>36b</sup> allows an optimal fit of the linker into HDAC6  
6  
7 which cannot be achieved in the case of other HDACs because of differing binding modes  
8 of the hydroxamic acid moiety. These binding modes, in turn, may interfere with an optimal  
9 alignment of the surface recognizing cap group. Moreover, a tyrosine replaces HDAC6  
10 F679 in HDAC2. The side chain hydroxyl possibly displaces the 4-methyl group of (*S*)-  
11 Marbostat-100 (**5a**) and/or weakens hydrophobic interactions of both isomers present in the  
12 case of HDAC6. HDAC7 contains a histidine in the position of HDAC6 Y782. The  
13 conformation of this histidine in HDAC7 structures does not enable a hydrogen bond  
14 replacing that between Y782 and the hydroxylamine oxygen of Marbostat-100 (**5a**).  
15  
16 Furthermore, HDAC7 contains a short helix between P807 and G811 two amino acids  
17 longer than the corresponding HDAC6 loop around L749. The course of this helix with two  
18 prolines may displace the diazocino moieties of both isomers from their positions in  
19 HDAC6. The hydrophobic contacts of the phenyl planes and the 4-methyl groups of (*R*)-and  
20 (*S*)-Marbostat-100 with HDAC6 L749 cannot be reproduced in an optimal way in case of  
21 the conformation of M274 replacing that leucine in HDAC8. Additionally, both isomers  
22 cannot interact with a hydrophobic amino acid of HDAC8 as with P501 in HDAC6 due to a  
23 far distant position of the short loop between HDAC8 L31 and K33 from the much longer  
24 HDAC6 loop between C493 and E502.  
25  
26  
27  
28  
29  
30  
31  
32  
33  
34  
35  
36  
37  
38  
39  
40  
41  
42  
43  
44  
45  
46  
47  
48  
49  
50  
51  
52  
53  
54  
55  
56  
57  
58  
59  
60

## Biology

We demonstrate that Marbostat-100 (**5a**) is a selective, potent, and rapid inhibitor of HDAC6 in various cell types. We see clear hyperacetylation of the HDAC6 target protein tubulin, but no accumulation of acetylated histones, which are targets of class I HDACs.<sup>4</sup> Regarding potency, we show that Marbostat-100 (**5a**) is superior over tubastatin A (**3**). Moreover, in contrast to the pan-HDACi LBH589, Marbostat-100 (**5a**) does not evoke a destruction of HDAC6 at longer treatment periods. An exception are unnecessarily high doses of Marbostat-100 that do not evoke any additional effect on tubulin acetylation. A comparison with the literature shows that Marbostat-100 (**5a**) is also more potent than other drugs that preferentially target HDAC6. For example, the HDAC6i HPB has to be applied in the  $\mu\text{M}$  dose range to evoke tubulin hyperacetylation in cells,<sup>20</sup> and ACY-1215 has some preference for HDAC6 but also blocks other HDACs at effective dose ranges impairing HDAC6.<sup>22</sup>

A potent inhibition of pancreatic cancer cell growth could be achieved with agents that target HDAC3 and HDAC6.<sup>23</sup> Additional work is required to dissect whether an inhibition of solely HDAC6 can reduce the growth of such cells that stem from a most aggressive and incurable cancer trait. Our previously collected data rather suggest that class I HDACs are pharmacologically relevant drug targets in pancreatic cancer.<sup>54, 55</sup>

The rapid induction of tubulin hyperacetylation may rely on the preference of HDAC6 for unpolymerized, free tubulin.<sup>56</sup> The hyperacetylation of tubulin and the lack of effects on H3 acetylation in the presence of Marbostat-100 (**5a**) are not due to gross cellular alterations or cytotoxic effects. Therefore, Marbostat-100 (**5a**) can be regarded as a selective HDAC6 inhibitor and as a true modulator of posttranslational protein modifications that depend on

1  
2  
3 HDAC6. Due to its non-cytotoxic effects, Marbostat-100 (**5a**) is equally a valid tool to  
4  
5 mirror the biology of HDAC6 knockout animals, which are viable and show no  
6  
7 abnormalities.<sup>12</sup> Apparently, HDAC6 can be targeted safely, without adverse effects on  
8  
9 normal cells.  
10  
11  
12  
13

### 14 15 ***In vivo* activity of Marbostat-100 (5a) in the CIA model**

16  
17 In rodent models of arthritis, protective effects have been shown by rather unspecific  
18  
19 inhibition of HDACs in rats with adjuvant induced arthritis (AIA)<sup>57-59</sup> and in SKG mice  
20  
21 which spontaneously develop autoimmune arthritis.<sup>60</sup> In collagen-induced (CIA) and in  
22  
23 collagen antibody-induced (CAIA) arthritis models, unspecific HDAC inhibition<sup>58, 61-63</sup> as  
24  
25 well as specific HDAC1<sup>64, 65</sup> or specific HDAC6 inhibition<sup>21, 66</sup> have shown anti-  
26  
27 inflammatory effects, the latter is consistent with our results. Others have demonstrated that  
28  
29 HDAC6 inhibition blocks the activation of macrophages, which was dependent on effects  
30  
31 on cell adhesion and microtubule acetylation.<sup>67</sup> In arthritis, this would imply an  
32  
33 immunosuppressive effect. Moreover, HDAC6 is a transcriptional activator of IL-10 gene  
34  
35 expression in antigen presenting cells.<sup>68</sup> This would imply that an inhibitor of HDAC6 is  
36  
37 also an inhibitor of IL-10, which was not tested in this study. However, others demonstrated  
38  
39 that HDAC inhibitors can support regulatory T cells and IL-10 secretion in experimental  
40  
41 stroke<sup>69</sup>, which was supported by others with a specific HDAC-6 inhibitor in a  
42  
43 lipopolysaccharide challenge of mice *in vivo*.<sup>70</sup> These latter two studies support a role for  
44  
45 HDAC-induced IL-10 as a possible beneficial effector, which might have played a role also  
46  
47 in arthritis.  
48  
49  
50  
51  
52  
53  
54  
55  
56  
57  
58  
59  
60

1  
2  
3 It should also be mentioned, That cellular knockdown of HDAC6 results in the  
4 inflammasome activation and IL-1 $\beta$  secretion.<sup>71</sup> This work was supported by a publication  
5 that demonstrated that HDAC6 inhibition prevents TNF-induced caspase 3 activation in  
6 lung endothelial cell and maintains cell-cell junctions.<sup>72</sup> In addition, overexpression of  
7 HDAC6 induces many other proinflammatory events in macrophages,<sup>73</sup> so that HDAC6  
8 inhibition should lead to opposite effects. If Marbostat100 would exert a similar effect, the  
9 proinflammatory pathway through the inflammasome, IL-1 $\beta$  and others can be blocked in  
10 clinical arthritis. These particular pathways might be good targets in a future investigation.  
11  
12

13  
14  
15  
16  
17  
18  
19  
20  
21  
22 Lee *et al.*<sup>66</sup> report a significant reduction of clinical scores by daily application of 100mg/kg  
23 tubastatin A (**3**), but not at 10 mg/kg or 50 mg/kg.<sup>66</sup> In order to investigate our newly  
24 developed HDAC6 inhibitor Marbostat-100 (**5a**) in CIA, we used Marbostat-100 (**5a**) at a  
25 dose of 30 mg/kg.  
26  
27

28  
29  
30  
31  
32 Our data suggest a significant reduction of clinical arthritis scores of about 25% and  
33 histological scores of about 50% for Marbostat-100 (**5a**) treatment. Importantly, we also  
34 observed significant effects regarding the clinical arthritis score and relative bone surface  
35 BS/BV for treating CIA with equimolar compound **5f** (42.3mg/kg). Regarding safety  
36 profiles, no significant changes in main blood parameters like red or white blood cell count  
37 and total hemoglobin were identified for all treatments (Marbostat-100 (**5a**), compound **5f**)  
38 as all values were within expected ranges for mice.<sup>74</sup> Thus, Marbostat-100 (**5a**) might also  
39 be a safe drug for clinical applications.  
40  
41  
42  
43  
44  
45  
46  
47  
48  
49  
50

## 51 52 53 **Conclusion**

54  
55  
56  
57  
58  
59  
60

1  
2  
3 The data shown above impressively demonstrate that Marbostat-100 (**5a**) is a highly  
4 selective and potent inhibitor of HDAC6, being superior over the established HDACi  
5 tubastatin A (**3**) and LBH589 in this respect. Hence, Marbostat-100 and its derivatives  
6 represent a novel class of precise tools for molecular and biochemical analyses of HDAC6  
7 and its functions *in vivo*.

8  
9  
10 Moreover, Marbostat-100 (**5a**) demonstrates *in vivo* anti-inflammatory activity in CIA.  
11  
12 Despite of impressive *in vitro* data of various HDAC inhibitors and the effectivity of  
13 givinostat for treatment of juvenile idiopathic arthritis,<sup>75</sup> as reviewed by Dinarello *et al.*<sup>76</sup>,  
14 achieving clinical success with HDAC inhibitors in RA needs further research since diverse  
15 inflammatory pathways are involved which might be controlled by different specific HATs  
16 and their corresponding specific HDACs. Nevertheless, inhibition of HDAC6 and other  
17 HDAC subtypes with small molecules remains a promising future alternative to escalating  
18 treatment of RA with biologicals.  
19  
20  
21  
22  
23  
24  
25  
26  
27  
28  
29  
30  
31  
32  
33  
34

## 35 **Experimental Section**

### 36 **Chemistry**

37  
38  
39  
40  
41 **General information.** The solvents and reagents were of analytical grade, purchased from  
42 commercial suppliers and used without further purification. Acetonitrile for HPLC  
43 (gradient grade) was from Merck (Darmstadt, Germany). Millipore water was used  
44 throughout for HPLC eluents (Astacus Membrane Pure, MembraPure GmbH, Bodenheim,  
45 Germany). Thin layer chromatography was performed on Merck silica gel 60 F<sub>254</sub> TLC  
46 aluminum plates. Geduran 60 (0.063 – 0.200 mm, Merck) was used for column  
47 chromatography. <sup>1</sup>H NMR and <sup>13</sup>C NMR spectra were measured with a Bruker Avance 300  
48  
49  
50  
51  
52  
53  
54  
55  
56  
57  
58  
59  
60

1  
2  
3 instrument (7.05 T,  $^1\text{H}$ : 300 MHz,  $^{13}\text{C}$ : 75 MHz) and a Bruker Avance 400 instrument (9.4  
4 T,  $^1\text{H}$ : 400 MHz,  $^{13}\text{C}$ : 101 MHz) (Bruker, Karlsruhe, Germany), using the respective solvent  
5  
6 as an internal standard. Specific NMR assignments if listed were determined by  
7  
8 multidimensional NMR ( $^1\text{H}/^{13}\text{C}$ -HMBC, NOSY and COSY) or decoupling experiments.  
9  
10 The multiplicity of carbon atoms ( $^{13}\text{C}$ -NMR) were determined by DEPT 135 and DEPT 90  
11  
12 (distortionless enhancement by polarization transfer): “+” primary and tertiary carbon atom  
13  
14 (positive DEPT 135 signal), “-“ secondary carbon atom (negative DEPT 135 signal),  
15  
16 “quat.” quaternary carbon atom.  
17  
18  
19  
20  
21

22 IR spectra (KBr) were reported with a Bruker Tensor 27 spectrometer. Melting points were  
23  
24 determined with a Büchi B-545 instrument and are uncorrected. Low-resolution mass  
25  
26 spectrometry (MS) was measured with a Finnigen Thermo Quest TSQ 7000 instrument  
27  
28 (Thermo Finnigan, San Jose, USA) with electrospray ionization (ESI) coupled to an Agilent  
29  
30 1100 Series HPLC (Agilent Technologies, Santa Clara, USA) or a Finnigan MAT SSQ 710  
31  
32 A with electron ionization (EI). High resolution mass spectrometry (HRMS) was performed  
33  
34 on an Agilent 6540 UHD Accurate-Mass Q-TOF LC/MS system with electrospray  
35  
36 ionization.  
37  
38  
39  
40

41 All reactions were carried out under nitrogen. Elemental analyzes were performed by the  
42  
43 Analytical Laboratory of the University of Regensburg. The x-ray structures were measured  
44  
45 by the Crystallography Laboratory of the University of Regensburg. Chemical names were  
46  
47 created using ChemDraw professional 15.0.0.107. Analytical HPLC analysis was performed  
48  
49 with a system from Merck (Darmstadt, Germany) consisting of a L-5000 controller, a  
50  
51 655A-12 pump, a 655A-40 autosampler and a L-4250 UV-VIS detector on a Eurospher-100  
52  
53 C18 column (250 × 4 mm, 5  $\mu\text{m}$ , Knauer, Berlin, Germany) at a flow rate of 0.8 mL / min.  
54  
55  
56  
57  
58  
59  
60

Mixtures of MeCN or 0.1 % TFA in MeCN and 0.1 % aq. TFA were used as mobile phase. Helium degassing was used throughout. Compound purities were either determined by elemental analysis or HPLC methods as given and calculated as the percentage peak area of the analyzed compound by UV detection at 220 nm. All compounds were confirmed to be of  $\geq 95\%$  purity.

For experimental and analytical details of further prepared intermediates see supporting information.

#### **Synthesis of the hydroxamates by cleavage of the tetrahydropyranyl-protecting group:**

The corresponding starting material (0.30 mmol) was dissolved in 10.0 mL of MeOH, optionally with gentle heating. Carefully 0.6 M aqueous HCl was added dropwise until a slight turbidity can be observed. Stirring at rt was continued until complete reaction is indicated by TLC control. The crystallization of the hydroxamic acid was completed by further addition of 0.6 M HCl. The crystalline product was filtered off and dried *in vacuo*.

#### **10-(4-(Hydroxycarbamoyl)benzyl)-1,2,3,4,5,10-hexahydro-2,5-methanoazepino[3,4-b]indol-2-ium 2,2,2-trifluoroacetate (4)**

According to GP3 from **75** the crude intermediate 4-((4,5-dihydro-1*H*-2,5-methanoazepino[3,4-*b*]indol-10(3*H*)-yl)methyl)-*N*-((tetrahydro-2*H*-pyran-2-yl)oxy)benzamide (**76**) (0.11 g; 0.25 mmol, 20 %) was obtained as a colorless oil after cc ( $\text{CH}_2\text{Cl}_2$  / MeOH /  $\text{NH}_3$  10:1:0,1) (see supporting information). In the following **76** was directly converted as described above. Yield 0.02 g (0.05 mmol, 20 %) colorless crystals after preparative HPLC with 0.10 % TFA / MeCN (80:20) gradient to  $\leq 0.10$  % TFA / MeCN (20:80). mp: 210.3-211.0 °C ( $\text{H}_2\text{O}$ ). IR (KBr): 1734  $\text{cm}^{-1}$ .  $^1\text{H}$  NMR (600 MHz, MeCN (20:80)).

1  
2  
3 MeOD):  $\delta$   $^1\text{H}$  NMR (600 MHz, MeOD)  $\delta$  7.68 (d,  $J$  = 8.3 Hz, 2H), 7.63 (d,  $J$  = 7.8 Hz, 1H),  
4 7.35 (d,  $J$  = 8.2 Hz, 1H), 7.21 – 7.16 (m, 1H), 7.15 – 7.12 (m, 1H), 7.09 (d,  $J$  = 8.3 Hz, 2H),  
5 5.44 (d,  $J$  = 17.3 Hz, 1H), 5.33 (d,  $J$  = 17.3 Hz, 1H), 4.81 (d,  $J$  = 15.5 Hz, 1H), 4.49 (d,  $J$  =  
6 15.3 Hz, 1H), 3.95 – 3.86 (m, 2H), 3.66 (d,  $J$  = 10.2 Hz, 1H), 3.61 (dd,  $J$  = 10.2, 3.1 Hz,  
7 1H), 3.44 – 3.36 (m, 1H), 2.54 – 2.43 (m, 1H), 2.40 – 2.31 (m,  $J$  = 11.3, 9.0 Hz, 1H).  
8  $^{13}\text{C}$ -NMR (151 MHz, DMSO- $d_6$ ):  $\delta$  163.74 (quat. CO), 157.87 (quat. CO (TFA)), 140.67  
9 (quat. Ar-C), 136.64 (quat. Ar-C), 131.87 (quat. Ar-C), 127.25 (+, (Ar-CH) $_2$ ), 126.57 (+,  
10 (Ar-CH) $_2$ ), 126.29 (CF $_3$ ), 125.40 (quat. Ar-C), 124.10 (quat. Ar-C), 121.79 (+, Ar-CH),  
11 119.67 (+, Ar-CH), 117.97 (+, Ar-CH), 113.86 (quat. Ar-C), 110.18 (+, Ar-CH), 57.02 (–,  
12 NCH $_2$ CH), 53.29 (–, NCH $_2$ CH $_2$ ), 53.03 (–, NCH $_2$ Ar), 46.19 (–, NCH $_2$ Ar (Benzyl)), 35.06  
13 (–, NCH $_2$ CH $_2$ ), 30.88 (+, NCH $_2$ CH) ESI-MS  $m/z$  (%): 348 [MH $^+$ ] (100). HRMS (ESI-MS  
14  $m/z$ ): Calcd.: 348.1709, found: 348.1707. RP-HPLC (220 nm): 97.9% (gradient: 0–30 min:  
15 MeCN/0.1% aq. TFA 20/80-95/5, 31-40 min: 95/5,  $t_R$  = 11.7 min).  
16  
17  
18  
19  
20  
21  
22  
23  
24  
25  
26  
27  
28  
29  
30  
31  
32

33  
34 ***N*-Hydroxy-4-((4-methyl-3,5-dioxo-3,4,5,6-tetrahydro-2,6-methano[1,3]diazocino[5,6-**  
35 ***b*]indol-11(*1H*)-yl)methyl)benzamide (Marbostat-100; **5a**)**  
36  
37

38  
39 As described above from 4-((4-methyl-3,5-dioxo-3,4,5,6-tetrahydro-2,6-  
40 methano[1,3]diazocino[5,6-*b*]indol-11(*1H*)-yl)methyl)-*N*-((tetrahydro-2*H*-pyran-2-  
41 yl)oxy)benzamide (**27a**) (0.16 g; 0.33 mmol). 0.06 g (0.148 mmol; 46 %) colorless crystals  
42 after crystallization from CH $_2$ Cl $_2$ /n-heptane. mp: 199.4-201.0 °C. IR (KBr): 1727, 1684 cm $^{-1}$ .  
43  $^1\text{H}$  NMR (400 MHz, DMSO- $d_6$ ):  $\delta$  11.17 (s, 1H, NHOH), 9.02 (s, 1H, NHOH), 7.68 (d,  $J$   
44 = 8.3 Hz, 2H, Ar-H), 7.57 – 7.51 (m, 1H, Ar-H), 7.41 (d,  $J$  = 7.2 Hz, 1H, Ar-H), 7.14 (d,  $J$   
45 = 8.3 Hz, 2H, Ar-H), 7.13 – 7.03 (m, 2H, Ar-H), 5.41 (s, 2H, NCH $_2$ Ar (Benzyl)), 4.87 (d,  $J$   
46 = 16.6 Hz, 1H, NCH $_A$ H $_B$ Ar), 4.58 (d,  $J$  = 16.6 Hz, 1H, NCH $_A$ H $_B$ Ar), 3.95 – 3.83 (m, 2H,  
47  
48  
49  
50  
51  
52  
53  
54  
55  
56  
57  
58  
59  
60

1  
2  
3 NCH<sub>A</sub>H<sub>B</sub>CH), 3.46 (d,  $J = 10.8$  Hz, 1H, NCH<sub>A</sub>H<sub>B</sub>CH), 2.91 (s, 3H, NCH<sub>3</sub>). <sup>13</sup>C NMR  
4 (101 MHz, DMSO-*d*<sub>6</sub>):  $\delta$  173.57 (quat. CO), 164.29 (quat. CO), 161.32 (quat. CO), 141.17  
5  
6 (quat. Ar-C), 136.40 (quat. Ar-C), 134.72 (quat. Ar-C), 132.37 (quat. Ar-C), 127.72 (+,  
7  
8 (Ar-CH)<sub>2</sub>), 127.09 (+, (Ar-CH)<sub>2</sub>), 126.19 (quat. Ar-C), 122.25 (+, Ar-CH), 120.31 (+, Ar-  
9  
10 CH), 118.32 (+, Ar-CH), 110.79 (+, Ar-CH), 105.82 (quat. Ar-C), 49.41 (–, NCH<sub>2</sub>Ar),  
11  
12 46.70 (–, NCH<sub>2</sub>CH), 46.47 (–, NCH<sub>2</sub>Ar (Benzyl)), 36.50 (+, NCH<sub>2</sub>CH), 27.89 (+, NCH<sub>3</sub>).  
13  
14 ESI-MS *m/z* (%): 422 [MNH<sub>4</sub><sup>+</sup>] (80), 405 [MH<sup>+</sup>] (100). Anal. calcd for C<sub>22</sub>H<sub>20</sub>N<sub>4</sub>O<sub>5</sub>: C  
15  
16 65.34; H 4.98; N 13.85; found: C 65.05; H 5.12; N 13.48.  
17  
18  
19  
20  
21

22  
23 ***N*-hydroxy-4-(((6*R*)-4-methyl-3,5-dioxo-3,4,5,6-tetrahydro-2,6-**  
24  
25 **methano[1,3]diazocino[5,6-*b*]indol-11(1*H*)-yl)methyl)benzamide (***R*-5a**)**  
26

27  
28 4-(((6*R*)-4-methyl-3,5-dioxo-3,4,5,6-tetrahydro-2,6-methano[1,3]diazocino[5,6-*b*]indol-  
29  
30 11(1*H*)-yl)methyl)-*N*-((tetrahydro-2*H*-pyran-2-yl)oxy)benzamide (***R*-27a**) (40 mg; 82  $\mu$ mol)  
31  
32 were dissolved in a mixture of MeOH/THF (10 mL; 1:1). A catalytic amount of Amberlyst  
33  
34 15 was added and the mixture stirred for 24 h at room temperature. The Amberlyst was  
35  
36 filtered off, the solvent removed under reduced pressure, the remaining solid dried in vacuo.  
37  
38 Yield 0.2 g (0.5 mmol; 52 %) colorless crystals after crystallization from diethylether. mp:  
39  
40 145.4-146.1 °C. IR (KBr): 1727, 1683 cm<sup>-1</sup>. <sup>1</sup>H NMR (400 MHz, DMSO-*d*<sub>6</sub>):  $\delta$  11.15 (s,  
41  
42 1H), 7.66 (d,  $J = 8.3$  Hz, 2H), 7.53 (dd,  $J = 6.8, 1.7$  Hz, 1H), 7.41 (d,  $J = 7.3$  Hz, 1H), 7.13  
43  
44 (d,  $J = 8.2$  Hz, 2H), 7.12 – 7.05 (m, 2H), 5.41 (s, 2H), 4.86 (d,  $J = 16.6$  Hz, 1H), 4.57 (d,  $J =$   
45  
46 16.5 Hz, 1H), 3.90 (d,  $J = 14.0$  Hz, 2H), 3.46 (dd,  $J = 12.9, 1.9$  Hz, 1H), 2.90 (s, 3H). <sup>13</sup>C  
47  
48 NMR (101 MHz, DMSO-*d*<sub>6</sub>)  $\delta$  173.59, 161.33, 164.32, 141.19, 136.40, 134.75, 132.38,  
49  
50 127.72, 127.10, 126.19, 122.26, 120.32, 118.33, 110.81, 105.82, 49.41, 46.70, 46.47, 36.49,  
51  
52  
53  
54  
55  
56  
57  
58  
59  
60

1  
2  
3 27.89.  $[\alpha]_{589}^{20}$  -136.190 (c 0.1; MeOH). Anal. calcd for C<sub>22</sub>H<sub>20</sub>N<sub>4</sub>O<sub>5</sub>: C 65.34; H 4.98; N  
4 13.85; found: C 65.15; H 4.99; N 13.71.  
5  
6

7  
8  
9 ***N*-Hydroxy-4-(((6*S*)-4-methyl-3,5-dioxo-3,4,5,6-tetrahydro-2,6-**  
10 **methano[1,3]diazocino[5,6-*b*]indol-11(1*H*)-yl)methyl)benzamide (*S*-5a)**

11  
12  
13  
14 Preparation as described above for the *R*-Enantiomer *R*-5a by use of 4-(((6*S*)-4-Methyl-3,5-  
15 dioxo-3,4,5,6-tetrahydro-2,6-methano[1,3]diazocino[5,6-*b*]indol-11(1*H*)-yl)methyl)-*N*-  
16 ((tetrahydro-2*H*-pyran-2-yl)oxy)benzamide (*S*-27a). Yield 0.12 g (0.3 mmol; 60 %)   
17 colorless crystals after recrystallization from diethylether. mp: 146.0-147.2 °C. IR (KBr):  
18 1727, 1681 cm<sup>-1</sup>. <sup>1</sup>H NMR (300 MHz, DMSO-*d*<sub>6</sub>): δ 11.17 (s, 1H), 9.03 (s, 1H), 7.66 (d, *J*  
19 = 8.2 Hz, 2H), 7.52 (dd, *J* = 6.4, 2.3 Hz, 1H), 7.41 (dd, 1H), 7.15 – 7.11 (m, 2H), 7.07 (dt, *J*  
20 = 7.1, 4.0 Hz, 2H), 5.41 (s, 2H), 4.86 (d, *J* = 16.6 Hz, 1H), 4.57 (d, *J* = 16.5 Hz, 1H), 3.90  
21 (d, *J* = 12.9 Hz, 2H), 3.46 (d, *J* = 11.2 Hz, 1H), 2.89 (s, 3H). <sup>13</sup>C NMR (101 MHz, DMSO)  
22 δ 173.59 (s), 164.30, 161.34 (s), 141.19 (s), 136.40 (s), 134.75 (s), 127.72 (s), 127.10 (s),  
23 126.19 (s), 122.26 (s), 120.32 (s), 118.33 (s), 110.81 (s), 105.82 (s), 49.41 (s), 46.69 (s),  
24 46.47 (s, *J* = 22.6 Hz), 36.49 (s), 27.89 (s).  $[\alpha]_{589}^{20}$  136.193 (c 0.1; MeOH). Anal. calcd for  
25 C<sub>22</sub>H<sub>20</sub>N<sub>4</sub>O<sub>5</sub>: C 65.34; H 4.98; N 13.85; found: C 65.27; H 5.02; N 13.62.  
26  
27  
28  
29  
30  
31  
32  
33  
34  
35  
36  
37  
38  
39  
40  
41

42 ***N*-Hydroxy-4-((8-methoxy-4-methyl-3,5-dioxo-3,4,5,6-tetrahydro-2,6-**  
43 **methano[1,3]diazocino[5,6-*b*]indol-11(1*H*)-yl)methyl)benzamide (5b)**

44  
45  
46  
47  
48 As described above from 4-((8-methoxy-4-methyl-3,5-dioxo-3,4,5,6-tetrahydro-2,6-  
49 methano[1,3]diazocino[5,6-*b*]indol-11(1*H*)-yl)methyl)-*N*-((tetrahydro-2*H*-pyran-2-  
50 yl)oxy)benzamide (**27b**) (0.10 g; 0.20 mmol). Yield 0.02 g (0.05 mmol; 25 %) colorless  
51 crystals after crystallization from water/MeOH; mp: 178.5 -179.4 °C. IR (KBr): 1716 cm<sup>-1</sup>.  
52  
53  
54  
55  
56  
57  
58  
59  
60

<sup>1</sup>H NMR (400 MHz, MeOD): δ 7.65 (d, *J* = 8.3 Hz, 2H), 7.17 (d, *J* = 8.9 Hz, 1H), 7.12 (d, *J* = 2.4 Hz, 1H), 7.06 (d, *J* = 8.3 Hz, 2H), 6.77 (dd, *J* = 8.9, 2.4 Hz, 1H), 5.37 – 5.25 (m, 2H), 4.81 (d, *J* = 16.5 Hz, 1H), 4.48 (d, *J* = 16.3 Hz, 1H), 3.93 (d, *J* = 13.2 Hz, 1H), 3.84 (s, 1H), 3.82 (s, 3H), 3.44 (dd, *J* = 13.2, 2.2 Hz, 1H), 3.01 (s, 3H). <sup>13</sup>C-NMR (101 MHz, DMSO-*d*<sub>6</sub>): δ 173.58 (quat. CO), 164.27 (quat. CO), 161.31 (quat. CO), 154.46 (quat. Ar-C), 141.28 (quat. Ar-C), 135.17 (quat. Ar-C), 132.33 (quat. Ar-C), 131.49 (quat. Ar-C), 127.68 (+, (Ar-CH)<sub>2</sub>), 127.02 (+, (Ar-CH)<sub>2</sub>), 126.64 (quat. Ar-C), 111.94 (+, Ar-CH), 111.64 (+, Ar-CH), 105.39 (quat. Ar-C), 100.32 (+, Ar-CH), 55.87 (+, OCH<sub>3</sub>), 49.44 (–, NCH<sub>2</sub>Ar), 46.72 (–, NCH<sub>2</sub>Ar (Benzyl)), 46.54 (–, NCH<sub>2</sub>CH), 36.47 (+, NCH<sub>2</sub>CH), 27.86 (+, NCH<sub>3</sub>). ESI-MS *m/z* (%): 435 [MH<sup>+</sup>-C<sub>5</sub>H<sub>8</sub>O] (100), 519 (11.65). RP-HPLC (220 nm): 98.4% (gradient: 0–30 min: MeCN/0.1% aq. TFA 20/80-95/5, 31-40 min: 95/5, t<sub>R</sub> = 13.3 min). HRMS (ESI) *m/z*: Calcd. 519.2238, found 519.2235.

**4-((8-(Benzyloxy)-4-methyl-3,5-dioxo-3,4,5,6-tetrahydro-2,6-methano[1,3]diazocino[5,6-*b*]indol-11(1*H*)-yl)methyl)-*N*-hydroxybenzamide (5c)**

As described above from 4-((8-(benzyloxy)-4-methyl-3,5-dioxo-3,4,5,6-tetrahydro-2,6-methano[1,3]diazocino[5,6-*b*]indol-11(1*H*)-yl)methyl)-*N*-((tetrahydro-2*H*-pyran-2-yl)oxy)benzamide (**27c**). Yield 0.15g (0.29 mmol; 44%). Colorless crystals; mp: 140.3–155.4 °C. IR (KBr): 1729, 1684, 1576 cm<sup>-1</sup>. <sup>1</sup>H NMR (300 MHz, DMSO-*d*<sub>6</sub>): δ 11.16 (s, 1H), 9.02 (s, 1H), 7.65 (d, *J* = 8.3 Hz, 2H), 7.48 (d, *J* = 6.8 Hz, 2H), 7.42 – 7.29 (m, 5H), 7.14 – 7.07 (m, 4H), 6.83 (dd, *J* = 8.9, 2.4 Hz, 1H), 5.36 (s, 2H), 5.08 (s, 2H), 4.83 (d, *J* = 16.7 Hz, 1H), 4.54 (d, *J* = 16.2 Hz, 1H), 3.89 (d, *J* = 12.9 Hz, 3H), 3.45 (d, *J* = 11.2 Hz, 1H), 2.90 (s, 3H). <sup>13</sup>C NMR (101 MHz, DMSO-*d*<sub>6</sub>) δ 173.56, 164.54, 161.48, 153.53, 141.27, 137.96, 135.34, 132.43, 131.70, 128.84, 128.17, 128.14, 127.71, 127.06, 126.66,

1  
2  
3 111.64, 105.41, 102.02, 70.35, 49.39, 46.73, 46.52, 36.50, 27.88. ESI-MS  $m/z$  (%):  
4 523.23 [MH<sup>+</sup>] (100), 1067.44 [2MNa<sup>+</sup>] (3.37). Anal. calcd for C<sub>29</sub>H<sub>26</sub>N<sub>4</sub>O<sub>5</sub> x 0.5 H<sub>2</sub>O: C,  
5 67.04; H, 5.24; N, 10.78; found: C 67.37; H 5.40; N 10.47.  
6  
7  
8  
9

10  
11 ***N*-Hydroxy-4-((9-methoxy-4-methyl-3,5-dioxo-3,4,5,6-tetrahydro-2,6-**  
12 **methano[1,3]diazocino[5,6-*b*]indol-11(*1H*)-yl)methyl)benzamide (5d)**  
13  
14

15  
16 As described above from 4-((9-methoxy-4-methyl-3,5-dioxo-3,4,5,6-tetrahydro-2,6-  
17 methano[1,3]diazocino[5,6-*b*]indol-11(*1H*)-yl)methyl)-*N*-((tetrahydro-2*H*-pyran-2-  
18 yl)oxy)benzamide (**27d**) (0.50 g; 0.97 mmol). Yield 0.18 g (0.41 mmol; 42 %) colorless  
19 crystals after crystallization from 0.5 N HCl<sub>aq</sub> / MeOH; mp: 169.4 -173.1 °C. IR (KBr):  
20 1725 cm<sup>-1</sup>. <sup>1</sup>H NMR (300 MHz DMSO-*d*<sub>6</sub>): δ 11.07 (s, 1H), 7.85 (s, 1H), 7.68 (d, *J* = 8.3  
21 Hz, 2H), 7.39 (d, *J* = 8.6 Hz, 1H), 7.14 (d, *J* = 8.3 Hz, 2H), 7.00 (d, *J* = 2.1 Hz, 1H), 6.73  
22 (dt, *J* = 6.6, 3.3 Hz, 1H), 5.40 (d, *J* = 17.5 Hz, 1H), 5.34 (d, *J* = 17.6 Hz, 1H), 4.79 (d, *J* =  
23 16.2 Hz, 1H), 4.49 (d, *J* = 16.2 Hz, 1H), 3.86 (d, *J* = 13.1 Hz, 1H), 3.79 (d, *J* = 18.6 Hz, 1H),  
24 3.71 (s, 3H), 3.41 (dd, *J* = 13.0, 1.9 Hz, 1H), 2.89 (s, 3H). <sup>13</sup>C NMR (75 MHz, DMSO-*d*<sub>6</sub>) δ  
25 173.10, 166.91, 163.71, 160.80, 155.90, 140.55, 136.64, 132.60, 131.68, 129.61, 127.14,  
26 126.55, 119.67, 118.35, 109.28, 105.23, 94.17, 55.32, 48.83, 46.14, 45.80, 35.82, 27.24.  
27 ESI-MS  $m/z$  (%): 435 [MH<sup>+</sup>] (100). Anal. calcd for C<sub>23</sub>H<sub>22</sub>N<sub>4</sub>O<sub>5</sub>: C 63.59; H 5.10; N 12.90;  
28 found: 63.25; H 5.07; N 12.75.  
29  
30  
31  
32  
33  
34  
35  
36  
37  
38  
39  
40  
41  
42  
43  
44  
45

46  
47 ***N*-Hydroxy-4-((8-hydroxy-4-methyl-3,5-dioxo-3,4,5,6-tetrahydro-2,6-**  
48 **methano[1,3]diazocino[5,6-*b*]indol-11(*1H*)-yl)methyl)benzamide (5e)**  
49  
50

51  
52 As described above from 4-((8-hydroxy-4-methyl-3,5-dioxo-3,4,5,6-tetrahydro-2,6-  
53 methano[1,3]diazocino[5,6-*b*]indol-11(*1H*)-yl)methyl)-*N*-((tetrahydro-2*H*-pyran-2-  
54  
55  
56  
57  
58  
59  
60

1  
2  
3 yl)oxy)benzamide (**27e**). Yield 0.10 g (0.24 mmol; 38 %) colorless crystals; mp: 259.8-  
4  
5 261.0 °C. IR (KBr): 2959, 1727, 1679, 1642, 1571  $\text{cm}^{-1}$ .  $^1\text{H}$  NMR (300 MHz,  $\text{DMSO-}d_6$ ):  $\delta$   
6  
7 11.17 (s, 1H), 9.02 (s, 1H), 8.89 (s, 1H), 7.65 (d,  $J = 8.2$  Hz, 2H), 7.18 (d,  $J = 8.8$  Hz, 1H),  
8  
9 7.11 (d,  $J = 8.2$  Hz, 2H), 6.86 (d,  $J = 2.2$  Hz, 1H), 6.58 (dd,  $J = 8.7, 2.3$  Hz, 1H), 5.31 (s,  
10  
11 2H), 4.81 (d,  $J = 16.5$  Hz, 1H), 4.52 (d,  $J = 16.5$  Hz, 1H), 3.87 (d,  $J = 12.9$  Hz, 1H), 3.75 (s,  
12  
13 2H), 4.81 (d,  $J = 16.5$  Hz, 1H), 4.52 (d,  $J = 16.5$  Hz, 1H), 3.87 (d,  $J = 12.9$  Hz, 1H), 3.75 (s,  
14  
15 1H), 3.43 (d,  $J = 13.2$  Hz, 1H), 2.89 (s, 3H).  $^{13}\text{C}$  NMR (101 MHz,  $\text{DMSO-}d_6$ )  $\delta$  173.67,  
16  
17 164.31, 161.38, 151.97, 141.43, 134.87, 132.30, 130.82, 127.67, 127.08, 126.99, 112.20,  
18  
19 111.30, 104.76, 102.47, 49.48, 46.79, 46.49, 36.60, 27.87. ESI-MS  $m/z$  (%): 421.15 [ $\text{MH}^+$ ]  
20  
21 (100), 841.29 [ $2\text{M}+\text{H}^+$ ] (27.57). Anal. calcd for  $\text{C}_{22}\text{H}_{20}\text{N}_4\text{O}_5 \times 0.33 \text{H}_2\text{O}$ : C 61.98; H 4.85;  
22  
23 N 13.15; found: 61.85; H 5.27; N 12.85.

24  
25  
26  
27 **4-(2-((11-(4-(Hydroxycarbamoyl)benzyl)-4-methyl-3,5-dioxo-1,3,4,5,6,11-hexahydro-**  
28  
29 **2,6-methano[1,3]diazocino[5,6-*b*]indol-8-yl)oxy)ethyl)morpholin-4-ium chloride (5f)**

30  
31  
32 To a stirred solution of 4-((4-methyl-8-(2-morpholinoethoxy)-3,5-dioxo-3,4,5,6-tetrahydro-  
33  
34 2,6-methano[1,3]diazocino[5,6-*b*]indol-11(1*H*)-yl)methyl)-*N*-((tetrahydro-2*H*-pyran-2-  
35  
36 yl)oxy)benzamide (**27f**) (1.15 g, 1.86 mmol) in  $\text{CH}_2\text{Cl}_2$  (40.0 mL) HCl in iso-propanol  
37  
38 (1.50 mL, 5-6N) was added dropwise. After 2 h stirring was stopped, the resulting solid  
39  
40 allowed to precipitate, the solvent decanted and the solid dissolved in the necessary amount  
41  
42 of MeOH. The solution obtained was added dropwise to a mixture of light petrol /  $\text{Et}_2\text{O}$   
43  
44 whilst stirring, the precipitating solid removed by filtration and the slightly wet solid dried  
45  
46 *in vacuo*. Yield 0.80 g (1.40 mmol, 75 %) pale yellow solid. mp: 158.4-162.0 °C. IR (KBr):  
47  
48 3433, 1671, 1468  $\text{cm}^{-1}$ ;  $^1\text{H}$  NMR (300 MHz,  $\text{DMSO-}d_6$ ):  $\delta$   $^1\text{H}$  NMR (300 MHz,  $\text{DMSO-}d_6$ )  
49  
50  $\delta$  11.19 (s, 1H), 10.75 (s, 1H), 9.03 (s, 1H), 7.66 (d,  $J = 8.2$  Hz, 2H), 7.35 (d,  $J = 8.9$  Hz,  
51  
52 1H), 7.09 (dd,  $J = 7.8, 5.3$  Hz, 3H), 6.83 (dd,  $J = 8.9, 2.3$  Hz, 1H), 5.38 (s, 2H), 4.84 (d,  $J =$   
53  
54  
55  
56  
57  
58  
59  
60

1  
2  
3 16.7 Hz, 1H), 4.56 (d,  $J = 16.5$  Hz, 1H), 4.37 (s, 2H), 4.02 – 3.72 (m, 6H), 3.50 (m, 5H),  
4  
5 3.28 – 3.15 (m, 2H), 2.90 (s, 3H).  $^{13}\text{C}$  NMR (101 MHz, DMSO- $d_6$ )  $\delta$  173.57 (s), 161.31 (s),  
6  
7 152.68 (s), 141.21 (s), 135.62 (s), 132.34 (s), 131.99 (s), 127.72 (s), 127.03 (s), 126.61 (s),  
8  
9 112.22 (s), 111.75 (s), 105.50 (s), 102.20 (s), 63.63 (s), 63.37 (s), 55.58 (s), 52.14 (s), 49.44  
10  
11 (s), 46.63 (d,  $J = 13.9$  Hz), 36.49 (s), 27.88 (s). ESI-MS  $m/z$  (%): 534.24 [ $\text{MH}^+$ ] (100). Anal.  
12  
13 calcd for  $\text{C}_{28}\text{H}_{32}\text{ClN}_5\text{O}_6 \times 1.75 \text{H}_2\text{O}$ : C 55.90; H 5.95; N 11.64; found: C 55.99; H 5.84; N  
14  
15 11.26.  
16  
17  
18  
19

20 **(*E*)-*N*-Hydroxy-3-(4-((4-Methyl-3,5-dioxo-3,4,5,6-tetrahydro-2,6-**  
21 **methano[1,3]diazocino[5,6-*b*]indol-11(*1H*)-yl)methyl)phenyl)acrylamide (6)**  
22  
23  
24

25 As described above from (*E*)-3-(4-((4-methyl-3,5-dioxo-3,4,5,6-tetrahydro-2,6-  
26 methano[1,3]diazocino[5,6-*b*]indol-11(*1H*)-yl)methyl)phenyl)-*N*-((tetrahydro-2*H*-pyran-2-  
27 yl)oxy)acrylamide (**86**). Yield 0.30 g (0.70 mmol; 72 %) colorless crystals; mp: 238.1-  
28 239.3 °C. IR (KBr): 3245, 1727, 1653  $\text{cm}^{-1}$ .  $^1\text{H}$  NMR (300 MHz, DMSO- $d_6$ ):  $\delta$  10.71 (s,  
29 1H), 9.07 (s, 1H), 7.61 – 7.34 (m, 5H), 7.16 – 6.96 (m, 4H), 6.40 (d,  $J = 15.8$  Hz, 1H), 5.37  
30 (s, 2H), 4.86 (d,  $J = 16.6$  Hz, 1H), 4.57 (d,  $J = 16.5$  Hz, 1H), 3.90 (d,  $J = 13.1$  Hz, 2H), 3.45  
31 (d,  $J = 11.3$  Hz, 1H), 2.89 (s, 3H).  $^{13}\text{C}$  NMR (75 MHz, DMSO- $d_6$ )  $\delta$  173.05, 162.62, 160.77,  
32 138.82, 137.76, 135.85, 134.13, 133.90, 127.74, 127.17, 125.60, 121.69, 119.73, 118.96,  
33 117.75, 110.24, 105.20, 48.85, 46.14, 45.95, 35.92, 27.34. ESI-MS  $m/z$  (%): 431 [ $\text{MH}^+$ ]  
34 (100). Anal. calcd for  $\text{C}_{24}\text{H}_{22}\text{N}_4\text{O}_4 \times \frac{2}{3} \text{H}_2\text{O}$ : C 65.15; H 5.32; N 12.66; found: C 64.94; H  
35 5.24; N 12.50.  
36  
37  
38  
39  
40  
41  
42  
43  
44  
45  
46  
47  
48  
49  
50

51 **(*E*)-*N*-Hydroxy-3-(3-((4-methyl-3,5-dioxo-3,4,5,6-tetrahydro-2,6-**  
52 **methano[1,3]diazocino[5,6-*b*]indol-11(*1H*)-yl)methyl)phenyl)acrylamide (7)**  
53  
54  
55  
56  
57  
58  
59  
60

As described above from (*E*)-3-(3-((4-methyl-3,5-dioxo-3,4,5,6-tetrahydro-2,6-methano[1,3]diazocino[5,6-*b*]indol-11(*1H*)-yl)methyl)phenyl)-*N*-((tetrahydro-2*H*-pyran-2-yl)oxy)acrylamide (**87**) (0.95 g; 1.84 mmol). Yield 0.25 g (0.56 mmol; 52 %) colorless crystals; mp: 218.1-219.0 °C. IR (KBr): 1727, 1684 cm<sup>-1</sup>. <sup>1</sup>H NMR (300 MHz, DMSO-*d*<sub>6</sub>): δ 10.77 (s, 1H), 9.06 (s, 1H), 7.56 – 7.25 (m, 6H), 7.17 – 6.98 (m, 3H), 6.41 (d, *J* = 15.8 Hz, 1H), 5.37 (s, 2H), 4.89 (d, *J* = 16.6 Hz, 1H), 4.61 (d, *J* = 16.5 Hz, 1H), 3.91 (d, *J* = 13.5 Hz, 2H), 3.48 (d, *J* = 11.2 Hz, 1H), 3.05 (dd, *J* = 13.1, 6.0 Hz, 1H), 2.90 (s, 3H). <sup>13</sup>C NMR (75 MHz, DMSO-*d*<sub>6</sub>) δ 173.06, 162.45, 160.80, 138.27, 135.82, 135.09, 134.20, 129.22, 127.67, 126.19, 126.06, 125.61, 121.69, 119.72, 119.40, 117.75, 110.27, 105.19, 48.90, 46.12, 45.34, 35.92, 27.32. ESI-MS *m/z* (%): 431 [MH<sup>+</sup>] (100). Anal. calcd for C<sub>24</sub>H<sub>22</sub>N<sub>4</sub>O<sub>4</sub> x H<sub>2</sub>O: C 64.28; H 5.39; N 12.49; found: C 64.60; H 5.58; N 12.37.

***N*-Hydroxy-4-((4-oxo-1,3,4,6,7,12*b*-hexahydroindolo[2,3-*a*]quinolizin-12(2*H*)-yl)methyl)benzamide (8)**

As described above from 4-((4-oxo-1,3,4,6,7,12*b*-hexahydroindolo[2,3-*a*]quinolizin-12(2*H*)-yl)methyl)-*N*-((tetrahydro-2*H*-pyran-2-yl)oxy)benzamide **92**. Yield 0.03 g (0.06 mmol, 64 %) colorless crystals after crystallization from MeOH / 0.5 N aqu. HCl; mp: 150.2-151.9 °C. IR (KBr): 2921, 1611 cm<sup>-1</sup>. <sup>1</sup>H NMR (300 MHz, acetone-*d*<sub>6</sub>): δ 10.91 (s, 1H), 8.45 (s, 1H), 7.77 (d, *J* = 8.3 Hz, 2H), 7.58 – 7.50 (m, 1H), 7.23 – 7.03 (m, 5H), 5.66 (d, *J* = 18.0 Hz, 1H), 5.49 (d, *J* = 18.0 Hz, 1H), 5.14 – 5.01 (m, 1H), 4.96 – 4.83 (m, 1H), 2.79 – 2.61 (m, 3H), 2.55 – 2.20 (m, 3H), 1.85 – 1.72 (m, 2H), 1.62 – 1.45 (m, 1H). <sup>13</sup>C-NMR (101 MHz, DMSO-*d*<sub>6</sub>): δ 169.05 (quat. CO), 168.01 (quat. CO), 141.83 (quat. Ar-C), 137.83 (quat. Ar-C), 136.06 (quat. Ar-C), 132.09 (quat. Ar-C), 127.67 (+, (Ar-CH)<sub>2</sub>), 126.73 (quat. Ar-C), 126.27 (+, (Ar-CH)<sub>2</sub>), 122.07 (+, Ar-CH), 119.84 (+, Ar-CH),

1  
2  
3 118.60 (+, Ar-CH), 110.57 (+, Ar-CH), 110.07 (quat. Ar-C), 54.24 (+,  
4 NCHCH<sub>2</sub>CH<sub>2</sub>CH<sub>2</sub>CO), 47.33 (-, NCH<sub>2</sub>Ar), 39.73 (-, NCH<sub>2</sub>CH<sub>2</sub>Ar), 32.11 (-,  
5 NCHCH<sub>2</sub>CH<sub>2</sub>CH<sub>2</sub>CO), 30.27 (-, NCHCH<sub>2</sub>CH<sub>2</sub>CH<sub>2</sub>CO), 21.69 (-, NCHCH<sub>2</sub>CH<sub>2</sub>CH<sub>2</sub>CO),  
6 19.28 (-, NCH<sub>2</sub>-CH<sub>2</sub>Ar). ESI-MS *m/z* (%): 390 [MH<sup>+</sup>] (100). RP-HPLC (220 nm): 98.1%  
7 (gradient: 0–30 min: MeCN/0.1% aq. TFA 20/80-95/5, 31-40 min: 95/5, *t<sub>R</sub>* = 15.1 min).  
8 HRMS (ESI) *m/z*: Calcd. 390.1812, found 390.1814.  
9  
10  
11  
12  
13  
14  
15  
16  
17

18 **(*E*)-*N*-Hydroxy-3-(4-((4-oxo-1,3,4,6,7,12*b*-hexahydroindolo[2,3-*a*]quinolizin-12(2*H*)-**  
19 **yl)methyl)phenyl)acrylamide (**9**)**  
20  
21  
22

23 As described above from (*E*)-3-(4-((4-Oxo-1,3,4,6,7,12*b*-hexahydroindolo[2,3-*a*]quinolizin-  
24 12(2*H*)-yl)methyl)phenyl)-*N*-((tetrahydro-2*H*-pyran-2-yl)oxy)acrylamide (**93**). Yield 0.05 g  
25 (0.11 mmol; 60 %) colorless crystals after crystallization from MeOH / 0.5 N aq. HCl; mp:  
26 185.0 – 188.0 °C. IR (KBr): 1703, 1652 cm<sup>-1</sup>. <sup>1</sup>H NMR (300 MHz, MeOD): δ 7.58 – 7.43  
27 (m, 4H), 7.19 – 6.96 (m, 5H), 6.41 (d, *J* = 15.8 Hz, 1H), 5.53 (d, *J* = 18.0 Hz, 1H), 5.38 (d,  
28 *J* = 18.0 Hz, 1H), 5.12 – 4.98 (m, 1H), 4.85 – 4.79 (m, 1H), 2.87 – 2.62 (m, 3H), 2.56 –  
29 2.28 (m, 3H), 1.86 – 1.63 (m, 2H), 1.60 – 1.41 (m, 1H). <sup>1</sup>H NMR (400 MHz, acetone-*D*<sub>6</sub>): δ  
30 7.61 – 7.48 (m, 4H), 7.22 – 7.17 (m, 1H), 7.13 – 7.03 (m, 4H), 6.54 (d, *J* = 15.8 Hz, 1H),  
31 5.54 (m, 2H), 5.13 – 5.04 (m, 1H), 4.84 – 4.94 (m, 1H), 2.85 – 2.64 (m, 3H), 2.58 – 2.48  
32 (m, 1H), 2.47 – 2.37 (m, 1H), 2.37 – 2.25 (m, 1H), 1.85 – 1.73 (m, 2H), 1.62 – 1.48 (m,  
33 1H). <sup>13</sup>C-NMR (101 MHz, DMSO-*d*<sub>6</sub>): δ 169.05 (quat. CO), 163.14 (quat. CO), 140.07  
34 (quat. Ar-C), 138.31 (quat. Ar-C), 137.88 (+, Ar-CH=CHCO), 136.05 (quat. Ar-C), 128.68  
35 (quat. Ar-C), 128.24 (+, (Ar-CH)<sub>2</sub>), 126.87 (+, (Ar-CH)<sub>2</sub>), 126.70 (quat. Ar-C), 125.48 (+,  
36 Ar-CH), 122.06 (+, Ar-CH), 119.81 (+, Ar-CH=CHCO, +, Ar-CH), 118.57 (+, Ar-CH),  
37 110.58 (+, Ar-CH), 110.03 (quat. Ar-C), 54.26 (+, NCHCH<sub>2</sub>CH<sub>2</sub>CH<sub>2</sub>CO), 47.38 (-,  
38  
39  
40  
41  
42  
43  
44  
45  
46  
47  
48  
49  
50  
51  
52  
53  
54  
55  
56  
57  
58  
59  
60

1  
2  
3 NCH<sub>2</sub>Ar), 39.77 (–, NCH<sub>2</sub>CH<sub>2</sub>Ar), 32.12 (–, NCHCH<sub>2</sub>CH<sub>2</sub>CH<sub>2</sub>CO), 30.28 (–,  
4 NCHCH<sub>2</sub>CH<sub>2</sub>CH<sub>2</sub>CO), 21.70 (–, NCHCH<sub>2</sub>CH<sub>2</sub>CH<sub>2</sub>CO), 19.29 (–, NCH<sub>2</sub>CH<sub>2</sub>Ar). ESI-MS  
5  
6 *m/z* (%): 416 [MH<sup>+</sup>] (100). Anal. calcd for C<sub>25</sub>H<sub>25</sub>N<sub>3</sub>O<sub>3</sub> x MeOH x H<sub>2</sub>O: C 67.08; H 6.71; N  
7  
8 9.03; found C 67.48; H 6.04; N 9.40.  
9  
10  
11

12  
13 ***N*-hydroxy-4-((9-methyl-8,10-dioxo-7,9,10,12-tetrahydro-7,11-  
14  
15  
16  
17  
18  
19  
20  
21  
22  
23  
24  
25  
26  
27  
28  
29  
30  
31  
32  
33  
34  
35  
36  
37  
38  
39  
40  
41  
42  
43  
44  
45  
46  
47  
48  
49  
50  
51  
52  
53  
54  
55  
56  
57  
58  
59  
60**  
**methanobenzo[*g*][1,3]diazocino[5,6-*b*]indol-13(8*H*)-yl)methyl)benzamide (10)**

According to GP3 from 4-((9-methyl-8,10-dioxo-7,9,10,12-tetrahydro-7,11-  
methanobenzo[*g*][1,3]diazocino[5,6-*b*]indol-13(8*H*)-yl)methyl)benzoic acid (**102**). The  
intermediate 4-((9-methyl-8,10-dioxo-7,9,10,12-tetrahydro-7,11-  
methanobenzo[*g*][1,3]diazocino[5,6-*b*]indol-13(8*H*)-yl)methyl)-*N*-((tetrahydro-2*H*-pyran-2-  
yl)oxy)benzamide was obtained in a yield of 0.45 g; 0.84 mmol (78 %) as a colorless foam  
after silica gel chromatography with CH<sub>2</sub>Cl<sub>2</sub> / EtOAc (1 : 1%). This crude product was  
used in the next step without further purification as described above. Yield 0.23 g; 0.51  
mmol (61 %) light beige crystals after crystallization from MeOH; mp: 193.4 – 194.4 °C  
(decomp.). IR (KBr): 3420, 1729, 1681 cm<sup>-1</sup>. <sup>1</sup>H NMR (300 MHz, DMSO-*d*<sub>6</sub>): δ 11.13 (s,  
1H), 9.00 (s, 1H), 8.14 – 8.05 (m, 1H), 7.97 – 7.89 (m, 1H), 7.72 (d, *J* = 8.6 Hz, 1H), 7.68 –  
7.56 (m, 3H), 7.38 – 7.30 (m, 2H), 7.03 (d, *J* = 8.0 Hz, 2H), 5.85 (s, 2H), 4.90 (d, *J* = 16.4  
Hz, 1H), 4.67 (d, *J* = 16.3 Hz, 1H), 4.04 (s, 1H), 4.01 – 3.93 (m, 1H), 3.62 – 3.49 (m, 1H),  
2.93 (s, 3H). <sup>13</sup>C NMR (75 MHz, DMSO-*d*<sub>6</sub>) δ 173.15, 163.81, 160.80, 140.67, 133.69,  
131.76, 130.80, 128.98, 128.64, 127.37, 125.54, 123.35, 122.90, 121.85, 121.49, 120.47,  
117.92, 106.88, 48.90, 48.88, 46.18, 35.83, 27.40. ESI-MS *m/z* (%): 455 [MH<sup>+</sup>] (100). Anal.  
calcd. for C<sub>26</sub>H<sub>22</sub>N<sub>4</sub>O<sub>4</sub> x H<sub>2</sub>O x MeOH: C 64.27; H 5.59; N 11.10; found: C 63.71; H 5.22;  
N 11.35.

1  
2  
3 ***N*-Hydroxy-4-((2-methyl-1,3-dioxo-2,3,5,6-tetrahydro-1*H*-imidazo[1',5':1,2]pyrido[4,3-**  
4 ***b*]indol-7(11*cH*)-yl)methyl)benzamide (11)**  
5  
6  
7

8  
9 As described above from 4-((2-Methyl-1,3-dioxo-2,3,5,6-tetrahydro-1*H*-  
10 imidazo[1',5':1,2]pyrido[4,3-*b*]indol-7(11*cH*)-yl)methyl)-*N*-((tetrahydro-2*H*-pyran-2-  
11 yl)oxy)benzamide (**36**). Yield 0.32 g (0.79 mmol; 79 %). mp: 248.1-251.7 °C; IR (KBr):  
12 3251, 1769, 1690, 1650cm<sup>-1</sup>; <sup>1</sup>H NMR (300 MHz, DMSO-*d*<sub>6</sub>): δ 11.14 (s, 1H), 9.02 (s,  
13 1H), 7.91 (dd, *J* = 6.6, 2.0 Hz, 1H), 7.65 (d, *J* = 8.2 Hz, 2H), 7.43 (d, *J* = 7.2 Hz, 1H), 7.20  
14 – 6.98 (m, 4H), 5.52 (s, 1H), 5.42 (s, 2H), 4.33 (dd, *J* = 13.5, 5.0 Hz, 1H), 3.28 – 3.19 (m,  
15 1H), 2.87 (s, 3H), 2.77 (d, *J* = 16.3 Hz, 2H). <sup>13</sup>C NMR (101 MHz, DMSO-*d*<sub>6</sub>) δ 171.93,  
16 164.41, 157.17, 141.53, 136.77, 134.41, 132.36, 127.76, 126.96, 124.85, 122.01, 120.44,  
17 120.01, 110.28, 103.24, 57.27, 45.96, 37.09, 25.03, 21.76. HRMS (ESI-MS) *m/z*: calcd.:  
18 405.1557 [MH<sup>+</sup>], found: 405.1558 [MH<sup>+</sup>]; Anal. calcd. for C<sub>22</sub>H<sub>20</sub>N<sub>4</sub>O<sub>4</sub> x 0.5 H<sub>2</sub>O: C 63.91;  
19 H 5.12; N 13.55; found: C 64.10; H 5.13; N 13.19.  
20  
21  
22  
23  
24  
25  
26  
27  
28  
29  
30  
31  
32  
33

34 ***N*-Hydroxy-4-((4-methyl-3-oxo-3,4,5,6-tetrahydro-2,6-methano[1,3]diazocino-[5,6-**  
35 ***b*]indol-11(1*H*)-yl)methyl)benzamide (12)**  
36  
37  
38  
39

40 0.20 g (0.42 mmol) of **42** were dissolved in 20 mL of MeOH, treated with 5 drops of 5N  
41 HCl in isopropanol and stirred at rt for 16 h. The solvent was removed under reduced  
42 pressure and the residue crystallized from MeOH. Yield 0.12 g (0.31 mmol, 74 %) colorless  
43 powder; mp: 245 °C. IR (KBr): 3454, 2838, 1623 cm<sup>-1</sup>. <sup>1</sup>H NMR (300 MHz, DMSO-*d*<sub>6</sub>): δ  
44 11.14 (s, 1H), 9.02 (s, 1H), 7.69 – 7.60 (m, 2H), 7.58 – 7.51 (m, 1H), 7.42 – 7.33 (m, 1H),  
45 7.17 – 6.98 (m, 4H), 5.44 – 5.24 (m, 2H), 4.68 (d, *J* = 16.5 Hz, 1H), 4.17 – 4.08 (m, 1H),  
46 3.78 – 3.66 (m, 1H), 3.45 – 3.38 (m, 2H), 3.29 – 3.11 (m, 2H), 2.71 (s, 3H). <sup>13</sup>C NMR (75  
47  
48  
49  
50  
51  
52  
53  
54  
55  
56  
57  
58  
59  
60

1  
2  
3 MHz, DMSO)  $\delta$  163.77, 162.92, 141.00, 136.20, 134.83, 131.69, 127.10, 126.56, 125.91,  
4  
5 121.06, 119.13, 117.60, 110.19, 109.97, 55.55, 48.87, 48.27, 45.77, 34.96, 25.86. ESI-MS  
6  
7  $m/z$  (%): 391 [MH]<sup>+</sup> (100). Anal. calcd for C<sub>22</sub>H<sub>22</sub>N<sub>4</sub>O<sub>3</sub> x 0.5 CH<sub>3</sub>OH: C 66.49; H 5.95; N  
8  
9 13.78; found: C 66.51; H 5.85; N 13.74.

10  
11  
12  
13 ***N*-Hydroxy-4-((4-methyl-3-oxo-5-thioxo-3,4,5,6-tetrahydro-2,6-**  
14  
15 **methano[1,3]diazocino[5,6-*b*]indol-11(*1H*)-yl)methyl)benzamide (13)**

16  
17  
18 As described above from 4-((4-methyl-3-oxo-5-thioxo-3,4,5,6-tetrahydro-2,6-  
19  
20 methano[1,3]diazocino[5,6-*b*]indol-11(*1H*)-yl)methyl)-*N*-((tetrahydro-2*H*-pyran-2-yl)oxy)  
21  
22 benzamide (**56**) (0.19 g; 0.38 mmol). Yield 0.10 g (0.23 mmol, 60 %) colorless crystals  
23  
24 from 0.5 N HCl<sub>aq</sub> / MeOH; mp: 169.2 – 170.7 °C; IR (KBr): 3252, 1702 cm<sup>-1</sup>. <sup>1</sup>H NMR  
25  
26 (300 MHz, DMSO-*d*<sub>6</sub>):  $\delta$  11.17 (s, 1H), 9.03 (s, 1H), 7.72 – 7.61 (m, 3H), 7.41 (dd, *J* = 6.5,  
27  
28 2.2 Hz, 1H), 7.22 – 7.02 (m, 4H), 5.56 – 5.30 (m, 2H), 4.94 (dd, *J* = 16.5, 5.3 Hz, 1H), 4.61  
29  
30 (d, *J* = 16.4 Hz, 1H), 4.44 (s, 1H), 3.91 (d, *J* = 12.8 Hz, 1H), 3.50 (dd, *J* = 13.1, 2.1 Hz, 1H),  
31  
32 3.30 (s, 3H). <sup>13</sup>C-NMR (101 MHz, DMSO-*d*<sub>6</sub>):  $\delta$  210.18 (quat. CS), 164.26 (quat. CO),  
33  
34 158.69 (quat. CO), 141.13 (quat. Ar-C), 136.46 (quat. Ar-C), 134.56 (quat. Ar-C), 132.37  
35  
36 (quat. Ar-C), 127.70 (+, (Ar-CH)<sub>2</sub>), 127.15 (+, (Ar-CH)<sub>2</sub>), 126.23 (quat. Ar-C), 122.19 (+,  
37  
38 Ar-CH), 120.29 (+, Ar-CH), 119.09 (+, Ar-CH), 110.82 (+, Ar-CH), 107.22 (quat. Ar-C),  
39  
40 50.23 (–, NCH<sub>2</sub>Ar), 47.61 (–, NCH<sub>2</sub>CH), 46.35 (–, NCH<sub>2</sub>Ar (Benzyl)), 35.05 (–,  
41  
42 NCH<sub>2</sub>CH), 32.16 (+, NCH<sub>3</sub>). ESI-MS  $m/z$  (%): 421 [MH<sup>+</sup>] (100). RP-HPLC (220 nm): 99.5  
43  
44 % (gradient: 0–30 min: MeCN/0.1% aq. TFA 20/80-95/5, 31-40 min: 95/5, tR = 21.1 min).  
45  
46  
47  
48  
49  
50  
51 HRMS (ESI)  $m/z$ : Calcd. 421.1329, found 421.1334.  
52  
53  
54  
55  
56  
57  
58  
59  
60

1  
2  
3 ***N*-Hydroxy-4-((4-methyl-5-oxo-3,4,5,6-tetrahydro-2,6-methano[1,3]diazocino-[5,6-**  
4  
5 ***b*]indol-11(*1H*)-yl)methyl)benzamide (14a)**  
6  
7

8 According to Saiga *et al.*<sup>77</sup> 2.15 g (31.00 mmol) of hydroxylamine hydrochloride were  
9 dissolved in 11.0 mL of MeOH by heating. A solution of 2.58 g (46.00 mmol) KOH in  
10 7 mL of MeOH was added and the mixture was stirred for 30 min at rt. The precipitate  
11 formed was filtered off and 1.58 g (4.05 mmol) of **46a** were dissolved in the filtrate. After 2  
12 days of stirring at rt the solution was adjusted to pH 6-7 with acetic acid and the solvent  
13 removed *in vacuo*. The residue was purified by cc on a short column (SiO<sub>2</sub>, EtOAc / MeOH  
14 2:1). When distilling off the solvent precipitation of a colorless solid occurred. It was  
15 filtered off, washed with MeOH and dried. 1.18 g (3.02 mmol; 75 %) colorless crystals; mp:  
16 190 °C (decomp.). IR (KBr): 3188, 2921, 1626 cm<sup>-1</sup>. <sup>1</sup>H NMR (300 MHz, DMSO-*d*<sub>6</sub>): δ  
17 11.15 (s, 1H), 9.02 (s, 1H), 7.70 – 7.62 (m, 2H), 7.57 – 7.48 (m, 1H), 7.38 – 7.31 (m, 1H),  
18 7.13 – 6.97 (m, 4H), 5.47 – 5.20 (m, 2H), 4.53 (d, *J* = 12.0 Hz, 1H), 4.38 (d, *J* = 17.9 Hz,  
19 1H), 4.20 – 4.11 (m, 2H), 3.57 – 3.44 (m, 2H), 3.12 (d, *J* = 12.7 Hz, 1H), 2.58 (s, 3H). <sup>13</sup>C  
20 NMR (75 MHz, DMSO) δ 169.39, 163.85, 141.00, 135.83, 134.11, 131.71, 127.18, 126.40,  
21 125.58, 120.87, 119.09, 117.98, 110.65, 109.61, 72.39, 50.67, 48.31, 45.75, 35.03, 29.64.  
22 ESI-MS *m/z* (%): 391 [MH]<sup>+</sup> (100). Anal. calcd for C<sub>22</sub>H<sub>22</sub>N<sub>4</sub>O<sub>3</sub> x 1.25 CH<sub>3</sub>OH: C 64.87; H  
23 6.32; N 13.01; found: C 64.67; H 6.15; N 13.15.  
24  
25  
26  
27  
28  
29  
30  
31  
32  
33  
34  
35  
36  
37  
38  
39  
40  
41  
42  
43  
44  
45

46 ***N*-Hydroxy-4-((8-methoxy-4-methyl-5-oxo-3,4,5,6-tetrahydro-2,6-**  
47 **methano[1,3]diazocino[5,6-*b*]indol-11(*1H*)-yl)methyl)benzamide (14b)**  
48  
49  
50

51 1.82 g (26.4 mmol) of hydroxylamine hydrochloride were dissolved in 10 mL of MeOH by  
52 heating. A solution of 2.19 (39.0 mmol) KOH in 6 mL of MeOH was added and the mixture  
53  
54  
55  
56  
57  
58  
59  
60

1  
2  
3 stirred for 30 min at rt. The precipitate was filtered off and 1.44 g (3:43 mmol) of **46b** were  
4 dissolved in the filtrate. After 2 days of stirring at rt the solution was adjusted to pH 6-7  
5 with acetic acid and the solvent removed *in vacuo*. When distilling off the solvent  
6 precipitation of a colorless solid occurred. It was filtered off, washed with MeOH and dried.  
7  
8 Crystallization from MeOH yielded 0.85 g (2.17 mmol; 63 %) colorless crystals; mp:  
9  
10 162 °C (decomp.). IR (KBr): 3202, 2940, 1631  $\text{cm}^{-1}$ .  $^1\text{H}$  NMR (300 MHz,  $\text{DMSO-}d_6$ ):  $\delta$   
11 11.16 (s, 1H), 9.03 (s, 1H), 7.65 (d,  $J = 8.0$  Hz, 2H), 7.23 (d,  $J = 8.8$  Hz, 1H), 7.06 (d,  $J =$   
12 8.0 Hz, 2H), 7.00 (d,  $J = 2.4$  Hz, 1H), 6.67 (dd,  $J = 8.7, 2.4$  Hz, 1H), 5.42 – 5.15 (m, 2H),  
13 4.52 (d,  $J = 12.0$  Hz, 1H), 4.35 (d,  $J = 17.9$  Hz, 1H), 4.19 – 4.07 (m, 2H), 3.75 (s, 3H), 3.51  
14 (d,  $J = 12.7$  Hz, 1H), 3.45 (s, 1H), 3.10 (d,  $J = 12.9$  Hz, 1H), 2.59 (s, 3H).  $^{13}\text{C}$  NMR (75  
15 MHz,  $\text{DMSO-}d_6$ )  $\delta$  169.51, 163.90, 153.56, 141.12, 134.66, 131.65, 130.99, 127.16, 126.33,  
16 125.98, 110.35, 100.19, 72.36, 55.27, 50.72, 48.35, 45.81, 35.00, 29.62. ESI-MS  $m/z$  (%):  
17 421  $[\text{MH}]^+$  (100). Anal. calcd for  $\text{C}_{23}\text{H}_{24}\text{N}_4\text{O}_4 \times 1.5 \text{CH}_3\text{OH}$ : C 62.81; H 6.45; N 11.96;  
18 found: C 62.58; H 6.20; N 11.83.  
19  
20  
21  
22  
23  
24  
25  
26  
27  
28  
29  
30  
31  
32  
33  
34  
35

36 ***N*-Hydroxy-4-((4-methyl-5-oxo-3-thioxo-3,4,5,6-tetrahydro-2,6-**  
37 **methano[1,3]diazocino[5,6-*b*]indol-11(*1H*)-yl)methyl)benzamide(15)**  
38  
39  
40

41 As described above from 4-((4-methyl-5-oxo-3-thioxo-3,4,5,6-tetrahydro-2,6-  
42 methano[1,3]diazocino[5,6-*b*]indol-11(*1H*)-yl)methyl)-*N*-((tetrahydro-2*H*-pyran-2-  
43 yl)oxy)benzamide (**52**) (0.42 g; 0.83 mmol). Yield 0.31 g (0.73 mmol; 88 %) slightly  
44 yellow crystals after crystallization from 0.5 N  $\text{HCl}_{\text{aq}}$  / MeOH. mp: 176.4-178.1 °C.  
45 IR (KBr): 1718, 1653  $\text{cm}^{-1}$ .  $^1\text{H}$  NMR (300 MHz,  $\text{DMSO-}d_6$ ):  $\delta$  11.17 (s, 1H), 9.01 (s, 1H),  
46 7.65 (d,  $J = 8.2$  Hz, 2H), 7.60 – 7.44 (m, 1H), 7.43 – 7.36 (m, 1H), 7.18 (d,  $J = 8.2$  Hz, 2H),  
47 7.14 – 6.92 (m, 2H), 5.56 (d,  $J = 16.1$  Hz, 1H), 5.44 (d,  $J = 14.6$  Hz, 2H), 5.06 (d,  $J = 16.0$   
48  
49  
50  
51  
52  
53  
54  
55  
56  
57  
58  
59  
60

1  
2  
3 Hz, 1H), 4.08 (d,  $J = 12.6$  Hz, 1H), 3.98 (s, 1H), 3.78 (dd,  $J = 12.8, 1.9$  Hz, 1H), 3.23 (s,  
4  
5 3H).  $^{13}\text{C}$ -NMR (101 MHz, DMSO- $d_6$ ):  $\delta$  193.01 (quat. CS), 170.39 (quat. CO), 164.23  
6  
7 (quat. CO), 154.53 (quat. COCH<sub>3</sub>), 141.06 (quat. Ar-C), 135.71 (quat. Ar-C), 132.31 (quat.  
8  
9 Ar-C), 131.44 (quat. Ar-C), 127.61 (+, (Ar-CH)<sub>2</sub>), 127.17 (+, (Ar-CH)<sub>2</sub>), 126.59 (quat. Ar-  
10  
11 C), 111.95 (+, Ar-CH), 111.74 (+, Ar-CH), 103.96 (quat. Ar-C), 100.23 (+, Ar-CH), 55.88  
12  
13 (+, COCH<sub>3</sub>), 49.07 (-, NCH<sub>2</sub>Ar), 48.45 (-, NCH<sub>2</sub>CH), 46.65 (-, NCH<sub>2</sub>Ar (Benzyl)), 36.48  
14  
15 (+, NCH<sub>2</sub>CH), 33.64 (+, NCH<sub>3</sub>). ESI-MS  $m/z$  (%): 421 [MH<sup>+</sup>] (100). Anal. calcd for  
16  
17 C<sub>22</sub>H<sub>20</sub>N<sub>4</sub>O<sub>5</sub> x  $\frac{1}{3}$  H<sub>2</sub>O: C 61.96; H 4.88, N 13.14, S 7.52; found: C 61.92; H 4.90; N 13.00,  
18  
19 S 7.43.  
20  
21  
22  
23

#### 24 25 **Methyl 2,3,4,9-tetrahydro-1*H*-pyrido[3,4-*b*]indole-4-carboxylate hydrochloride (16a)**<sup>77</sup>

26  
27 Methyl 3-amino-2-(1*H*-indol-3-yl)propanoate hydrochloride (**79a**)<sup>31</sup> (2.54 g; 10.00 mmol)  
28  
29 and formaldehyde (**43**) (12.00 mmol; 1.06 mL 35 % in H<sub>2</sub>O) were dissolved in MeOH and  
30  
31 heated to 60 °C for 1 h. The solution was cooled to rt and stirred overnight. After addition  
32  
33 of Et<sub>2</sub>O (20.0 mL) the colorless product was filtered off, washed with Et<sub>2</sub>O and dried.  
34  
35 Yield 2.29 g (86 %) colorless crystals. mp: 245.3-245.4 °C. IR (KBr): 3166, 1729 cm<sup>-1</sup>.  
36  
37  $^1\text{H}$  NMR (300 MHz, DMSO- $d_6$ ):  $\delta$  11.28 (s, 1H), 9.38 (s, 2H), 7.52 (d,  $J = 7.7$  Hz, 1H),  
38  
39 7.39 (d,  $J = 8.0$  Hz, 1H), 7.12 (dd,  $J = 11.0, 4.1$  Hz, 1H), 7.05 (dd,  $J = 10.9, 4.0$  Hz, 1H),  
40  
41 4.43 – 4.27 (m, 2H), 4.24 (t,  $J = 4.8$  Hz, 1H), 3.71 (dd, 1H,  $J = 12.9, 4.6$  Hz, 1H), 3.70 (s,  
42  
43 3H), 3.53 (dd,  $J = 12.9, 5.3$  Hz, 1H). ESI-MS  $m/z$  (%): 272 [MH<sup>+</sup> + CH<sub>3</sub>CN] (100),  
44  
45 231 [MH<sup>+</sup>] (65).  
46  
47  
48  
49  
50

#### 51 52 **Methyl 2-(methylcarbamoyl)-2,3,4,9-tetrahydro-1*H*-pyrido[3,4-*b*]indole-4-carboxylate** 53 54 **(19a)**

1  
2  
3 Methyl 2,3,4,9-tetrahydro-1*H*-pyrido[3,4-*b*]indole-4-carboxylate hydrochloride (**16a**)  
4 (0.67 g; 2.50 mmol) was suspended in MeCN (13.4 mL). With stirring  
5  
6 diisopropylethylamine (2.5 mL) was added. After addition of *N*-succinimidyl-*N*-methyl-  
7  
8 carbamate (**18**) (0.52 g; 3.00 mmol) stirring was continued for 16 h atrt. The mixture was  
9  
10 poured into water and the crude product was extracted with EtOAc (3 x 50 mL). The  
11  
12 combined organic layers were dried (Na<sub>2</sub>SO<sub>4</sub>) and evaporated. Crystallization from EtOAc  
13  
14 yielded 0.66 g (2.30 mmol; 92 %) colorless crystals; mp: 202.5-203.1 °C. IR (KBr): 3380,  
15  
16 3275, 2945, 1716 cm<sup>-1</sup>. <sup>1</sup>H NMR (300 MHz, DMSO-*d*<sub>6</sub>): δ 11.06 (s, 1H), 7.33 (d, *J* = 8.0  
17  
18 Hz, 2H), 7.10 – 7.01 (m, 1H), 7.00 – 6.89 (m, 1H), 6.65 (q, *J* = 4.0 Hz, 1H), 4.61 (d, *J* =  
19  
20 16.4 Hz, 1H), 4.51 (d, *J* = 16.2 Hz, 1H), 4.03 – 3.87 (m, 2H), 3.73 (dd, *J* = 12.7, 3.9 Hz,  
21  
22 1H), 3.64 (s, 3H), 2.61 (d, *J* = 4.3 Hz, 3H). <sup>13</sup>C NMR (101 MHz, DMSO): δ 173.35, 158.53,  
23  
24 136.39, 133.48, 126.57, 121.31, 119.28, 118.29, 111.60, 105.28, 52.16, 44.56, 41.96, 39.00,  
25  
26 27.74. ESI-MS *m/z* (%): 575 [2M+H<sup>+</sup>] (100), 288 [MH<sup>+</sup>] (35). Anal. calcd for C<sub>15</sub>H<sub>17</sub>N<sub>3</sub>O<sub>3</sub>:  
27  
28 C 62.71; H 5.96; N 14.63; found: C 62.39; H 6.26; N 14.62.  
29  
30  
31  
32  
33  
34  
35

#### 36 **4-Methyl-6,11-dihydro-2,6-methano[1,3]diazocino[5,6-*b*]indole-3,5(1*H*,4*H*)-dione (20a)**

37  
38  
39 To a solution of methyl 2-(methylcarbamoyl)-2,3,4,9-tetrahydro-1*H*-pyrido[3,4-*b*]indole-4-  
40  
41 carboxylate (**19a**) (0.48 g; 1.67 mmol) in dioxane (50 mL) was added Cs<sub>2</sub>CO<sub>3</sub> (1.20 equ.,  
42  
43 0.65 g; 2.00 mol) under nitrogen atmosphere. After being stirred for 4 h under reflux, the  
44  
45 mixture was filtered. The clear solution was charged with silica gel (5-10 mL) and the  
46  
47 solvent was removed under reduced pressure. Silica gel chromatography by “dry load  
48  
49 method” afforded the desired product. Yield 0.31 g (1.21 mmol; 72 %) colorless crystals  
50  
51 after cc (SiO<sub>2</sub>; CH<sub>2</sub>Cl<sub>2</sub>, EtOAc; 1:1) from EtOAc; mp: 248.7-249.0 °C. IR (KBr): 3357,  
52  
53 1717, 1687 cm<sup>-1</sup>. <sup>1</sup>H NMR (300 MHz DMSO-*d*<sub>6</sub>): δ 11.14 (s, 1H), 7.48 (d, *J* = 7.4 Hz, 1H),  
54  
55  
56  
57  
58  
59  
60

1  
2  
3 7.34 (d,  $J = 7.4$  Hz, 1H), 7.00-7.11 (m, 2H), 4.67 (s, 2H), 3.89 (dd,  $J = 13.1, 1.2$  Hz, 1H),  
4  
5 3.82 (s, 1H), 3.44 (dd,  $J = 13.1, 2.3$  Hz, 1H), 2.89 (s, 3H).  $^{13}\text{C}$ -NMR (101 MHz,  $\text{DMSO-}d_6$ ):  
6  
7  $\delta$  173.74 (quat. CO), 161.51 (quat. CO), 136.01 (quat. Ar-C), 133.57 (quat. Ar-C), 126.24  
8  
9 (quat. Ar-C), 121.89 (+, Ar-CH), 119.75 (+, Ar-CH), 117.93 (+, Ar-CH), 112.04 (+, Ar-  
10  
11 CH), 105.33 (quat. Ar-C), 50.10 (-,  $\text{NCH}_2\text{Ar}$ ), 46.97 (-,  $\text{NCH}_2\text{CH}$ ), 36.53 (+,  $\text{NCH}_2\text{CH}$ ),  
12  
13 27.82 (+,  $\text{NCH}_3$ ). ESI-MS  $m/z$  (%): 297 [ $\text{MH}^+ + \text{CH}_3\text{CN}$ ] (100), 256 [ $\text{MH}^+$ ] (7). Anal. calcd  
14  
15 for  $\text{C}_{14}\text{H}_{13}\text{N}_3\text{O}_2$ : C 65.87; H 5.13; N 16.46; found: C 65.69; H 5.28; N 16.32.  
16  
17  
18  
19

20 **General procedure 1. Modification a (GP1a):** Under nitrogen a solution of the carboline  
21  
22 derivative (2.00 mmol) in DMF (10.0 mL) was cooled to 0 °C. After addition of NaH (2.20  
23  
24 mmol; 60 % in paraffin) the mixture was stirred for 10 min. The alkylating agent (2.20  
25  
26 mmol) was added and stirring at rt continued until completion of the reaction (TLC). The  
27  
28 mixture was poured into water. The crude product was isolated by filtration or extraction of  
29  
30 the aqueous phase with  $\text{CH}_2\text{Cl}_2$  (4 x 50.0 mL). In both cases silica gel chromatography  
31  
32 afforded the desired product.  
33  
34  
35  
36

37 ***tert*-Butyl 4-((4-methyl-3,5-dioxo-3,4,5,6-tetrahydro-2,6-methano[1,3]diazocino[5,6-**  
38  
39 ***b*]indol-11(1*H*)-yl)methyl)benzoate (22a)**  
40  
41

42 According to GP1a from 4-methyl-6,11-dihydro-2,6-methano[1,3]diazocino[5,6-*b*]indole-  
43  
44 3,5-(1*H*,4*H*)-dione (**20a**) (0.51 g; 2.00 mmol) and *tert*-butyl 4-(bromomethyl)benzoate  
45  
46 (**21**)<sup>78</sup>. Yield 0.65 g (1.46 mmol; 73 %) colorless crystals after recrystallization from  
47  
48  $\text{CH}_2\text{Cl}_2$ /n-heptane; mp: 191.5-191.9 °C. IR (KBr): 1714, 1687  $\text{cm}^{-1}$ .  $^1\text{H}$  NMR (300 MHz  
49  
50  $\text{DMSO-}d_6$ ):  $\delta$  7.82 (d,  $J = 8.3$  Hz, 2H), 7.53 (dd,  $J = 6.2, 2.5$  Hz, 1H), 7.41 (dd,  $J = 6.5, 2.1$   
51  
52 Hz, 1H), 7.16 (d,  $J = 8.5$  Hz, 2H), 7.12 – 6.95 (m, 2H), 5.45 (s, 2H), 4.83 (d,  $J = 16.6$  Hz,  
53  
54  
55  
56  
57  
58  
59  
60

1  
2  
3 1H), 4.54 (d,  $J = 16.6$  Hz, 1H), 3.90 (d,  $J = 12.1$  Hz, 2H), 3.45 (dd,  $J = 13.6, 2.6$  Hz, 1H),  
4  
5 2.89 (s, 3H), 1.51 (s, 9H).  $^{13}\text{C}$  NMR (101 MHz, DMSO- $d_6$ ):  $\delta$  173.58, 165.07, 161.32,  
6  
7 143.10, 136.46, 134.74, 130.92, 129.89, 127.25, 126.19, 122.29, 120.33, 118.33, 110.75,  
8  
9 105.94, 81.17, 49.37, 46.68, 46.50, 36.48, 28.21, 27.89. ESI-MS  $m/z$  (%): 463 [ $\text{MNH}_4^+$ ]  
10  
11 (70), 446 [ $\text{MH}^+$ ] (100). Anal. calcd from  $\text{C}_{26}\text{H}_{27}\text{N}_3\text{O}_4$ : C 70.09; H 6.11; N 9.43; found: C  
12  
13 70.02; H 6.02; N 9.35.  
14  
15  
16  
17

18 **General procedure 2. (GP2):** Deprotection of *tert*-butyl carbamates. A solution of the *tert*-  
19  
20 butyl carbamate (0.50 mmol) in trifluoroacetic acid (5.0 mL) was stirred for 15 min at rt.  
21  
22 After completion of the reaction (TLC monitoring) the mixture was poured into water. The  
23  
24 carboxylic acid was collected by filtration und dried. If the molecule contains an  
25  
26 amino group, the excess of trifluoroacetic acid was removed under reduced pressure and the  
27  
28 product was obtained as its trifluoroacetic acid salt.  
29  
30  
31  
32

33 **4-((4-Methyl-3,5-dioxo-3,4,5,6-tetrahydro-2,6-methano[1,3]diazocino[5,6-*b*]indol-**  
34  
35 **11(1*H*)-yl)methyl)benzoic acid (24a)**  
36  
37

38 According to GP2 from *tert*-butyl 4-((4-methyl-3,5-dioxo-3,4,5,6-tetrahydro-2,6-  
39  
40 methano[1,3]diazocino[5,6-*b*]indol-11(1*H*)-yl)methyl)benzoate (**22a**) (0.50 g; 1.12 mmol).  
41  
42 0.44 g (1.11 mmol; 99 %) colorless crystals; mp: 285.1-286.0 °C. IR (KBr): 1726, 1684  $\text{cm}^{-1}$   
43  
44  $^1\text{H}$  NMR (300 MHz, DMSO- $d_6$ ):  $\delta$  12.93 (s, 1H), 7.86 (d,  $J = 8.3$  Hz, 2H), 7.53 (dd,  $J =$   
45  
46 6.4, 2.3 Hz, 1H), 7.42 (dd,  $J = 6.7, 1.9$  Hz, 1H), 7.16 (d,  $J = 8.3$  Hz, 2H), 7.13 – 6.98 (m,  
47  
48 2H), 5.45 (s, 2H), 4.83 (d,  $J = 16.6$  Hz, 1H), 4.55 (d,  $J = 16.5$  Hz, 1H), 3.90 (d,  $J = 11.9$  Hz,  
49  
50 2H), 3.45 (dd,  $J = 13.4, 2.5$  Hz, 1H), 2.89 (s, 3H).  $^{13}\text{C}$  NMR (101 MHz, DMSO- $d_6$ )  $\delta$   
51  
52 173.58, 167.44, 161.31, 143.08, 136.48, 134.76, 130.35, 130.27, 127.21, 126.17, 122.31),  
53  
54  
55  
56  
57  
58  
59  
60

1  
2  
3 120.34, 118.34, 110.76, 105.92, 49.36, 46.59, 36.48, 27.88. ESI-MS  $m/z$  (%): 431 [MH<sup>+</sup>+  
4 CH<sub>3</sub>CN] (80), 390 [MH<sup>+</sup>] (100). Anal. calcd for C<sub>22</sub>H<sub>19</sub>N<sub>3</sub>O<sub>4</sub> x ¼ H<sub>2</sub>O: C 67.08; H 4.99; N  
5 10.67; found: C 67.03; H 4.97; N 10.34.  
6  
7  
8  
9

10 **General procedure 3. (GP3):** The carboxylic acid (0.50 mmol) was dissolved in DMF  
11 (5.00 mL). After addition of benzotriazol-1-yloxy-tris (dimethylamino)  
12 phosphoniumhexafluorophosphate (**25**, BOP) (0.50 mmol), triethylamine (1.50 mmol) and  
13 *O*-(tetrahydro-2*H*-pyran-2-yl)hydroxylamine (**26**) (2.00 mmol) the mixture was stirred at rt  
14 until the reaction was completed (TLC monitoring). If the product crystallized, it was  
15 filtered off and dried in vacuo. Alternatively, the mixture was extracted with CH<sub>2</sub>Cl<sub>2</sub> (4 x  
16 25.0 mL), the combined organic phases were washed with brine (25.0 mL) and dried over  
17 Na<sub>2</sub>SO<sub>4</sub>. The solvent was removed and the residue dried *in vacuo*. Purification by  
18 chromatography on silica gel using (CH<sub>2</sub>Cl<sub>2</sub>, EtOAc (1:2)) or the indicated eluent.  
19  
20  
21  
22  
23  
24  
25  
26  
27  
28  
29  
30  
31

32 **4-((4-Methyl-3,5-dioxo-3,4,5,6-tetrahydro-2,6-methano[1,3]diazocino[5,6-*b*]indol-  
33 11(1*H*)-yl)methyl)-*N*-((tetrahydro-2*H*-pyran-2-yl)oxy)benzamide (**27a**)**  
34

35 According to GP3 from 4-((4-methyl-3,5-dioxo-3,4,5,6-tetrahydro-2,6-  
36 methano[1,3]diazocino[5,6-*b*]indol-11(1*H*)-yl)methyl) benzoic acid (**24a**) (0.45 g; 1.16  
37 mmol). Yield 0.37 g (0.76 mmol; 65 %) colorless crystals from CH<sub>2</sub>Cl<sub>2</sub> by addition of  
38 heptane; mp: 197.7-198.5 °C. IR (KBr): 2952, 1727, 1680 cm<sup>-1</sup>. <sup>1</sup>H NMR (300 MHz,  
39 DMSO-*d*<sub>6</sub>): δ 11.59 (s, 1H), 7.68 (d, *J* = 8.3 Hz, 2H), 7.52 (dd, *J* = 6.3, 2.4 Hz, 1H), 7.41  
40 (dd, *J* = 6.6, 2.0 Hz, 1H), 7.15 (d, *J* = 8.3 Hz, 2H), 7.12 – 6.99 (m, 2H), 5.42 (s, 1H), 4.96  
41 (s, 1H), 4.86 (d, *J* = 16.6 Hz, 1H), 4.56 (d, *J* = 16.5 Hz, 1H), 4.07-3.96 (m, 1H), 3.90 (d, *J* =  
42 12.8 Hz, 2H), 3.47 (t, *J* = 11.4 Hz, 2H), 2.90 (s, 3H), 1.70 (s, 3H), 1.53 (s, 3H). <sup>13</sup>C NMR  
43  
44  
45  
46  
47  
48  
49  
50  
51  
52  
53  
54  
55  
56  
57  
58  
59  
60

(101 MHz, DMSO-*d*<sub>6</sub>)  $\delta$  173.59 (s), 161.33 (s), 142.10 – 140.90 (m), 136.42 (s), 134.75 (s), 132.15 – 131.76 (m), 128.09 (s), 127.13 (s), 126.19 (s), 122.27 (s), 120.32 (s), 118.33 (s), 110.80 (s), 105.86 (s), 101.44 (s), 61.85 (s), 49.42 (s), 46.70 (s), 46.49 (s), 36.49 (s), 28.33 (s), 27.90 (s), 25.17 (s), 18.76 (s). ESI-MS *m/z* (%): 506 [MNH<sub>4</sub><sup>+</sup>] (38), 489 [MH<sup>+</sup>] (100). Anal. calcd for C<sub>27</sub>H<sub>28</sub>N<sub>4</sub>O<sub>5</sub>: C, 66.38; H, 5.78; N, 11.47; found: C, 65.57, H, 5.97, N, 11.16.

### Cell culture and treatment conditions

MV4-11, HEL, Jurkat and BV173 cells were maintained in Roswell Park Memorial Institute (RPMI) medium containing 10 % fetal calf serum (Gibco) and 1% penicillin/streptomycin (Sigma). HEK293T cells were grown in Dulbecco's Modified Eagle's medium (DMEM) (Sigma) containing the same additives. All cells were cultured at 37 °C and 5% CO<sub>2</sub> atmosphere. For further details see supporting information.

### Western blot and antibodies

For details please see supporting information.

### Molecular Modeling

Models were generated with the modeling suite SYBYL-X 2.0 (Certara, L.P., St. Louis, USA). Docking approaches were based on the crystal structure of zebrafish HDAC6 CD II in complex with N-hydroxy-4-[[2-hydroxyethyl)(phenylacetyl)amino]methyl]benzamid (PDB 5WGK)<sup>36b</sup>. Both enantiomers of Marbostat-100 (**5a**) were manually docked retaining the binding mode of the phenylhydroxamic acid moiety of the cocrystallized inhibitor. Models were prepared as follows: Hydrogens were added and charges were assigned (proteins and water molecules – AMBER\_FF99, ligands – Gasteiger-Hueckel, Zn<sup>2+</sup> ion –

1  
2  
3 formal charge of 2). Complexes were refined in two steps: First, minimization with fixed  
4 inhibitor using the AMBER\_FF99 force field.<sup>79</sup> Second, subset minimization of Marbostat-  
5 100 and the surrounding (distance up to 6 Å) protein residues (Tripos force field<sup>80</sup>). In both  
6  
7  
8  
9  
10  
11  
12  
13  
14  
15  
16  
17  
18  
19  
20  
21  
22  
23  
24  
25  
26  
27  
28  
29  
30  
31  
32  
33  
34  
35  
36  
37  
38  
39  
40  
41  
42  
43  
44  
45  
46  
47  
48  
49  
50  
51  
52  
53  
54  
55  
56  
57  
58  
59  
60

formal charge of 2). Complexes were refined in two steps: First, minimization with fixed inhibitor using the AMBER\_FF99 force field.<sup>79</sup> Second, subset minimization of Marbostat-100 and the surrounding (distance up to 6 Å) protein residues (Tripos force field<sup>80</sup>). In both minimization steps, the Powell conjugate gradient method with termination at a root-mean-square force of  $0.05 \text{ kcal/mol} \times \text{Å}^{-1}$  was applied. Molecular surfaces and lipophilic potentials (protein variant with the new Crippen parameter table)<sup>81, 82</sup> were calculated and visualized by the program MOLCAD (MOLCAD, Darmstadt, Germany) contained within SYBYL.

## Animals

Male DBA/1J mice (6-8 weeks old) were purchased from Janvier (France). They were housed in a specific pathogen-free environment with unrestricted access to chow and water. Five animals lived in one cage, and they were acclimated to the environment during one week before the experiments. The Government of Unterfranken, Germany, approved all experiments according to institutional and governmental regulations for animal use (Az. 55.2 DMS-2532-2-124).

## Induction, assessment of arthritis and scoring

Arthritis was induced by a single injection of 100 µg of bovine type II collagen (MD Bioproducts, Zurich, Switzerland) emulsified in an equal volume of complete Freund adjuvant (Sigma, Deisenhofen, Germany) intradermally at the base of the tail. After immunization, animals were inspected daily for signs of joint swelling in front and hind limbs<sup>83</sup>. For further details of assessment and scoring see supporting information.

## Treatment

Sterile and freshly prepared equimolar solutions of Marbostat-100 (**5a**) or **5f** were injected intraperitoneally every morning at a concentration of 30 mg/kg, or (equimolar) 42.3 mg/kg, respectively. Treatment was initiated for each mouse after a clinical arthritis score of 8 or higher was reached (therapeutic treatment approach), and was continued for 12-14 consecutive days until all mice were killed. Injection of vehicle (sterile solution of PBS, Cremophor, 1-methyl-2-pyrrolidinone and DMSO, all Sigma) alone served as control.

## Blood count and removal of organs

Immediately after killing the mice, whole blood was obtained by cardiac puncture and transferred into EDTA coated tubes (Sarstedt, Germany) for blood count analysis. Hemoglobin, erythrocytes and leukocytes were determined with a full automatic counter, which is also used for patient blood sampling (University Hospital Regensburg, Department of clinical chemistry and laboratory medicine). Organs were removed immediately, packed in vials and snap frozen in liquid nitrogen.

## Statistical analysis

If not stated otherwise, results are presented as box plots with the 10<sup>th</sup>, 25<sup>th</sup>, 50<sup>th</sup> (median), 75<sup>th</sup>, and 90<sup>th</sup> percentile (in the animal experiments for scoring results). The non-parametric Mann-Whitney test was used to compare two groups. A two-way ANOVA test using the Holm Sidak method was used to compare groups (Sigma Plot, Version 11, Systat Software GmbH, Erkrath, Germany). We considered p-values below 0.05 as statistically significant. Data from flow cytometry were analyzed with FACS Diva Software (Version 7.0, BD Biosciences GmbH, Heidelberg, Germany) Image Studio Lite (Version 4.0, LI-COR

1  
2  
3 Biosciences Inc., Lincoln, USA) was used to analyze the data from Western blot. The  
4  
5 graphs were illustrated using Prism 6 (Graph Pad Inc., La Jolla, USA).  
6  
7  
8  
9  
10  
11  
12  
13  
14  
15  
16

### 17 **Supporting Information.**

18  
19  
20 Experimental details for synthesis of all intermediates, x-ray data, molecular formula  
21  
22 strings, procedures for Western blot analysis, induction, assessment of arthritis and scoring  
23  
24 as well as hemoglobin analysis. This material is available free of charge via the Internet at  
25  
26 the ACS Publications website at DOI:  
27  
28  
29  
30  
31  
32  
33

### 34 **AUTHOR INFORMATION**

#### 35 36 37 **Corresponding Author**

38  
39  
40 \*Corresponding author, E-mail: [Siavosh.mahboobi@chemie.uni-regensburg.de](mailto:Siavosh.mahboobi@chemie.uni-regensburg.de)  
41  
42

#### 43 **Author Contributions**

44  
45 The manuscript was written with contributions from all authors. ‡Senior authors who  
46  
47 contributed equally.  
48  
49

50  
51 Andreas Sellmer, Elisabeth Grünstein, Michel Leonhardt, Oliver H. Krämer<sup>‡</sup>, Herwig  
52  
53 Pongratz, Emerich Eichhorn, Sigurd Elz and Siavosh Mahboobi<sup>‡</sup> were responsible for drug  
54  
55 design, synthesis and interpretation of enzyme inhibition data.  
56  
57  
58  
59  
60

1  
2  
3 Hubert Stangl, Zsuzsa Jenei-Lanzl, Elisabeth Grünstein and Rainer H. Straub<sup>‡</sup> were  
4 responsible for the *in vivo* experiments and interpretation of the anti-inflammatory and  
5  
6  
7  
8  
9  
10  
11  
12  
13  
14  
15  
16  
17  
18  
19  
20  
21  
22  
23  
24  
25  
26  
27  
28  
29  
30  
31  
32  
33  
34  
35  
36  
37  
38  
39  
40  
41  
42  
43  
44  
45  
46  
47  
48  
49  
50  
51  
52  
53  
54  
55  
56  
57  
58  
59  
60

Hubert Stangl, Zsuzsa Jenei-Lanzl, Elisabeth Grünstein and Rainer H. Straub<sup>‡</sup> were responsible for the *in vivo* experiments and interpretation of the anti-inflammatory and antirheumatic effects in the collagen type II – induced arthritis model.

Mandy Beyer and Oliver H. Krämer<sup>‡</sup> were responsible for all cell cultures and biochemical experiments.

Stefan Dove<sup>‡</sup> performed docking and investigated the binding mode of Marbostat-100

Birgit Striegl was responsible for preparation and measurement of the microcomputed tomography images.

#### ACKNOWLEDGMENT

Dedicated to Prof. Dr. rer. nat. Dr. phil. Wolfgang Wiegand on the occasion of his 85th birthday. We thank Thorsten Heinzl and Sabine Scheiding (University of Jena, CMB, Germany) and Ina Oehme and Olaff Witt (DKFZ Heidelberg, Germany) for helpful discussions and technical support. We also thank Michael Bodensteiner, University of Regensburg, Germany, and his department for measurement of the x-ray structure and editing of the crystallographic data. We thank Rudolf Vasold and Peter Kreitmeier, University of Regensburg, Germany, for performance of the HPLC measurements.

#### FUNDING SOURCES

We mainly thank the Deutsche Forschungsgemeinschaft (KR 2291/4-1 and MA2183/1-1, STR 511/31-1 and INST 102/11-1 FUGG) for financial support. Additional support came from the Deutsche Forschungsgemeinschaft (KR2291/5-1 and KR2291/7-1 to O.H.K),

1  
2  
3 German Cancer Aid (#110909 and #110125), the Wilhelm Sander-Stiftung (#2010.078.2),  
4 and intramural and NMFZ funding to O.H.K.  
5  
6

7  
8 The authors declare the following competing financial interest: Andreas Sellmer, Herwig  
9 Pongratz, Michel Leonhardt, Oliver H. Krämer and Siavosh Mahboobi are also the  
10 inventors of this entity: Appl. (2016), WO 2016020369 A1 20160211.  
11  
12  
13  
14  
15  
16  
17

#### 18 ABBREVIATIONS

19  
20  
21 acH3, Acetylated histone 3  
22

23  
24 ac-tubulin, Acetylated tubulin  
25

26  
27 BOP, Benzotriazol-1-yloxy-tris(dimethylamino)phosphoniumhexafluorophosphate  
28

29  
30 CAIA, collagen antibody-induced arthritis  
31

32  
33 cc, column chromatography  
34

35  
36 CD, Catalytic Domain  
37

38  
39 CDI, 1,1'-Carbonyldiimidazole  
40

41  
42 CIA, Collagen type II - induced arthritis  
43

44  
45 DMFDMA, *N,N*-Dimethylformamide-dimethylacetal  
46

47  
48 EDTA, Ethylenediaminetetraacetic acid  
49

50  
51 ELISA, Enzyme linked immunosorbent assay  
52

53  
54 FLS, Fibroblast like synoviocyte  
55  
56  
57  
58  
59  
60

1  
2  
3 HDACi, Histone deacetylase inhibitor  
4

5  
6 IL-6, Interleukin 6  
7

8  
9 IgG, Immunoglobulin G  
10

11  
12 NH<sub>2</sub>OTHP, O-(tetrahydro-2*H*-pyran-4-yl)hydroxylamine  
13

14  
15 PBS, Phosphate buffer solution  
16

17  
18 RA, Rheumatoid arthritis  
19

20  
21 rt, Room temperature  
22

23  
24 TLC, Thin layer chromatography  
25  
26  
27  
28  
29  
30  
31  
32  
33  
34  
35

## 36 REFERENCES

37  
38  
39  
40

41 1. Seto, E.; Yoshida, M. Erasers of histone acetylation: the histone deacetylase  
42 enzymes. *Cold Spring Harb Perspect Biol* **2014**, *6*, 1-27.  
43

44 2. Beier, U. H.; Akimova, T.; Liu, Y.; Wang, L.; Hancock, W. W. Histone/protein  
45 deacetylases control Foxp3 expression and the heat shock response of T-regulatory cells.  
46  
47  
48  
49  
50  
51  
52  
53  
54  
55  
56  
57  
58  
59  
60

3. Krämer, O. H. HDAC2: a critical factor in health and disease. *Trends Pharmacol Sci*  
**2009**, *30*, 647-655.

- 1  
2  
3 4. Krämer, O. H.; Mahboobi, S.; Sellmer, A. Drugging the HDAC6-HSP90 interplay in  
4 malignant cells. *Trends Pharmacol. Sci.* **2014**, *35*, 501-509.  
5  
6
- 7 5. Zhang, L.; Zhang, Y.; Chou, C. J.; Inks, E. S.; Wang, X.; Li, X.; Hou, J.; Xu, W.  
8 Histone deacetylase inhibitors with enhanced enzymatic inhibition effects and potent in  
9 vitro and in vivo antitumor activities. *ChemMedChem* **2014**, *9*, 638-648.  
10  
11
- 12 6. Li, Y.; Shin, D.; Kwon, S. H. Histone deacetylase 6 plays a role as a distinct  
13 regulator of diverse cellular processes. *FEBS* **2013**, *280*, 775-793.  
14  
15
- 16 7. Zwick, V.; Simoes-Pires, C. A.; Nurisso, A.; Petit, C.; Dos Santos Passos, C.;  
17 Randazzo, G. M.; Martinet, N.; Bertrand, P.; Cuendet, M. Synthesis of a selective HDAC6  
18 inhibitor active in neuroblasts. *Bioorg Med Chem Lett* **2016**, *26*, 4955-4959.  
19  
20
- 21 8. Iaconelli, J.; Huang, J. H.; Berkovitch, S. S.; Chattopadhyay, S.; Mazitschek, R.;  
22 Schreiber, S. L.; Haggarty, S. J.; Karmacharya, R. HDAC6 inhibitors modulate Lys49  
23 acetylation and membrane localization of  $\beta$ -catenin in human iPSC-derived neuronal cells.  
24 *ACS Chem Biol* **2015**, *10*, 883-890.  
25  
26
- 27 9. Pontiki, E.; Hadjipavlou-Litina, D. Histone deacetylase inhibitors (HDACIs).  
28 Structure-activity relationships: history and new QSAR perspectives. *Med Res Rev* **2012**,  
29 *32*, 1-165.  
30  
31
- 32 10. Tang, G.; Wong, J. C.; Zhang, W.; Wang, Z.; Zhang, N.; Peng, Z.; Zhang, Z.; Rong,  
33 Y.; Li, S.; Zhang, M.; Yu, L.; Feng, T.; Zhang, X.; Wu, X.; Wu, J. Z.; Chen, L.  
34 Identification of a novel aminotetralin class of HDAC6 and HDAC8 selective inhibitors. *J.*  
35 *Med. Chem.* **2014**, *57*, 8026-8034.  
36  
37
- 38 11. Witt, O.; Deubzer, H. E.; Milde, T.; Oehme, I. HDAC family: What are the cancer  
39 relevant targets? *Cancer Lett* **2009**, *277*, 8-21.  
40  
41  
42  
43  
44  
45  
46  
47  
48  
49  
50  
51  
52  
53  
54  
55  
56  
57  
58  
59  
60

- 1  
2  
3 12. Zhang, Y.; Kwon, S.; Yamaguchi, T.; Cubizolles, F.; Rousseaux, S.; Kneissel, M.;  
4 Cao, C.; Li, N.; Cheng, H.-L.; Chua, K.; Lombard, D.; Mizeracki, A.; Matthias, G.; Alt, F.  
5  
6 W.; Khochbin, S.; Matthias, P. Mice lacking histone deacetylase 6 have hyperacetylated  
7  
8 tubulin but are viable and develop normally. *Mol Cell Biol* **2008**, *28*, 1688-1701.  
9  
10  
11  
12 13. Haggarty, S. J.; Koeller, K. M.; Wong, J. C.; Grozinger, C. M.; Schreiber, S. L.  
13  
14 Domain-selective small-molecule inhibitor of histone deacetylase 6 (HDAC6)-mediated  
15  
16 tubulin deacetylation. *Proc Natl Acad Sci* **2003**, *100*, 4389-4394.  
17  
18  
19 14. Butler, K. V.; Kalin, J.; Brochier, C.; Vistoli, G.; Langley, B.; Kozikowsky, A. P.  
20  
21 Rational design and simple chemistry yield a superior neuroprotective HDAC6 inhibitor,  
22  
23 tubastatin A. *J. Am. Chem. Soc.* **2010**, *132* 10842-10846.  
24  
25  
26 15. Dallavalle, S.; Pisano, C.; Zunino, F. Development and therapeutic impact of  
27  
28 HDAC6-selective inhibitors. *Biochem Pharmacol* **2012**, *84*, 756-765.  
29  
30  
31 16. Kalin, J. H.; Bergman, J. A. Development and therapeutic implications of selective  
32  
33 histone deacetylase 6 inhibitors. *J. Med. Chem.* **2013**, *56*, 6297-6313.  
34  
35  
36 17. Kalin, J. H.; Butler, K. V.; Akimova, T.; Hancock, W. W.; Kozikowski, A. P.  
37  
38 Second-generation histone deacetylase 6 inhibitors enhance the immunosuppressive effects  
39  
40 of Foxp3+ T-regulatory cells. *J. Med. Chem.* **2012**, *55*, 639-651.  
41  
42  
43 18. Oehme, I.; Linke, J.-P.; Bock, B. C.; Milde, T.; Lodrini, M.; Hartenstein, B.;  
44  
45 Wiegand, I.; Eckert, C.; Roth, W.; Kool, M.; Kaden, S.; Grone, H.-J.; Schulte, J. H.;  
46  
47 Lindner, S.; Hamacher-Brady, A.; Brady, N. R.; Deubzer, H. E.; Witt, O. Histone  
48  
49 deacetylase 10 promotes autophagy-mediated cell survival. *Proc Natl Acad Sci* **2013**, *110*,  
50  
51 2592-2601.  
52  
53  
54  
55  
56  
57  
58  
59  
60

- 1  
2  
3 19. Jochems, J.; Boulden, J.; Lee, B. G.; Blendy, J. A.; Jarpe, M.; Mazitschek, R.; Van  
4 Duzer, J. H.; Jones, S.; Berton, O. Antidepressant-like properties of novel HDAC6-selective  
5 inhibitors with improved brain bioavailability. *Neuropsychopharmacology* **2014**, *39*, 389-  
6 400.  
7  
8  
9  
10  
11  
12 20. Lee, J.-H.; Ngo, L.; Venta-Perez, G.; Choy, M. L.; Marks, P. A.; Yao, Y.;  
13 Mahendran, A.; Breslow, R. Creation of a histone deacetylase 6 inhibitor and its biological  
14 effects [corrected]. *Proc Natl Acad Sci* **2015**, *112*, 12005-12010.  
15  
16  
17  
18  
19 21. Vishwakarma, S.; Iyer, L. R.; Muley, M.; Singh, P. K.; Shastry, A.; Saxena, A.;  
20 Kulathingal, J.; Vijaykanth, G.; Raghul, J.; Rajesh, N.; Rathinasamy, S.; Kachhadia, V.;  
21 Kilambi, N.; Rajgopal, S.; Balasubramanian, G.; Narayanan, S. Tubastatin, a selective  
22 histone deacetylase 6 inhibitor shows anti-inflammatory and anti-rheumatic effects. *Int.*  
23 *Immunopharmacol.* **2013**, *16*, 72-78.  
24  
25  
26  
27  
28  
29  
30  
31 22. Santo, L.; Hideshima, T.; Kung, A. L.; Tseng, J. C.; Tamang, D.; Yang, M.; Jarpe,  
32 M.; van Duzer, J. H.; Mazitschek, R.; Ogier, W. C.; Cirstea, D.; Rodig, S.; Eda, H.; Scullen,  
33 T.; Canavese, M.; Bradner, J.; Anderson, K. C.; Jones, S. S.; Raje, N. Preclinical activity,  
34 pharmacodynamic, and pharmacokinetic properties of a selective HDAC6 inhibitor, ACY-  
35 1215, in combination with bortezomib in multiple myeloma. *Blood* **2012**, *119*, 2579-2589.  
36  
37  
38  
39  
40  
41  
42 23. Kozikowski, A. P.; Tapadar, S.; Luchini, D. N.; Kim, K. H.; Billadeau, D. D. Use of  
43 the nitrile oxide cycloaddition (NOC) reaction for molecular probe generation: a new class  
44 of enzyme selective histone deacetylase inhibitors (HDACIs) showing picomolar activity at  
45 HDAC6. *J Med Chem* **2008**, *51*, 4370-4373.  
46  
47  
48  
49  
50  
51 24. Lohman, R.-J.; Iyer, A.; Fairlie, T. J.; Cotterell, A.; Gupta, P.; Reid, R. C.; Vesey,  
52 D. A.; Sweet, M. J.; Fairlie, D. P. Differential anti-inflammatory activity of HDAC  
53  
54  
55  
56  
57  
58  
59  
60

1  
2  
3 inhibitors in human macrophages and rat arthritis. *J Pharmacol Exp Ther* **2016**, *356*, 387-  
4  
5 396.

6  
7  
8 25. Cleophas, M. C. P.; Crisan, T. O.; Lemmers, H.; Toenhake-Dijkstra, H.; Fossati, G.;  
9  
10 Jansen, T. L.; Dinarello, C. A.; Netea, M. G.; Joosten, L. A. B. Suppression of monosodium  
11  
12 urate crystal-induced cytokine production by butyrate is mediated by the inhibition of class  
13  
14 I histone deacetylases. *Ann Rheum Dis* **2016**, *75*, 593-600.

15  
16  
17 26. Gillespie, J.; Savic, S.; Wong, C.; Hempshall, A.; Inman, M.; Emery, P.; Grigg, R.;  
18  
19 McDermott, M. F. Histone deacetylases are dysregulated in rheumatoid arthritis and a novel  
20  
21 histone deacetylase 3-selective inhibitor reduces interleukin-6 production by peripheral  
22  
23 blood mononuclear cells from rheumatoid arthritis patients. *Arthritis Rheum.* **2012**, *64*, 418-  
24  
25 422.

26  
27  
28 27. Li, S.; Fossati, G.; Marchetti, C.; Modena, D.; Pozzi, P.; Reznikov, L. L.; Moras, M.  
29  
30 L.; Azam, T.; Abbate, A.; Mascagni, P.; Dinarello, C. A. Specific inhibition of histone  
31  
32 deacetylase 8 reduces gene expression and production of proinflammatory cytokines in vitro  
33  
34 and in vivo. *J. Biol. Chem.* **2015**, *290*, 2368-2378.

35  
36  
37 28. Grabiec, A. M.; Korchynskyi, O.; Tak, P. P.; Reedquist, K. A. Histone deacetylase  
38  
39 inhibitors suppress rheumatoid arthritis fibroblast-like synoviocyte and macrophage IL-6  
40  
41 production by accelerating mRNA decay. *Ann. Rheum. Dis.* **2012**, *71*, 424-431.

42  
43  
44 29. Wang, X.; Song, Y.; Jacobi, J. L.; Tuan, R. S. Inhibition of histone deacetylases  
45  
46 antagonized FGF2 and IL-1 $\beta$  effects on MMP expression in human articular chondrocytes.  
47  
48 *Growth Factors* **2009**, *27*, 40-49.

49  
50  
51 30. Angiolilli, C.; Grabiec, A. M.; Ferguson, B. S.; Ospelt, C.; Fernandez, B. M.; van  
52  
53 Es, I. E.; van Baarsen, L. G. M.; Gay, S.; McKinsey, T. A.; Tak, P. P.; Baeten, D. L.;

1  
2  
3 Reedquist, K. A. Inflammatory cytokines epigenetically regulate rheumatoid arthritis  
4 fibroblast-like synoviocyte activation by suppressing HDAC5 expression. *Ann Rheum Dis*  
5  
6 **2016**, *75*, 430-438.  
7

8  
9  
10 31. Bartoli, G.; Bosco, M.; Giuli, S.; Giuliani, A.; Lucarelli, L.; Marcantoni, E.; Sambri,  
11 L.; Torregiani, E. Efficient preparation of 2-indolyl-1-nitroalkane derivatives employing  
12 nitroalkenes as versatile michael sceptors: New practical linear approach to alkyl 9H- $\beta$ -  
13 carboline-4-carboxylate. *J. Org. Chem.* **2005**, *70*, 1941-1944.  
14  
15

16  
17 32. Palmieri, A.; Gabrielli, S.; Ballini, R. Low impact synthesis of  $\beta$ -nitroacrylates  
18 under fully heterogeneous conditions. *Green Chem.* **2013**, *15*, 2344-2348.  
19  
20

21  
22 33. Yi, W.-B.; Wang, X.; Cai, C. Nitroaldol reaction in fluorous media. An important  
23 improvement of the chemoselective addition of aldehyde. *Catal. Commun.* **2007**, *8*, 1995-  
24 1998.  
25  
26

27  
28 34. Ballini, R.; Gabrielli, S.; Palmieri, A.; Petrini, M. Improved preparation of alkyl 2-  
29 (3-indolyl)-3-nitroalkanoates under fully heterogenous conditions: stereoselective synthesis  
30 of alkyl (*E*)-2-(3-indolyl)-alkenoates. *Tetrahedron* **2008**, *64*, 5435-5441.  
31  
32

33  
34 35. Shi, X.-X.; Liu, S.-L.; Xu, W.; Xu, Y.-L. Highly stereoselective Pictet-spengler  
35 reaction of D-tryptophan methyl ester with piperonal: convenient syntheses of Cialis  
36 (Tadalafil), 12a-epi-Cialis, and their deuterated analogues. *Tetrahedron: Asymmetry* **2008**,  
37 *19*, 435-442.  
38  
39

40  
41 36. Motoshima, K.; Ishikawa, M.; Hashimoto, Y.; Sugita, K. Peroxisome proliferator-  
42 activated receptor agonists with phenethylphenylphthalimide skeleton derived from  
43 thalidomide-related liver X receptor antagonists: Relationship between absolute  
44 configuration and subtype selectivity. *Bioorg. Med. Chem.* **2011**, *19*, 3156-3172.  
45  
46  
47  
48  
49  
50  
51  
52  
53  
54  
55  
56  
57  
58  
59  
60

- 1  
2  
3 37. Walton, J. G. A.; Patterson, S.; Liu, G.; Haraldsen, J. D.; Hollick, J. J.; Slawin, A.  
4 M. Z.; Ward, G. E.; Westwood, N. J. Synthesis and biological evaluation of functionalised  
5 tetrahydro- $\beta$ -carboline analogues as inhibitors of *Toxoplasma gondii* invasion. *Org. Biomol.*  
6 *Chem.* **2009**, *7*, 3049-3060.  
7  
8  
9  
10  
11  
12 38. Kumar, V.; Khatik, G. L.; Pal, A.; Praneeth, M. R.; Bhattarai, S.; Nair, V. A. A  
13 facile synthesis and chemoselective reactions of dihydrothiouracils. *Synlett* **2012**, *23*, 2357-  
14 2362.  
15  
16  
17  
18  
19 39. Ganesh, M.; Seidel, D. Catalytic enantioselective additions of indoles to  
20 nitroalkenes. *J. Am. Chem. Soc.* **2008**, *130*, 16464-16465.  
21  
22  
23  
24 40. Cheng, Y.; Prusoff, W. H. Relationship between the inhibition constant (K<sub>1</sub>) and the  
25 concentration of inhibitor which causes 50 per cent inhibition (I<sub>50</sub>) of an enzymatic  
26 reaction. *Biochem Pharmacol* **1973**, *22*, 3099-3108.  
27  
28  
29  
30  
31 41. Lobera, M.; Madauss, K. P.; Pohlhaus, D. T.; Wright, Q. G.; Trocha, M.; Schmidt,  
32 D. R.; Baloglu, E.; Trump, R. P.; Head, M. S.; Hofmann, G. A.; Murray-Thompson, M.;  
33 Schwartz, B.; Chakravorty, S.; Wu, Z.; Mander, P. K.; Kruidenier, L.; Reid, R. A.;  
34 Burkhart, W.; Turunen, B. J.; Rong, J. X.; Wagner, C.; Moyer, M. B.; Wells, C.; Hong, X.;  
35 Moore, J. T.; Williams, J. D.; Soler, D.; Ghosh, S.; Nolan, M. A. Selective class IIa histone  
36 deacetylase inhibition via a nonchelating zinc-binding group. *Nat. Chem. Biol.* **2013**, *9*,  
37 319-325.  
38  
39  
40  
41  
42  
43  
44  
45  
46  
47 42. Hai, Y.; Christianson, D. W. Histone deacetylase 6 structure and molecular basis of  
48 catalysis and inhibition. *Nat. Chem. Biol.* **2016**, *12*, 741-747.  
49  
50  
51  
52  
53  
54  
55  
56  
57  
58  
59  
60

- 1  
2  
3 43. Porter, N. J.; Mahendran, A.; Breslow, R.; Christianson, D. W. Unusual zinc-  
4 binding mode of HDAC6-selective hydroxamate inhibitors. *Proc. Natl. Acad. Sci. U. S. A.*  
5 **2017**, *114*, 13459-13464.  
6  
7  
8  
9  
10 44. Zou, H.; Wu, Y.; Navre, M.; Sang, B.-C. Characterization of the two catalytic  
11 domains in histone deacetylase 6. *Biochem. Biophys. Res. Commun.* **2006**, *341*, 45-50.  
12  
13  
14 45. Espallergues, J.; Teegarden, S. L.; Veerakumar, A.; Boulden, J.; Challis, C.;  
15 Jochems, J.; Chan, M.; Petersen, T.; Deneris, E.; Matthias, P.; Hahn, C.-G.; Lucki, I.; Beck,  
16 S. G.; Berton, O. HDAC6 regulates glucocorticoid receptor signaling in serotonin pathways  
17 with critical impact on stress resilience. *The Journal of Neuroscience* **2012**, *32*, 4400-4416.  
18  
19  
20  
21 46. Li, Y.; Zhang, X.; Polakiewicz, R. D.; Yao, T.-P.; Comb, M. J. HDAC6 is required  
22 for epidermal growth factor-induced beta-catenin nuclear localization. *J Biol Chem* **2008**,  
23 *283*, 12686-12690.  
24  
25  
26  
27 47. Iaconelli, J.; Lalonde, J.; Watmuff, B.; Liu, B.; Mazitschek, R.; Haggarty, S. J.;  
28 Karmacharya, R. Lysine deacetylation by HDAC6 regulates the kinase activity of AKT in  
29 human neural progenitor cells. *ACS Chem Biol* **2017**, *12*, 2139-2148.  
30  
31  
32  
33 48. Buchwald, M.; Pietschmann, K.; Müller, J. P.; Böhmer, F. D.; Heinzl, T.; Krämer,  
34 O. H. Ubiquitin conjugase UBCH8 targets active FMS-like tyrosine kinase 3 for  
35 proteasomal degradation. *Leukemia* **2010**, *24*, 1412-1421.  
36  
37  
38  
39 49. Boyault, C.; Sadoul, K.; Pabion, M.; Khochbin, S. HDAC6, at the crossroads  
40 between cytoskeleton and cell signaling by acetylation and ubiquitination. *Oncogene* **2007**,  
41 *26*, 5468-5476.  
42  
43  
44  
45 50. Bradner, J. E.; Mak, R.; Tanguturi, S. K.; Mazitschek, R.; Haggarty, S. J.; Ross, K.;  
46 Chang, C. Y.; Bosco, J.; West, N.; Morse, E.; Lin, K.; Shen, J. P.; Kwiatkowski, N. P.;  
47  
48  
49  
50  
51  
52  
53  
54  
55  
56  
57  
58  
59  
60

1  
2  
3 Gheldof, N.; Dekker, J.; Deangelo, D. J.; Carr, S. A.; Schreiber, S. L.; Golub, T. R.; Ebert,  
4 B. L. Chemical genetic strategy identifies histone deacetylase 1 (HDAC1) and HDAC2 as  
5 therapeutic targets in sickle cell disease. *Proc Natl Acad Sci* **2010**, *107*, 12617-12622.  
6  
7

8  
9  
10 51. Noack, K.; Mahendrarajah, N.; Hennig, D.; Schmidt, L.; Grebien, F.; Hildebrand,  
11 D.; Christmann, M.; Kaina, B.; Sellmer, A.; Mahboobi, S.; Kubatzky, K.; Heinzl, T.;  
12 Krämer, O. H. Analysis of the interplay between all-trans retinoic acid and histone  
13 deacetylase inhibitors in leukemic cells. *Arch Toxicol* **2017**, *91*, 2191-2208.  
14  
15

16  
17  
18 52. Lauffer, B. E. L.; Mintzer, R.; Fong, R.; Mukund, S.; Tam, C.; Zilberleyb, I.; Flicke,  
19 B.; Ritscher, A.; Fedorowicz, G.; Vallero, R.; Ortwine, D. F.; Gunzner, J.; Modrusan, Z.;  
20 Neumann, L.; Koth, C. M.; Lupardus, P. J.; Kaminker, J. S.; Heise, C. E.; Steiner, P.  
21 Histone deacetylase (HDAC) inhibitor kinetic rate constants correlate with cellular histone  
22 acetylation but not transcription and cell viability. *J. Biol. Chem.* **2013**, *288*, 26926-26943.  
23  
24

25  
26  
27 53. Vannini, A.; Volpari, C.; Filocamo, G.; Casavola, E. C.; Brunetti, M.; Renzoni, D.;  
28 Chakravarty, P.; Paolini, C.; De Francesco, R.; Gallinari, P.; Steinkuehler, C.; Di Marco, S.  
29 Crystal structure of a eukaryotic zinc-dependent histone deacetylase, human HDAC8,  
30 complexed with a hydroxamic acid inhibitor. *Proc Natl Acad Sci* **2004**, *101*, 15064-15069.  
31  
32

33  
34  
35 54. Schäfer, C.; Göder, A.; Beyer, M.; Kiweler, N.; Mahendrarajah, N.; Rauch, A.;  
36 Nikolova, T.; Stojanovic, N.; Wieczorek, M.; Reich, T. R.; Tomicic, M. T.; Linnebacher,  
37 M.; Sonnemann, J.; Dietrich, S.; Sellmer, A.; Mahboobi, S.; Heinzl, T.; Schneider, G.;  
38 Krämer, O. H. Class I histone deacetylases regulate p53/NF- $\kappa$ B crosstalk in cancer cells.  
39 *Cell. Signalling* **2017**, *29*, 218-225.  
40  
41

42  
43  
44 55. Stojanovic, N.; Hassan, Z.; Wirth, M.; Wenzel, P.; Beyer, M.; Schäfer, C.; Brand,  
45 P.; Krömer, A.; Stauber, R. H.; Schmid, R. M.; Arlt, A.; Sellmer, A.; Mahboobi, S.; Rad,  
46  
47  
48  
49  
50  
51  
52  
53  
54  
55  
56  
57  
58  
59  
60

- R.; Reichert, M.; Saur, D.; Krämer, O. H.; Schneider, G. HDAC1 and HDAC2 integrate the expression of p53 mutants in pancreatic cancer. *Oncogene* **2017**, *36*, 1804-1815.
56. Miyake, Y.; Keusch, J. J.; Wang, L.; Saito, M.; Hess, D.; Wang, X.; Melancon, B. J.; Helquist, P.; Gut, H.; Matthias, P. Structural insights into HDAC6 tubulin deacetylation and its selective inhibition. *Nat Chem Biol* **2016**, *12*, 748-754.
57. Nakamura, T.; Kukita, T.; Shobuike, T.; Nagata, K.; Wu, Z.; Ogawa, K.; Hotokebuchi, T.; Kohashi, O.; Kukita, A. Inhibition of histone deacetylase suppresses osteoclastogenesis and bone destruction by inducing IFN- $\beta$  production. *J. Immunol.* **2005**, *175*, 5809-5816.
58. Joosten, L. A. B.; Leoni, F.; Meghji, S.; Mascagni, P. Inhibition of HDAC activity by ITF2357 ameliorates joint inflammation and prevents cartilage and bone destruction in experimental arthritis. *Mol. Med.* **2011**, *17*, 391-396.
59. Hsieh, I. N.; Liou, J. P.; Lee, H. Y.; Lai, M. J.; Li, Y. H.; Yang, C. R. Preclinical anti-arthritic study and pharmacokinetic properties of a potent histone deacetylase inhibitor MPT0G009. *Cell Death Dis.* **2014**, *5*, e1166; doi:10.1038/cddis.2014.133; published online 10 April 2014 (accessed Mar 22, 2018).
60. Misaki, K.; Morinobu, A.; Saegusa, J.; Kasagi, S.; Fujita, M.; Miyamoto, Y.; Matsuki, F.; Kumagai, S. Histone deacetylase inhibition alters dendritic cells to assume a tolerogenic phenotype and ameliorates arthritis in SKG mice. *Arthritis Res. Ther.* **2011**, *13*, R77, <http://arthritis-research.com/content/13/3/R77> (accessed Mar 22, 2018).
61. Lin, H. S.; Hu, C. Y.; Chan, H. Y.; Liew, Y. Y.; Huang, H. P.; Lepescheux, L.; Bastianelli, E.; Baron, R.; Rawadi, G.; Clement-Lacroix, P. Anti-rheumatic activities of

1  
2  
3 histone deacetylase (HDAC) inhibitors in vivo in collagen-induced arthritis in rodents. *Br.*  
4  
5 *J. Pharmacol.* **2007**, *150*, 862-872.

6  
7  
8 62. Nasu, Y.; Nishida, K.; Miyazawa, S.; Komiyama, T.; Kadota, Y.; Abe, N.; Yoshida,  
9  
10 A.; Hirohata, S.; Ohtsuka, A.; Ozaki, T. Trichostatin A, a histone deacetylase inhibitor,  
11  
12 suppresses synovial inflammation and subsequent cartilage destruction in a collagen  
13  
14 antibody-induced arthritis mouse model. *Osteoarthritis Cartilage* **2008**, *16*, 723-732.

15  
16  
17 63. Saouaf, S. J.; Li, B.; Zhang, G.; Shen, Y.; Furuuchi, N.; Hancock, W. W.; Greene,  
18  
19 M. I. Deacetylase inhibition increases regulatory T cell function and decreases incidence  
20  
21 and severity of collagen-induced arthritis. *Exp. Mol. Pathol.* **2009**, *87*, 99-104.

22  
23  
24 64. Hawtree, S.; Muthana, M.; Wilkinson, J. M.; Akil, M.; Wilson, A. G. Histone  
25  
26 deacetylase 1 regulates tissue destruction in rheumatoid arthritis. *Hum. Mol. Genet.* **2015**,  
27  
28 *24*, 5367-5377.

29  
30  
31 65. Cantley, M. D.; Fairlie, D. P.; Bartold, P. M.; Marino, V.; Gupta, P. K.; Haynes, D.  
32  
33 R. Inhibiting histone deacetylase 1 suppresses both inflammation and bone loss in arthritis.  
34  
35 *Rheumatology (Oxford)* **2015**, *54*, 1713-1723.

36  
37  
38 66. Lee, J.; Hong, E. C.; Jeong, H.; Hwang, J. W.; Kim, H.; Bae, E.-K.; Ahn, J. K.;  
39  
40 Choi, Y.-L.; Han, J.; Cha, H.-S.; Koh, E.-M. A novel histone deacetylase 6-selective  
41  
42 inhibitor suppresses synovial inflammation and joint destruction in a collagen antibody-  
43  
44 induced arthritis mouse model. *Int. J. Rheum. Dis.* **2015**, *18*, 514-523.

45  
46  
47 67. Yan, B.; Xie, S.; Ran, J.; Li, Y.; Wang, J.; Yang, Y.; Zhou, J.; Li, D.; Liu, Z.; Liu,  
48  
49 M. HDAC6 deacetylase activity is critical for lipopolysaccharide-induced activation of  
50  
51 macrophages. In *PLoS One*, 2014; Vol. 9, p e110718. doi:10.1371/journal.pone.0110718;  
52  
53 published online 16 October 2014 (accessed Mar 22, 2018).

- 1  
2  
3 68. Cheng, F.; Lienlaf, M.; Perez-Villarroel, P.; Wang, H.-W.; Lee, C.; Woan, K.;  
4 Woods, D.; Knox, T.; Bergman, J.; Pinilla-Ibarz, J.; Kozikowski, A.; Seto, E.; Sotomayor,  
5 E. M.; Villagra, A. Divergent roles of histone deacetylase 6 (HDAC6) and histone  
6 deacetylase 11 (HDAC11) on the transcriptional regulation of IL10 in antigen presenting  
7 cells. *Mol Immunol* **2014**, *60*, 44-53.  
8  
9  
10  
11  
12  
13  
14 69. Liesz, A.; Zhou, W.; Na, S.-Y.; Haemmerling, G. J.; Garbi, N.; Karcher, S.;  
15 Mracsko, E.; Backs, J.; Rivest, S.; Veltkamp, R. Boosting regulatory T cells limits  
16 neuroinflammation in permanent cortical stroke. *J. Neurosci.* **2013**, *33*, 17350-17362.  
17  
18  
19  
20  
21 70. Wang, B.; Rao, Y.-H.; Inoue, M.; Hao, R.; Lai, C.-H.; Chen, D.; McDonald, S. L.;  
22 Choi, M.-C.; Wang, Q.; Shinohara, M. L.; Yao, T.-P. Microtubule acetylation amplifies p38  
23 kinase signalling and anti-inflammatory IL-10 production. *Nature Communications* **2014**, *5*,  
24 3479.  
25  
26  
27  
28  
29  
30  
31 71. Hwang, I.; Lee, E.; Jeon, S.-A.; Yu, J.-W. Histone deacetylase 6 negatively  
32 regulates NLRP3 inflammasome activation. *Biochem Biophys Res Commun* **2015**, *467*, 973-  
33 978.  
34  
35  
36  
37 72. Yu, J.; Ma, M.; Ma, Z.; Fu, J. HDAC6 inhibition prevents TNF- $\alpha$ -induced caspase 3  
38 activation in lung endothelial cell and maintains cell-cell junctions. *Oncotarget* **2016**, *7*,  
39 54714-54722.  
40  
41  
42  
43 73. Youn, G. S.; Lee, K. W.; Choi, S. Y.; Park, J. Overexpression of HDAC6 induces  
44 pro-inflammatory responses by regulating ROS-MAPK-NF- $\kappa$ B/AP-1 signaling pathways in  
45 macrophages. *Free Radic Biol Med* **2016**, *97*, 14-23.  
46  
47  
48  
49  
50  
51 74. Wolfensohn, S.; Lloyd, M. *Handbook of Laboratory Animal - Management and*  
52 *Welfare*. Third Edition ed.; Blackwell Publishing: Oxford, UK, 2003.  
53  
54  
55  
56  
57  
58  
59  
60

- 1  
2  
3 75. Vojinovic, J.; Damjanov, N.; D'Urzo, C.; Furlan, A.; Susic, G.; Pasic, S.; Iagaru, N.;  
4  
5 Stefan, M.; Dinarello, C. A. Safety and efficacy of an oral histone deacetylase inhibitor in  
6  
7 systemic-onset juvenile idiopathic arthritis. *Arthritis Rheum.* **2011**, *63*, 1452-1458.  
8  
9  
10 76. Dinarello, C. A.; Fossati, G.; Mascagni, P. Histone deacetylase inhibitors for  
11  
12 treating a spectrum of diseases not related to cancer. *Mol. Med.* **2011**, *17*, 333-352.  
13  
14  
15 77. Saiga, Y.; Iijima, I.; Ishida, A.; Miyagishima, T.; Takamura, N.; Ohishi, T.;  
16  
17 Matsumoto, M.; Matsuoka, Y. Synthesis of 1,2,3,4-tetrahydro- $\beta$ -carboline derivatives as  
18  
19 hepatoprotective agents. IV. Positional isomers of 1,2,3,4-tetrahydro-2-  
20  
21 methylthiothiocarbonyl- $\beta$ -carboline-3-carboxylic acid and its 1-alkylated derivatives. *Chem.*  
22  
23 *Pharm. Bull.* **1987**, *35*, 3705-3712.  
24  
25  
26 78. Andrianjara, C.; Ortwine, D. F.; Pavlovsky, A. G.; Roark, W. H. Preparation of  
27  
28 substituted Isophthalic Acid Derivatives, multicyclic Pyrimidinediones and Analogs thereof  
29  
30 as Matrix Metalloproteinase Inhibitors. WO2002064080A2, 2002.  
31  
32  
33 79. Cornell, W. D.; Cieplak, P.; Bayly, C. I.; Gould, I. R.; Merz, K. M. J.; Ferguson, D.  
34  
35 M.; Spellmeyer, D. C.; Fox, T.; Caldwell, J. W.; Kollman, P. A. A second generation force  
36  
37 field for the simulation of proteins and nucleic acids. *J. Am. Chem. Soc.* **1995**, *117*, 5179-  
38  
39 5197.  
40  
41  
42 80. Clark, M.; Cramer, R. D. I.; Van Opdenbosch, N. Validation of the general purpose  
43  
44 tripos 5.2 force field. *J Comp Chem* **1989**, *10*, 982-1012.  
45  
46  
47 81. Heiden, W.; Möckel, G.; Brickmann, J. A new approach to analysis and display of  
48  
49 local lipophilicity/hydrophilicity mapped on molecular surfaces. *J Comput Aided Mol Des*  
50  
51 **1993**, *7*, 503-514.  
52  
53  
54  
55  
56  
57  
58  
59  
60

1  
2  
3 82. Ghose, A. K.; Viswanadhan, V. N.; Wendoloski, J. J. Prediction of hydrophobic  
4 (lipophilic) properties of small organic molecules using fragmental methods: An analysis of  
5 ALOGP and CLOGP Methods. *J. Phys. Chem.* **1998**, *102*, 3762-3772.  
6  
7

8  
9  
10 83. Jenei-Lanzl, Z.; Capellino, S.; Kees, F.; Fleck, M.; Lowin, T.; Straub, R. H. Anti-  
11 inflammatory effects of cell-based therapy with tyrosine hydroxylase-positive  
12 catecholaminergic cells in experimental arthritis. *Ann. Rheum. Dis.* **2015**, *74*, 444-451.  
13  
14  
15  
16  
17  
18  
19  
20  
21  
22  
23  
24  
25  
26  
27  
28  
29

### 30 Table of Contents Graphic

